DTIC FILE COPY

DISTRIBUTION STATEMENT A
Approved for public release;
Distribution Unlimited

(2)

SECURITY CLASSIFICATION OF THIS PAGE

DTIC

REPORT DOCUMENTATION PAGE

Form Approved
OMB No. 0704-0188

1a. AD-A224 012

1b. RESTRICTIVE MARKINGS
NA

2a.

3. DISTRIBUTION/AVAILABILITY OF REPORT
Distribution Unlimited

2b. NA

4. PERFORMING ORGANIZATION REPORT NUMBER(S)
University of California, Davis

5. MONITORING ORGANIZATION REPORT NUMBER(S)
NA

6a. NAME OF PERFORMING ORGANIZATION	6b. OFFICE SYMBOL (If applicable)	7a. NAME OF MONITORING ORGANIZATION
University of California, Davis	NA	Office of Naval Research

6c. ADDRESS (City, State, and ZIP Code)	7b. ADDRESS (City, State, and ZIP Code)
1603 Alhambra Blvd. Sacramento, CA 95816	800 N. Quincy Street Arlington, VA 22217-5000

8a. NAME OF FUNDING/SPONSORING ORGANIZATION	8b. OFFICE SYMBOL (If applicable)	9. PROCUREMENT INSTRUMENT IDENTIFICATION NUMBER
Office of Naval Research	ONR	N00014-88-K-0395

8c. ADDRESS (City, State, and ZIP Code)	10. SOURCE OF FUNDING NUMBERS			
	PROGRAM ELEMENT NO.	PROJECT NO.	TASK NO.	WORK UNIT ACCESSION NO.
800 N. Quincy Street Arlington, VA 22217-5000	61153N	RR04108	441q805	

11. TITLE (Include Security Classification)
Intracellular Signalling in Retinal Ischemia

12. PERSONAL AUTHOR(S) Burns, Margaret Sue; Bellhorn, Roy William; Panattoni, Cory Marcus; Rheinhardt, Jeannette; Hitzman, Chuck; Tyler, Nancy K.

13a. TYPE OF REPORT	13b. TIME COVERED	14. DATE OF REPORT (Year, Month, Day)	15. PAGE COUNT
Annual	FROM 7-1-89 TO 7-1-90	90-7-1	

16. SUPPLEMENTARY NOTATION

17. COSATI CODES			18. SUBJECT TERMS (Continue on reverse if necessary and identify by block number)
FIELD	GROUP	SUB-GROUP	
08			Calcium; Retina; Brain; Ischemia; Glutamate; Secondary Ion Mass Spectrometry; Electrolytes; Permeability; Laser; Vein Occlusion; Angiography (TES)

19. ABSTRACT (Continue on reverse if necessary and identify by block number)

In vivo models of retinal ischemia, using laser induced vein obstruction were created and evaluated by non-invasive measurement of vessel permeability and flow, and by histofluorescence of intravenously injected dyes, fluorescein and Evans Blue. We concluded that this model was not reproducible enough to use for the ischemia studies. We have begun experiments with a global retinal vessel ligation model, which will occlude both the retinal and choroidal circulation. We will use this model to evaluate the in vivo characteristics of calcium mobilization and the ability of slected drugs that could affect ischemic injury, reperfusion injury and calcium mobilization.

20. DISTRIBUTION/AVAILABILITY OF ABSTRACT	21. ABSTRACT SECURITY CLASSIFICATION
☒ UNCLASSIFIED/UNLIMITED ☐ SAME AS RPT. ☐ DTIC USERS	U

22a. NAME OF RESPONSIBLE INDIVIDUAL	22b. TELEPHONE (Include Area Code)	22c. OFFICE SYMBOL
Dr. J.A. Majde	202/696-4055	ONR

DD Form 1473, JUN 86 *Previous editions are obsolete.* SECURITY CLASSIFICATION OF THIS PAGE

S/N 0102-LF-014-6603

"Original contains color plates: All DTIC reproductions will be in black and white"

Electrolyte localization and relative quantitation were evaluated in primary retinal cultures and compared to normal, in vivo localization. Influx of exogenous calcium was studied using the stable isotope, ^{42}Ca, and direct ion imaging using secondary ion mass spectrometry. There was loss of the normal calcium isotope, ^{40}Ca, from all retinal layers during incubation under control conditions, ischemia, glutamate, high K^+, and A23187. However, the loss of the normal isotope was compensated for by influx of the stable calcium isotope, but at the same levels of total calcium that are found in normal retinas. There were no major differences between the different experimental conditions with regard to calcium localization or quantitation. There was no massive influx of calcium into the retinas during experimental conditions, up to 6 hours, that was different from control incubations. We conclude the calcium homeostasis is still tightly controlled in these circumstances, and that these studies support redistribution of intracellular calcium as a mechansism of cell death. Future studies will include the influence of different drugs on the calcium exchange. The appearance of high calcium in the synaptic layers of the photoreceptor cells could, speculatively, be related to their normal function.

Another related study in the laboratory has shown an absolute increase in inter-glial (primarily inter-astrocyte) gap junctions in the inner retina following photoreceptor degeneration in rats. We attribute this to an attempt of the retinal glial cells to buffer an increasingly abnormal extracellular space, as could be created by ischemic processes.

An additional study of photoreceptor degeneration in rats has shown that the epithelial layer of the retina is specifically vascularized by new vessels growing in from the retina. Two aspects of this finding are remarkable. First, the neovascularization occurs in the epithelium simultaneously with vascular degeneration in the adjacent retina, and in the presence of high oxygen concentrations from the choroid. This suggests that the epithelial cell exerts as a specific neovascularization stimulus, which has applicability to ischemia studies, in that lack of oxygen alone is not a necessary condition to stimulate neovascularization. Secondly, the phenotype of the new vessels is changed dramatically to a leaky, fenestrated, new endothelial cell. This phenomenon appears also to be induced by the epithelial cell and could be pertinent in the neovascularization of ischemia.

Retinal Vein Occlusion in Rats as a Model of Ischemic CNS Injury

Roy W. Bellhorn, D.V.M.[1]
Margaret S. Burns, Ph.D.[2]
Jeanette M. Rheinhardt, B.S.[1]
Cory M. Panattoni, B.S.[2]

[1] Department of Surgery, School of Veterinary Medicine, University of California, Davis, 95616

[2] Department of Ophthalmology, School of Medicine, University of California, Davis, 95616

Abstract

Retinal neuronal and glial cell ischemia was produced by occluding a major retinal vein with repeated argon laser applications to the vessel. Flow patterns and vascular permeability in the ischemic retinal region were assessed using direct visual observations and fundus fluorescein angiography. Retrograde flow occurred in the venules proximal to the occlusion and then via the capillary network into adjacent non-occluded venous beds. Patchy areas of altered permeability were scattered throughout the ischemic region. Employing NaFl and Evan's blue as permeability markers, fluorescence microscopic assessment of freeze-dried retina from the ischemic region showed altered permeability to primarily non-proteinaceous edema fluid at the level of the capillaries and post-capillary venules. The patchiness of the edematous process in this model, however, has not provided good potential for reliably repeatable studies. Thus a model of complete retinal ischemia, i.e. ligation of intraorbital pre-retinal vessels, is also being developed for further studies.

Introduction

Cerebral ischemia has been extensively studied in a variety of animal models (1,2,3,4,5). Such studies, though, are hampered by the fact that direct cerebral and vascular observations cannot be accomplished without extensive alteration of the brain's normal environment (e.g. surgically removing cranial bones, etc). The retina, on the other hand, is a peripheral extension of the central nervous system that can be directly visualized and studied in many ways without altering its normal environment (e.g. ophthalmoscopy, fluorescein angiography). It is also generally thought that the blood-

brain and blood-retinal "barriers" have considerably similar physiologic and morphologic characteristics. We are developing animal models of retinal ischemia that provide opportunities to obtain in vivo data that in turn can be correlated with in vitro data obtained via cellular and subcellular investigative techniques.

Sodium fluorescein (NaFl) is a dye utilized extensively for clinically assessing the permeability characteristics of the retinal vasculature in both humans and non-humans. Under the conditions of fluorescein angiographic photography, NaFl is not evident outside the retinal vessels in normal subjects; in turn, its presence within neural tissue indicates an altered permeability of the retinal vessels. However, since the molecules of NaFl are not all tightly bound to serum proteins (6), its presence outside the vessels and within tissues does not reflect the nature of the edema fluid, i.e. proteinaceous vs non-proteinaceous. We have utilized fluoresceinated dextrans (FITC-dextrans) of selected molecular weights to assess the role of molecular size in retinal vascular permeability (7). One drawback is that only 1 size can be assessed at any one time, and thus the ability to assess, for example, proteinaceous versus non-proteinaceous components of edema fluid in the same sample is lacking. However, experimental studies of cerebral edema have utilized the combination of NaFl and EB to help define the nature of the edema fluid since EB tightly binds to the serum protein, albumin (8). In our studies we will also utilize the NaFl/EB combination to help understand the nature of the edema fluid.

This report describes our initial clinicopathologic studies, results and interpretations regarding certain aspects of acute retinal ischemia.

Materials and Methods

Adult female albino (WKY) and pigmented (Long-Evans) laboratory rats were anesthetized with sodium pentobarbital (40-50 mg/kg) intraperitoneally. Their pupils were dilated with 1% atropine sulfate and a femoral vein was exteriorized and cannulated. The rat was positioned at an ophthalmic argon laser (CVL-100; CooperVision) and a glass cover slip was affixed to the cornea using a 2% methylcellulose solution to negate the optical power of the air/cornea interface. Using an initial power setting of 1.25 watts, 200 ms exposure and 100 micron aperture, a segment of the selected vein was spasmed first somewhat away from and then immediately adjacent to the optic nerve head. The occluded segment was then repeatedly treated with argon laser low power burns (power setting of 0.40-0.50 watts) until the blood column was coagulated (See Figure 1). Visual observation through the laser delivery system biomicroscope provided initial assessment of blood flow in the compromised venous region.

Selected animals were then immediately moved to the fluorescein angiographic camera (Topcon TRC---VT), the coverslip removed and an injection of NaFl 2.5% (17 mg/kg) and/or Evan's blue 2.0% (20 mg/kg) was administered via the femoral vein cannula. The subsequent angiographic series was recorded on black/white film (ASA 400) which was routinely processed.

Fifteen minutes after the initial injection of NaFl and/or Evan's blue (EB), the eyes were enucleated, flash frozen in liquid nitrogen cooled isopentane, and freeze-dried at -35 degrees C in a molecular sieve apparatus. Non-lasered and non-injected eyes were similarly freeze-dried processed. Slices of the dried tissue were embedded in paraffin,

sectioned at 10 u and examined with a fluorescence microscope equipped with a computer-driven monochromator (Zonax System, Zeiss, Inc.) for assessment of fluorescent wavelengths in the tissues. The voltage and gain, the microscope objective and the aperture of the monochromator were consistent at each recording session.

Other animals were injected with the NaFl/EB solution at 1, 3, or, after re-anesthetizing, 24 hours after laser-induced venous closure. Again, 15 minutes after injection, eyes were enucleated, processed and assessed as described above.

After enucleation, all animals were humanely destroyed using an overdose of anesthetic.

Results

Following closure of a retinal vein, direct observation of the retinal vessels by fundus biomicroscopy showed that the blood flow was characterized in that region by a marked slowing of the flow rate into the occluded vein (the flow was slowed to the extent that red blood cells could be observed). Flow did continue, however, in the following manner: the blood moving into the occluded vein slowly exited the compromised area by retrograde flow via the venules near the site of the occlusion that normally would empty into the occluded vein; the retrograde flow continued distally from the occluded vein into adjacent capillary beds that were being drained by adjacent, open veins (Figure 2).

Fluorescein angiography not only confirmed the above observations, but demonstrated leakage of dye from capillary beds in the ischemic region (Figure 2). The

leakage was characterized as being patchy rather than diffuse, and this was also apparent upon examining the freeze-dried tissue prior to embedding (Figure 3).

Fluorescence microscopic examination of the retinal tissues demonstrated the presence of NaFl (both visually and spectrally, peak wavelengths 530-550 nm) in the neural tissue at the sites of dye leakage (Figures 4, 5A & B). In many areas, there was no frank evidence of dye leakage, but rather simply evidence of vessel dilation (Figures 6A & B). In some instances, though, dye was detected by the monochromator in those areas. Evan's blue (peak wavelengths 640-690 nm) was infrequently noted, and when noted, it was to a much lesser degree as compared to the presence of NaFl (Figure 7). Readings taken from the lumen of major retinal blood vessels (Figure 8) provided the basic ratio for comparing the presence of NaFl to EB in the tissues. The presence of both NaFl and EB was greater in any given area the closer the readings were taken to a retinal vessel.

Discussion

A basic question to be answered by our studies is the applicability of retinal ischemia investigations to the understanding of cerebral ischemia. There are several generalizations which suggest that it should be applicable. For example, both the brain and retina are central nervous system tissue "housed" within an unyielding structure (i.e. the cranium and the sclera respectively); both the brain and the retina lack lymphatics; both have extensive and intricate extracellular spaces; and the intracerebral and intraretinal vasculatures possess autoregulatory mechanisms. In addition, the morphologic, physiologic and pathologic characteristics of the blood-brain and blood-

retinal barriers have been shown to be markedly similar, as attested to by the information presented at 2 symposia concerning those neural and vascular interactions (9,10). Thus it is apparent that studies of retinal ischemia have a significant basis for extending that knowledge into the understanding of cerebral ischemia.

The major finding in this clinicopathologic study was that in acute retinal venous blockage, at least in the rat and under our conditions, the edema fluid was primarily non-proteinaceous. In essence, the edema was generated primarily by the increased hydrostatic pressure forcing increased quantities of non-proteinaceous fluid across the endothelial cells of the vessels. The stretching and associated thinning of the endothelial cells as the vessels became congested would also facilitate the passage of non-proteinaceous fluid in the face of increased hydrostatic pressure. The paucity of proteinaceous edema fluid indicates that opening of the intercellular tight junctions did not occur to any significant extent. It would appear that the insult undergone by the endothelial cells was, therefore, insufficiently damaging such that the tight junctions were able to remain intact. There are several factors that most likely accounted for the relatively minimal insult to the vessels. First is the observed fact that flow within the occluded vessel did not totally cease. It was evident that a slowed flow continued through the major vessel lumen, but that it could occur only because of the retrograde flow of blood from the lumen into venules that normally would drain into the major vein. Thus this retrograde flow provided a reduction of the pressure head within the lumen of the major vein that was apparently of sufficient magnitude to minimize the stretching of the endothelial cells. Another factor was the sometime transient nature of the occlusion itself. On occasion it was even observed within the first few minutes that the clot would

be freed and move along the vein toward the optic nerve head and out of the eye. In those instances, of course, relatively normal flow would resume quite quickly. It is likely, therefore, that the severity of the edematous process would be lessened in proportion to the shorter periods of time that the vein remained occluded.

As can be seen, it became apparent that the single vein closure model of retinal edema produces an edematous process that is minimal in severity, that is unpredictably transient and, therefore, not readily reproducible. While important information can be extracted, especially in relation to minimal, transient insult, for our purposes it became necessary to consider other models. Closure of 2 adjacent veins readily produced a much more severe edematous process. However, once again the occlusions were transient to varying degrees and it was decided that this model would not meet our needs. Ligation of all the vessels entering the posterior aspect of the eye was then considered. Because the rat has a relatively open orbit, it was not difficult to surgically expose the area of the optic nerve. The intraretinal vessels and the choroidal vessels enter the globe adjacent to the optic nerve immediately adjacent to the sclera. Thus, ligating the optic nerve would effectively cause total ischemia of the retina by depriving it of both its intraretinal and choroidal vascular supply. It is readily ascertained that total occlusion has occurred in that ophthalmoscopically viewing the back of the albino rat's eye provides direct visualization of both the retinal and choroidal vascular systems. And, the absence of blood within the vessels confirms the occlusion. Also, ligation, unlike laser-induced occlusion, is permanent. Because of the distinct advantages provided by this model, it will now be the model of choice for our continued studies of retinal ischemia.

References

1. Cohn, R. and Hurley, C.W.: Cerebral hemodynamics in experimental ischemia in the gerbil. In Advances in Neurology, Vol. 28; Brain Edema, J. Cervos-Navarro and R. Ferszt, eds. Raven Press, New York, 1980. pp 39-54

2. Westergaard, E.: Ultrastructural permeability properties of cerebral microvasculature under normal and experimental conditions after application of tracer. Ibid, pp 55-74.

3. Garcia, J.H.,Conger, K.A., Morawetz, R. and Halsey, Jr., J.H.: Postischemic brain edema: quantitation and evolution. Ibid, pp 147-169.

4. Sutton, L.N., Bruce, D.A., Welsh, F.A. and Jaggi, J.L.: Metabolic and electrophysiologic consequences of vasogenic edema. Ibid, pp 241-254.

5. Klatzo, I., Chui, E., Fujiwara, K. and Spatz, M.: Resolution of vasogenic brain edema. Ibid, pp 359-373.

6. Coscas, G.: Fluorescein angiography and the blood-retinal barrier. In Blood-Retinal Barriers, J.G. Cuhna-Vaz, ed. NATO Advanced Study Institutes Series. Series A: Life Sciences, Vol 32. Plenum Press, New York & London, 1980. pg 212.

7. Bellhorn, M., Bellhorn, R. and Poll, D.: Permeability of fluorescein-labelled dextrans in fundus angiography of rats and birds. Experimental Eye Research 24:595-605, 1976.

8. Klatzo, I., Wisniewski, H., Steinwall, O. and Streicher, E.: Dynamics of cold injury edema. In Brain Edema, I. Klatzo and F. Seitelberger, eds. Springer-Verlag, New York, 1967. pp 554-563.

9. The Cerebral Microvasculature: Investigation of the Blood-Brain Barrier, H.M. Eisenberg and R.L. Suddith, eds. Advances in Experimental Medicine and Biology, Vol. 131. Raven Presss, New York & London, 1979.

10. The Blood-Retinal Barriers, J.G. Cuhna-Vaz, ed. NATO Advanced Study Institutes Series, Series A: Life Sciences, Vol. 32. Plenum Press, New York & London, 1980.

Figure Legends

Figure 1. Fundus photograph of rat showing laser-induced occlusion of a major retinal vein (arrowhead). A venule providing retrograde flow from the occluded vein is visible (small arrow).

Figure 2. Fundus fluorescein angiographic photograph showing 1) extensive leakage of dye at the laser burn sites (*), 2) lack of dye in occluded segment of vessel (open arrowhead), 3) dilated and tortuous venule providing retrograde flow from occluded vessel (small arrow), and 4) patches of leaked dye within the neuroretinal tissue (solid arrowheads). Optic nerve head (O).

Figure 3. Macrophotograph of a freeze-dried quadrant of the posterior ocular segment showing patches of leaked dye (arrows) in the drainage field of the occluded vein. Laser site (L) and optic nerve (O) are noted.

Figure 4. Photomicrograph of freeze-dried tissue showing presence of NaFl adjacent to a capillary in the deep capillary bed of the retina (white arrow). The dilated major vein is also evident (white arrowhead). Sclera (s) and choroid (c) are also noted.

Figure 5 A. Monochromator wavelength printout from non-injected/non-lasered control rat showing peak fluorescence at 550 nm (.1481) which is typical for tissue autofluorescence.

Figure 5 B. Monochromator wavelength printout from lasered rat showing increased evidence of fluorescence and peak fluorescence of 540 nm (.5212) which is typical for NaFl. Reading was taken adjacent to a medium sized vessel at the level of the inner plexiform layer.

Figure 6 A. Photomicrograph of freeze-dried tissue showing presence of Evans blue within normal retinal vasculature (small arrows) and choroid (c). Evans blue on outer surface of sclera (arrowhead) indicates presence of blood resulting from the enucleation procedure.

Figure 6 B. Photomicrograph of freeze-dried tissue showing Evans blue within dilated retinal vessels (arrows). Visual evidence of Evans blue outside the vessels is lacking.

Figure 7. Monochromator wavelength printout from lasered rat showing presence of NaFl (.2525-.2606) and to a much smaller extent the presence of Evans blue (.0505) in neuroretinal tissue adjacent to a dilated capillary.

Figure 8. Monochromator wavelength printout showing fluorescent values for NaFl and Evans blue in intravascular blood. Note that in comparison to Figure 7 the values are relatively equal for the 2 fluorescent dyes.

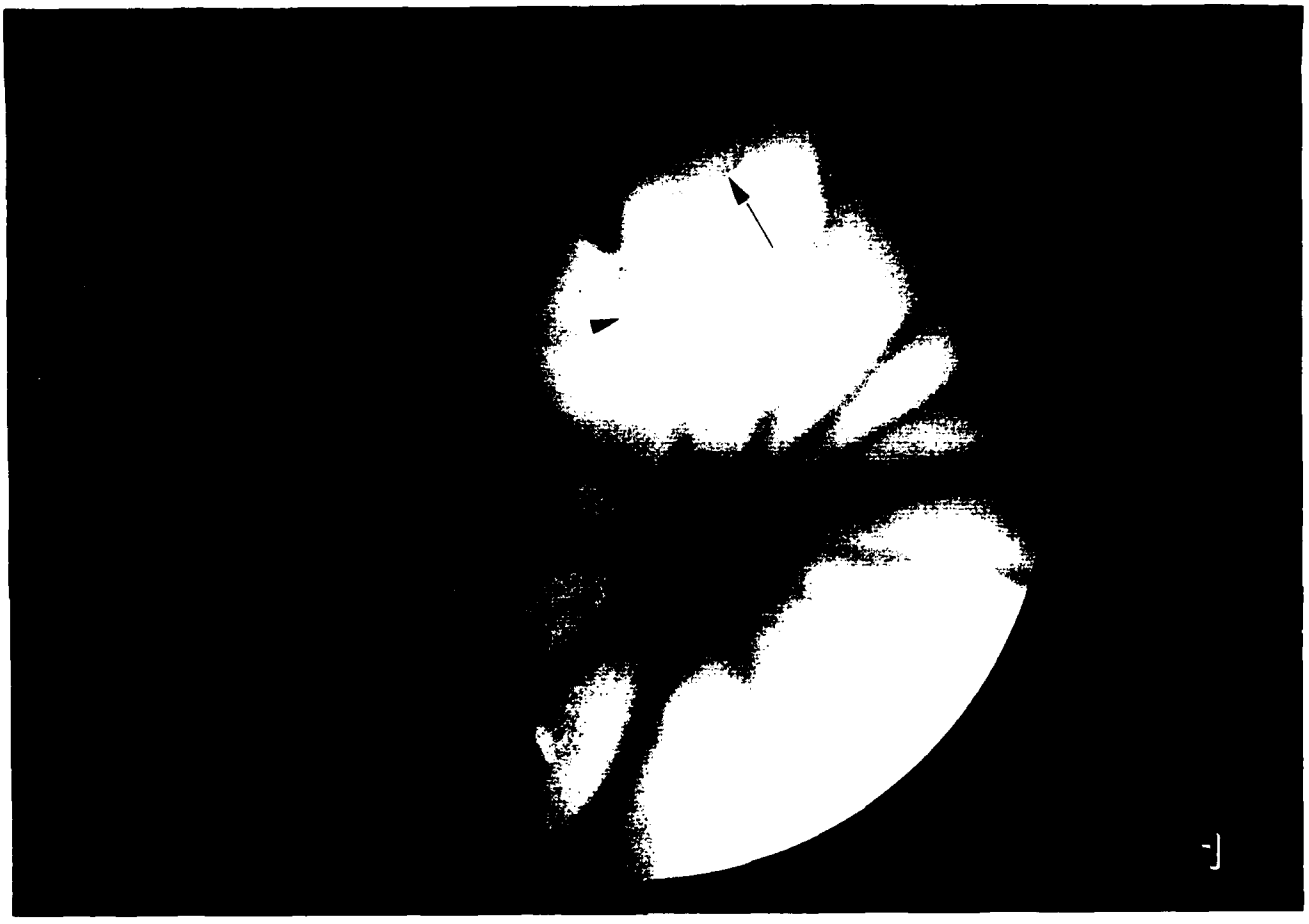

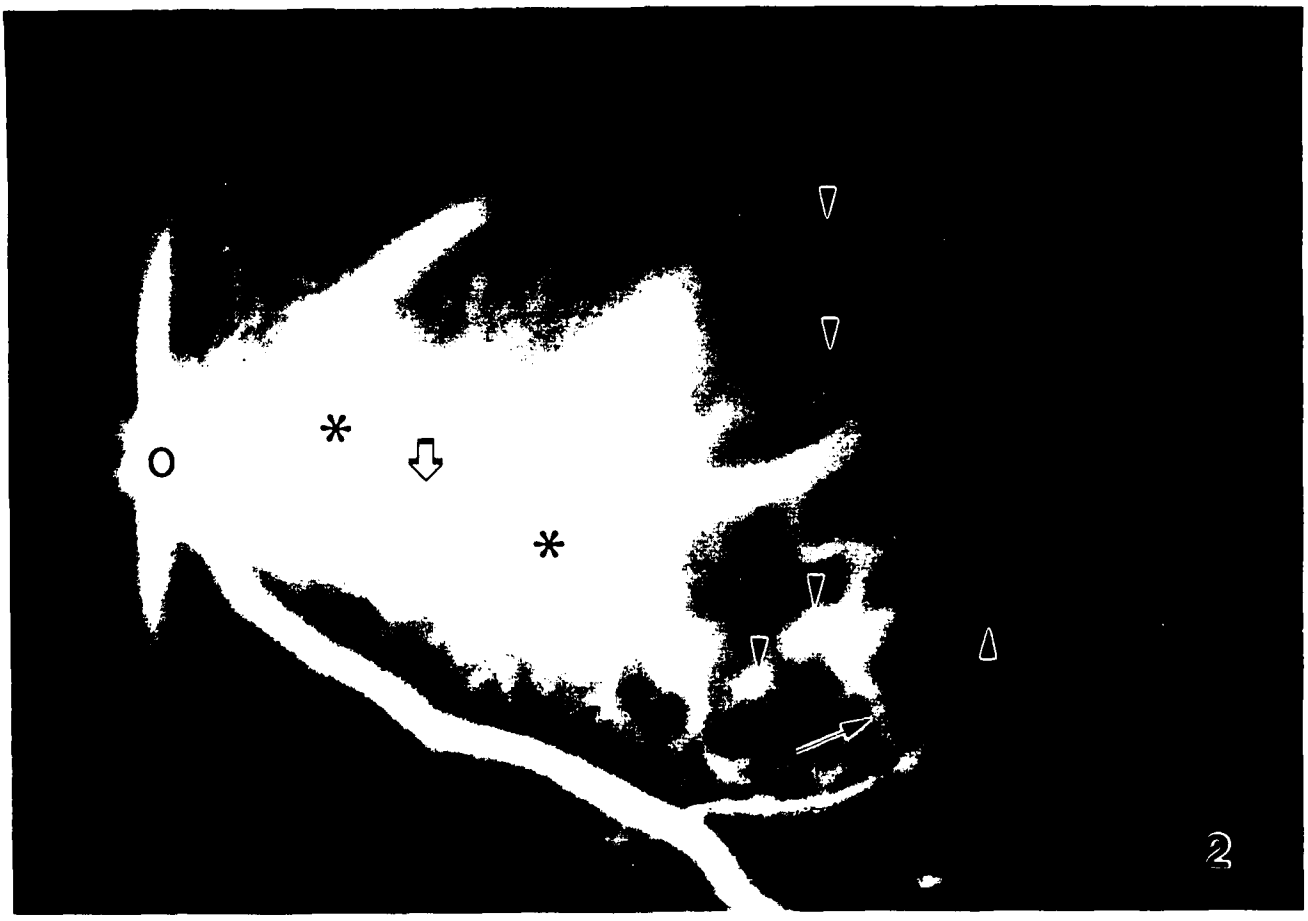

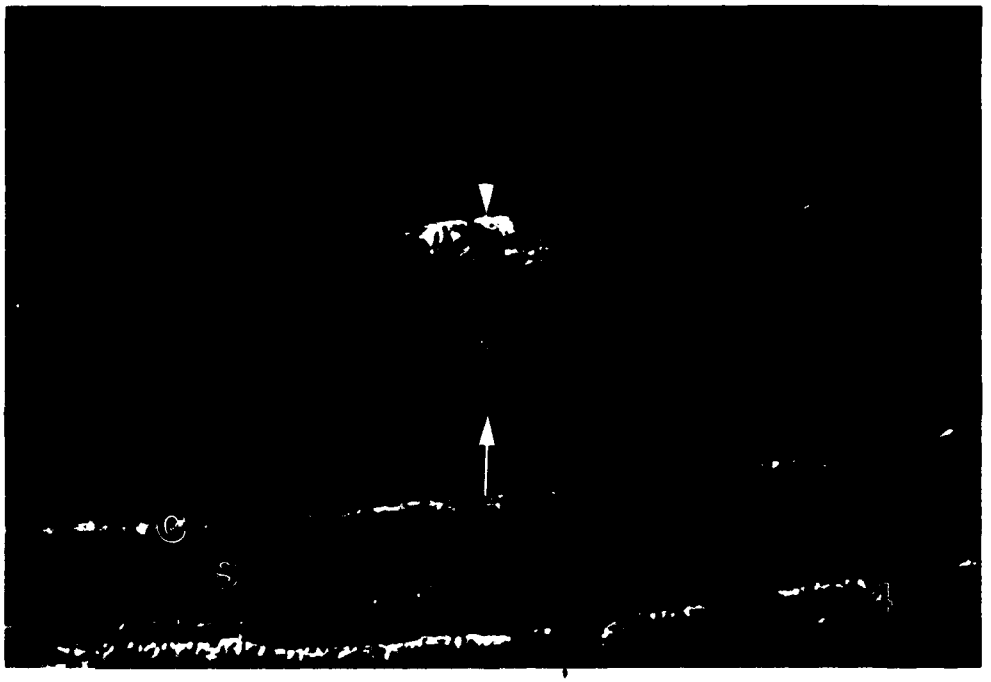

I2065-,0,0,OSA,IPL,FP,iK/iK,0.25,40X-DAY2, NEAR RV

WAVELENGTH	VALUE	
400	.0406	*
410	.0457	*
420	.0365	*
430	.042	*
440	.0536	*
450	.052	*
460	.0494	*
470	.0568	*
480	.0502	*
490	.0518	*
500	.039	*
510	.0476	*
520	.0656	*
530	.0983	*
540	.1439	*
550	.1481	*
560	.1153	*
570	.123	*
580	.1046	*
590	.1071	*
600	.0889	*
610	.0695	*
620	.0588	*
630	.0649	*
640	.0545	*
650	.0584	*
660	.0421	*
670	.0508	*
680	.0559	*
690	.0437	*
700	.0461	*

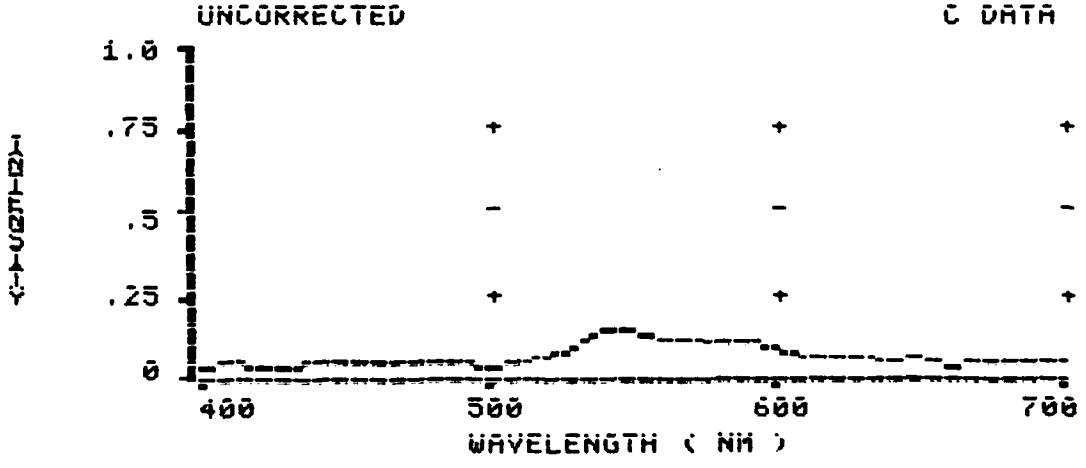

Figure 5A

KK1095.L,FE,OSA,FP.IPL,1K/1K,.25,40X,NEAR MEDIUM VESSEL

WAVELENGTH	VALUE	
400	.0373	*
410	.0439	*
420	.0571	*
430	.0495	*
440	.0354	*
450	.0463	*
460	.0346	*
470	.0485	*
480	.0361	*
490	.0379	*
500	.0447	*
510	.0815	*
520	.2959	*
530	.5202	*
540	.5212	*
550	.4771	*
560	.385	*
570	.2924	*
580	.2042	*
590	.179	*
600	.1567	*
610	.1194	*
620	.0858	*
630	.0812	*
640	.0585	*
650	.0677	*
660	.0662	*
670	.0563	*
680	.0673	*
690	.0634	*
700	.0657	*

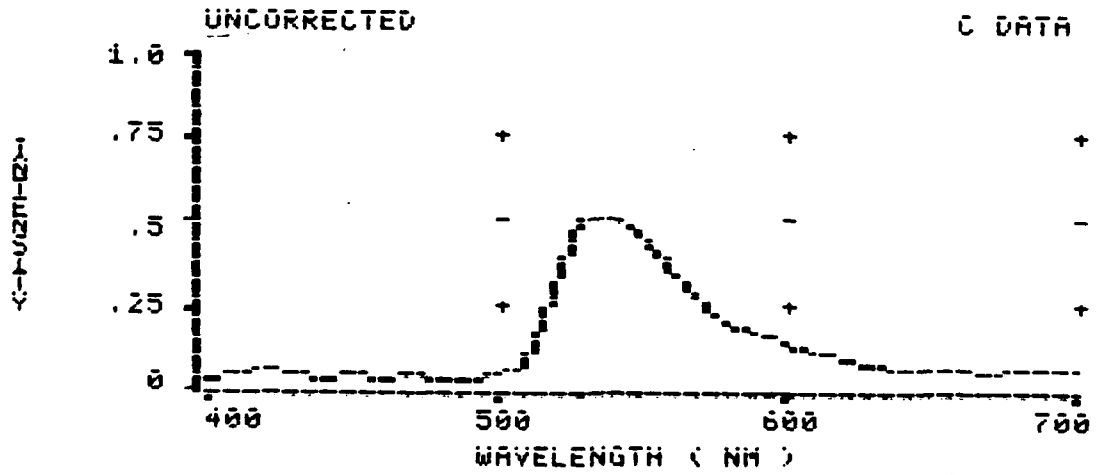

Figure 5B

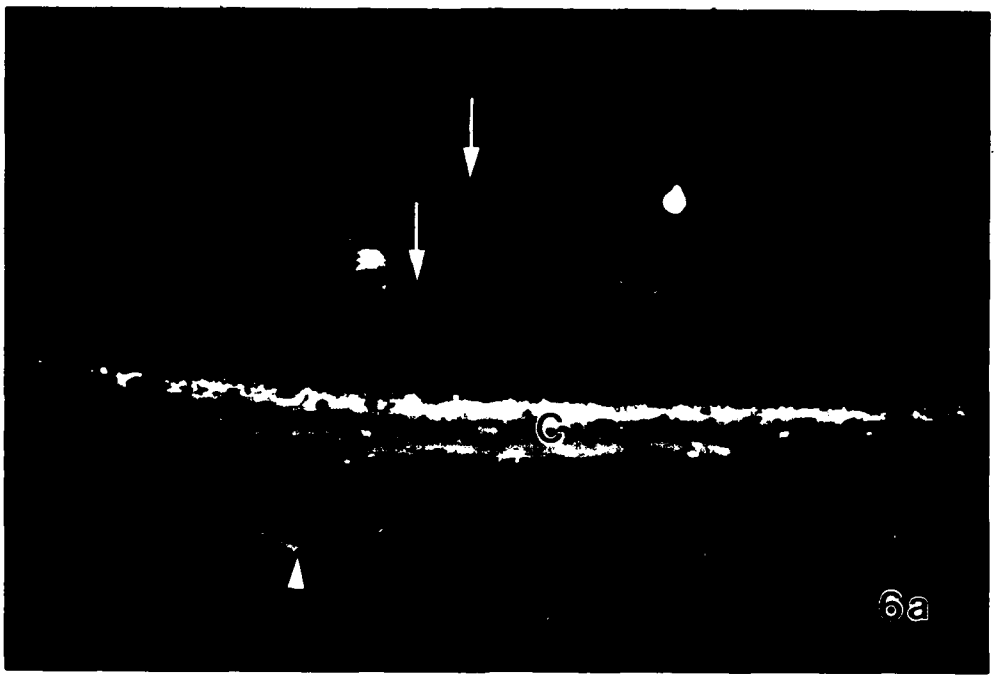

6a

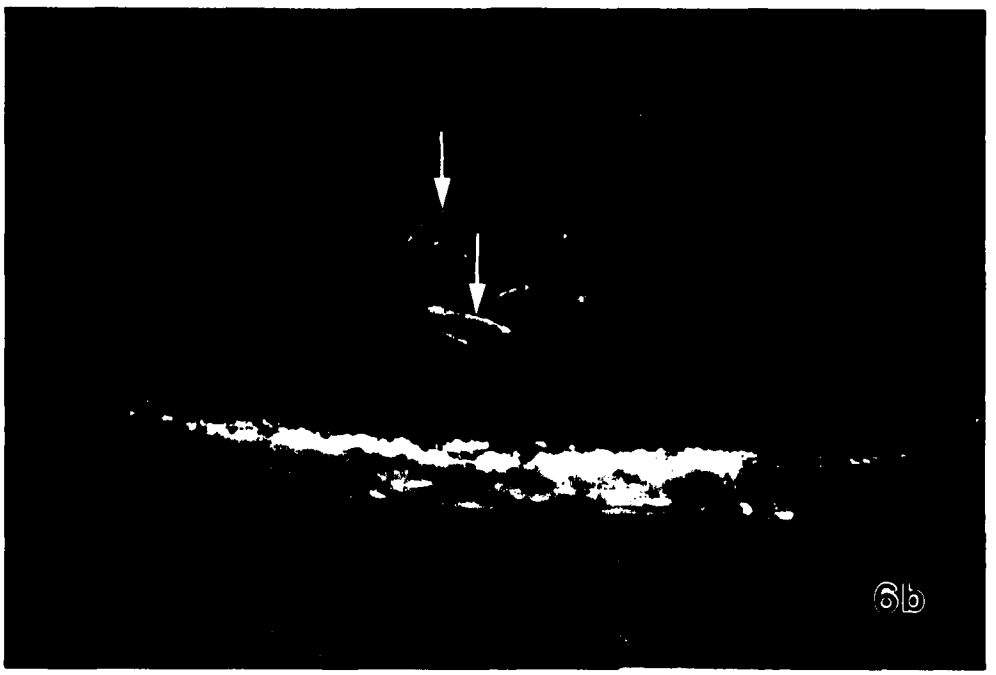

6b

A246W,L,FE,OSA,FP,ONL,1K/1K,.25,40X,NEAR DILATED CAPILLARY

WAVELENGTH	VALUE	
400	.0297	*
410	.0288	*
420	.0394	*
430	.0611	*
440	.0432	*
450	.0515	*
460	.0472	*
470	.0369	*
480	.0349	*
490	.0498	*
500	.047	*
510	.0512	*
520	.1234	*
530	.2233	*
540	.2525	*
550	.2605	*
560	.2114	*
570	.1756	*
580	.1336	*
590	.1295	*
600	.0991	*
610	.0971	*
620	.0759	*
630	.0691	*
640	.0543	*
650	.0391	*
660	.0505	*
670	.04	*
680	.0471	*
690	.034	*
700	.0411	*

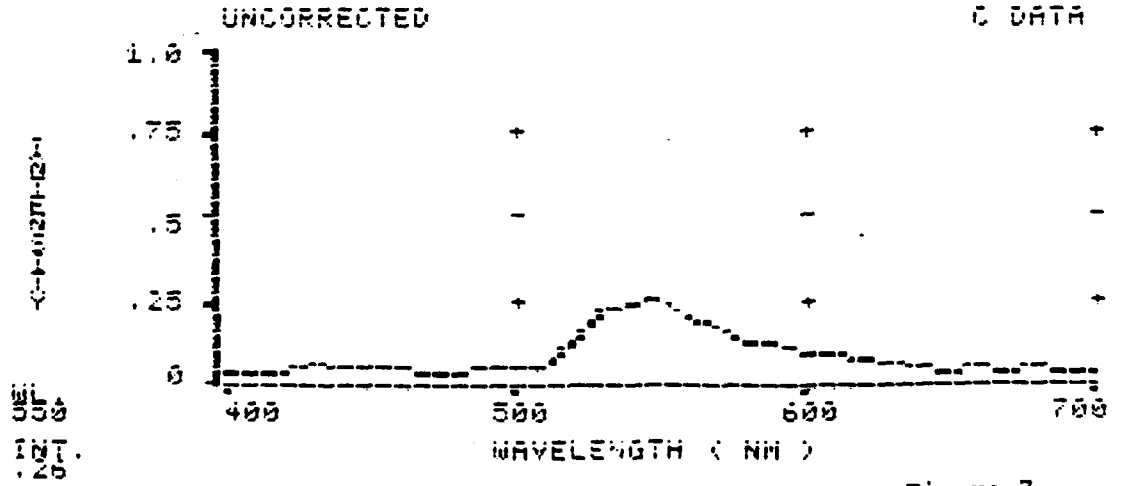

Figure 7

I245M,L,FE,OSA,FP,RV,1K/1K),.25,LUMEN MEDIUM VESSEL

WAVELENGTH	VALUE
400	.0408
410	.0456
420	.0375
430	.055
440	.0437
450	.0411
460	.0519
470	.0452
480	.0451
490	.0576
500	.0736
510	.0929
520	.1345
530	.1862
540	.2258
550	.3353
560	.4753
570	.4021
580	.2659
590	.2008
600	.1524
610	.1372
620	.1854
630	.2345
640	.4138
650	.4913
660	.5899
670	.5813
680	.5736
690	.5527
700	.4738

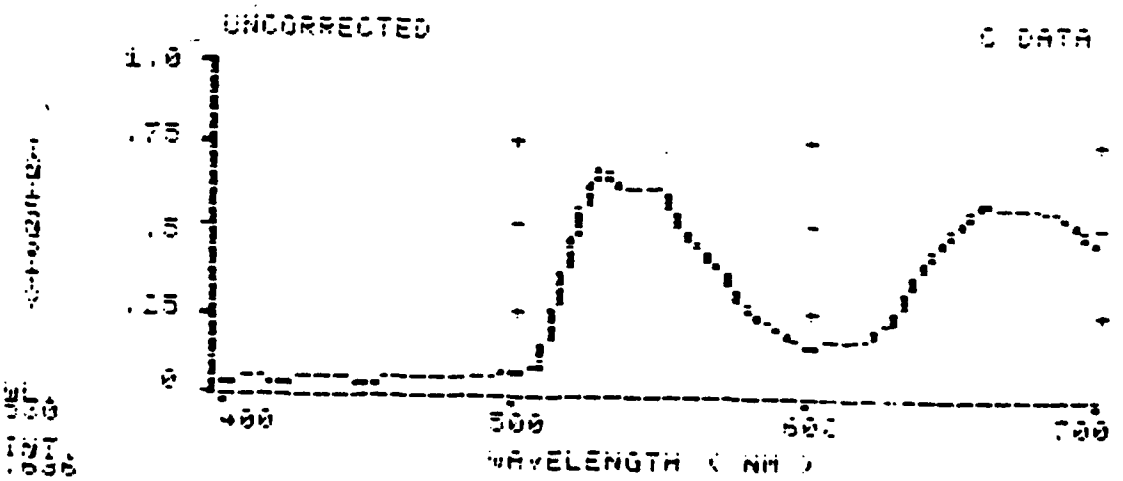

Figure 8

MICROLOCALIZATION OF ELECTROLYTES (NA, K, MG, CA) IN RAT RETINA DURING ISCHEMIA IN VITRO

Margaret S. Burns[1], Cory M. Panattoni[1] and Chuck Hitzman[2]

[1] Department of Ophthalmology, School of Medicine, University of California, Davis, CA 95616

[2] Charles Evans and Associates, 301 Chesapeake Drive, Redwood City, CA 94063

ABSTRACT

Calcium homeostasis in cells is tightly controlled. Increases in intracellular calcium have been postulated to be important in cell death, particularly in the central nervous system in which the neuronal and glial cells have little capacity for renewal. One aspect of this question is whether intracellular calcium arises from redistribution of intracellular stores or from exogenous calcium. We have examined this question in retina under various in vitro conditions: control incubation in Ames' medium; ischemia in 100% N_2 atmosphere; high glutamate concentration; high KCl concentration; and in the presence of A23187.

All incubation conditions resulted in some swelling and distortion of the retina, particularly in the inner nuclear layer at times up to 6 hours. Cell death was greater in glutamate incubation than other conditions. Radioactive ^{45}Ca uptake occurred in all incubated retinas, and was approximately twice as much at 30 minutes in all experimental conditions than the control.

Analysis of electrolyte localization was made by secondary ion mass spectrometry (SIMS). Na, K, and Mg localization is qualitatively the same in incubated retinas as in normal, in vivo retinas. Calcium also shows a similar distribution, except that the outer plexiform layer (OPL) has high calcium emission in all conditions except glutamate incubation, and this layer represents the synaptic contacts of the photoreceptor cells with second order neurons. When the retinas were incubated with the stable isotope, ^{42}Ca, in the medium the exogenous calcium was also very high in the OPL.

Digital image analysis of relative quantitation of electrolytes showed the following: 1) Sodium was increased in control, in vitro, incubations compared to normal retina; 2) Na was further increased in ischemic and high glutamate incubation, particularly in the inner nuclear layer; 3) K distribution was not appreciably different from normal in the incubated retinas; 4) Mg distribution was fairly even in the normal retina, but was more prominent in the nuclear layers than the plexiform layers in incubated retina, the opposite distribution of calcium; 5) Calcium exchange in all retinal layers occurred by 6 hours and was 50% to 70% of the total calcium, although the total calcium level was maintained and not increased; 6) With the exception of the OPL, the endogenous ^{40}Ca and exogenous ^{42}Ca distribution was the same in control, ischemic and glutamate incubated samples at 6 hours.

These data show appreciable calcium exchange in incubated retinas, which does not rise above normal levels. At prolonged incubation times, there is no difference in control, ischemia and glutamate incubation. These data suggest that there is considerable control of calcium homeostasis during in vitro incubations since increases in total calcium levels have not been observed. This suggests that redistribution of intracellular calcium may be the dominant mechanism for cell death under these circumstances.

INTRODUCTION

Calcium homeostasis in cells is tightly controlled and regulated. Alterations in calcium homeostasis, either transient or prolonged, can result from specific stimuli such as neurotransmitter binding. There is increasing evidence that increases in intracellular calcium could be a common final pathway that results in cell death (1,2,3). The relationship between cell ischemia and increases in cellular calcium concentration have been explored in many systems, but is of particular interest in central nervous system neural tissues, since these neurons and glia have little capacity for renewal and therefore, cell death leads to loss of CNS function.

One aspect of this questions which is difficult to approach, is whether increased intracellular calcium arises from redistribution of intracellular calcium stores and/or from influx of extracellular calcium. We have begun studies on this question using Secondary Ion Mass Spectrometry (SIMS), a technique which permits direct imaging of elements and their isotopes, thus giving both a quantitative analysis and a microlocalization of the elements with approximately 1 μm spatial resolution (4,5).

As a model system of brain ischemia, we have used the CNS tissue of retina, which has been referred to as "the little brain" (6). In these initial experiments, we have used an in vitro culture system of rat retina, in order to be able to more closely control the extracellular milieu than is possible in vivo. Several experimental modifications have been studied, which each bear on some aspect of ischemia: 1) total ischemia is created with a 100% N_2 environment; 2) high concentrations of glutamate are thought to mimic

ischemic CNS injury; 3) depolarizing conditions are created with 40 mM KCl; 4) the calcium ionophore, A23187, could increase calcium entry into cells. These experimental conditions are compared both to an in vitro control and to retina immediately removed from the animal (normal retina). Electrolyte (K, Na, Mg and Ca) localization and relative quantitation was assessed in individual retinal cell layers, using SIMS. By including the stable calcium isotope, ^{42}Ca, in the medium, influx of extracellular calcium could also be measured. Radioactive ^{45}Ca uptake into total tissue was also compared.

MATERIALS AND METHODS

Retinal Isolation and Maintenance In Vitro: Adult Long-Evans (LE) rats weighing 200-275 g were obtained from Charles River Laboratories. All were maintained on a 12 h light/dark cycle and received food and water ad libitum. Animals were anesthetized with sodium pentobarbital (35 mg/kg) given intraperitoneally. The eye was enucleated, removing the cornea and lens, then bisected through the optic nerve. The vitreous was discarded and the retina was isolated from the choroid and sclera with gentle manipulation and placed in 20 ml of control medium at approximately 37°C equilibrated with a 5% CO_2/95% air atmosphere. This large volume of medium should have the effect of diluting residual anesthetic that could be in the retina. Euthanasia of animals was performed after enucleation with an intracardiac injection of EUTHA-6 C-II.

Retinas were incubated in 10 ml of medium contained in 6-well tissue culture plates. The control medium consisted of 119.5 mM NaCl , 3.6 mM KCl, 1.15 mM $CaCl_2$-

$2H_2O$, 1.2 mM $MgSO_4$, 22.6 mM $NaHCO_3$ and 10 mM glucose (Ames medium). All chemicals were cell culture tested from Sigma Chemical Company. This was supplemented with 10 ml/L MEM Vitamins (100X) solution, 20 ml/L BME Amino Acids (50X) solution and 10 ml/L Penicillin-Streptomycin (10,000 units/10,000 mcg/ml) solution (Sigma). Control retinas were maintained at 35-37°C under 5% CO_2/95% air and 100% humidity. They remained in control medium for periods ranging from 1 to 360 minutes.

Experimental Procedures: Immediately prior to the experiments, the control medium was replaced with experimental medium having a similar composition but modified for individual experiments. 1) In the ischemia experiment, control medium was used but it was equilibrated with 100% N_2. 2) 5 mM glutamic acid (Sigma) was added to the medium. 3) KCl was increased from 3.6 mM to 40 mM with a concommitant decrease in NaCl to 83.04 mM to preserve the osmolality of the medium. 4) Calcium ionophore A23187 (Sigma) was prepared in dimethyl sulfoxide (DMSO) at 2 mg/ml and was added to cultures for a final concentration of 4 μM A23187. An equivalent volume of DMSO was added to control cultures, approximately 0.1%. All experimental retinas were incubated at 35-37°C under 5% CO_2/95% air and 100% humidity except the ischemia experiment in which incubation was at 35-37%°C in a 100% N_2 atmosphere (Modular Incubator Chamber).

Calcium Uptake: ^{45}Ca chloride (Amersham) was added to cultures to measure the influx of calcium into the retina under the varying experimental conditions. A 100 uCi stock solution of ^{45}Ca chloride was prepared in 1 ml control medium and 10 μl were

added to each culture. Retinas were cultured from 1 to 360 minutes, then removed and washed three times in 10 ml medium to remove excess calcium. Each retina was then homogenized in 200 μl of phosphate buffered saline (PBS). ^{45}Ca was measured in the medium, the three washes and the homogenate with a liquid scintillation counter. Remaining homogenate was used to measure total protein of the retina using the Bio-Rad Protein Assay kit.

Light Microscopy: Tissues were fixed with 3% glutaraldehyde in 0.1 M phosphate buffer for 24 h at 4°C, followed by phosphate buffer rinses, dehydration through graded ethanol and propylene oxide and embedded in PolyBed-812. Tissue damage was assessed both qualitatively and quantitatively through morphological observation and by counting the number of surviving, nonpyknotic nuclei in the inner nuclear layer in 3 photographic fields per specimen at high power (100X).

GFAP Expression - techniques: Tissues fixed and embedded for light microscopy were immunocytochemically labeled for glial fibrillary acidic protein (GFAP) as described previously (7).

SIMS: Cultures were incubated for 1 or 360 minutes in control medium with 10 μl of ^{45}Ca chloride stock solution or 360 minutes with 10 μl ^{45}Ca chloride solution in which usual $CaCl_2$ (^{40}Ca) had been totally replaced in the medium with the stable isotope ^{42}Ca carbonate (Oak Ridge National Research Laboratories). The ^{42}Ca was 93.77% pure. Samples were then removed and washed three times in 10 ml maintenance medium to remove excess calcium. The culture medium and the three washes were counted for ^{45}Ca content.

Since the electrolytes of interest are readily diffusible, tissues were quick frozen in isopentene cooled in liquid nitrogen to prevent translocation of calcium and other electrolytes (5). Tissues were freeze dried at -30°C and dry embedded in Polybed-812 under vacuum. Ten micron thick sections of tissues were dry cut and pressure mounted on conductive silicon wafers, and overcoated with 99.999% Au to provide charge conductance (5).

SIMS analysis was performed with a Cameca IMS 4f operated in stigmatic ion imaging beam mode with a positively charged O_2^+ primary ion beam of ca. 100 nA current. A 250 μm x 250 μm crater was sputtered through the gold coating before analysis began. Images of 150 μm diameter of the retina were formed, selected areas were isolated and counted using a digital image processing system.

RESULTS

Morphology: The freeze-drying method used for preservation of electrolyte distribution results in adequate preservation of morphological detail at the light microscopic level (Figure 1). Eyecups containing retina which were removed from the animal and immediately quick frozen appeared completely normal (Figure 1a). There is some evidence of ice crystal formation, but it does not disrupt electrolyte distribution (5).

All incubation conditions resulted in some swelling and distortion of the retina (Figure 1b to 1f). The inner nuclear layer (INL) which contains the cell bodies of the horizontal, bipolar and amacrine neuronal cells and the Müller glial cell, was distorted, even if the remainder of the retina looked relatively normal. The nerve fiber layer (NFL) was sometimes also swollen. The outer nuclear layer (ONL), the nuclei of the

photoreceptor cells, was usually relatively intact. The photoreceptor cell outer and inner segments were commonly somewhat distorted, but this is possibly due to their mechanical separation from the retinal pigment epithelium (RPE) as well as the incubation conditions. The incubation in high K^+ resulted in the worst morphological damage, with the entire retina being uniformly distorted (Figure 1e). There was some variability of morphology within a single specimen.

All incubation conditions, including the control, resulted in loss of surviving, nonpyknotic nuclei in the INL during the 6 hours of incubation (Table I). The counts of nuclei were made from glutaraldehyde fixed specimens, rather than the illustrations of freeze-dried material shown in Figure 1. In the fixed material the differentiation of healthy and pyknotic nuclei is much easier. There is an approximately 33% loss of nuclei in the control incubated retina over 6 hours. Some of the variability in morphology can be appreciated from the standard deviations of the averages in this table. Ischemic and A23187 incubation showed essentially the same rate of loss of INL nuclei (Figure 2), which was not different from control incubation conditions. Both glutamate and high K^+ incubation resulted in rapid loss of INL nuclei within 30 minutes, but in high K^+ medium there was no further loss after 2 hours, and the numbers of normal INL nuclei matched the control at 4 and 6 hours. However, in the glutamate medium, INL nuclei survival decreased over 6 hours and was consistently 25% less than in control incubation.

Müller cells of the retina express glial fibrillary acidic protein (GFAP) under many conditions of damage or stress (7), so we performed immunohistochemical staining

for GFAP in the retinas incubated for 6 hours under all conditions. Although GFAP was found in the astrocytes of the inner retina, where it normally occurs, it was not present in the Müller cell radial fibers under any incubation conditions (data not shown).

Radioactive ^{45}Ca uptake: There is uptake of ^{45}Ca by the retina incubated under control conditions (Figure 3). This uptake rises gradually during the first hour and then the uptake rate is slower for the next 5 hours of incubation.

A common feature of ^{45}Ca uptake in all the experimental conditions is that the initial rise is faster than in the control retinas (Figure 3). At 30 minutes, the uptake under all experimental conditions is the same, and is approximately twice as much as in control incubations.

At later time periods, the curves for ^{45}Ca uptake vary for each of the experimental conditions. In ischemic conditions, there is no further increase in ^{45}Ca in the retina until the 6 hour time point (Figure 3a). With incubation in glutamate, ^{45}Ca uptake increases for the first 2 hours and then the amount stays the same until 6 hours (Figure 3a). In high K^+ medium, calcium increases for 2 hours and then plateaus and, at 6 hours, has the same value as the control incubations (Figure 3b). Incubation with the calcium ionophore, A23187, has the initial rapid rise in ^{45}Ca in the retina and then a slower, but steady, increase in ^{45}Ca uptake throughout the 6 hours of incubation (Figure 3b).

SIMS Analysis, Ion Images: Images of electrolytes in the normal, in vivo retina were the same as previously described (Figure 4) (8). Sodium emission is particularly intense in the choroid and RPE layer due to the melanin granules present in these areas (8). The ONL and INL are different in emission from the plexiform layers, both OPL

and IPL, as well as the photoreceptor outer segments (ROS). These electrolytes are absent from the epoxy resin (E). The potassium emission is generally brighter than the sodium, since the tissue is mostly cellular with little extracellular space present. The normal calcium isotope, ^{40}Ca, is also present in high concentrations in the choroid and RPE, but within the retina is more emissive in the plexiform layers, the regions of synaptic contact, than in the nuclear layers. An image of ^{42}Ca barely shows any counts, since the natural abundance of this isotope is only 0.64%, compared to 97.0% for ^{40}Ca, and no ^{42}Ca was added to this sample. An image of 12^+ from this area is uniform, reflecting a homogeneous emission of carbon from the tissue and from the epoxy resin (not shown).

The ion images of rat retina that had been incubated in control medium for 6 hours are shown in Figure 5, and correspond to the light micrograph shown in Figure 1b. The electrolyte distributions of sodium and potassium correspond to the same layers as was seen in the normal, in vivo retina, although there is, of course, no choroid or RPE in the dissected samples. The emission from the INL is more diffuse, probably due to the disruption of this layer during incubation. A difference in the incubated samples is seen in the ^{40}Ca image. A line of heavy ^{40}Ca emission is seen in the outer plexiform layer, corresponding to the synaptic endings of the photoreceptor cells with second order neurons. An image of ^{24}Mg shows an inverse relationship to calcium, in that the nuclear layers are more emissive than the plexiform layers. Using high mass resolution analysis, we have found 10% or less contribution of $^{24}C_2^+$ to the magnesium signal.

Rat retinas incubated under ischemic conditions showed similar ion images of

sodium and potassium (Figure 6), although the distinction of electrolyte distribution in the inner layers was less obvious. Again ^{40}Ca showed a bright, emissive line corresponding to the outer plexiform layer, and another emissive line at the level of the outer edge of the ONL. The OPL concentration of ^{40}Ca was seen in all incubated samples except for incubation in glutamate.

The distribution of ^{42}Ca in four incubated rat retinas is shown in Figure 7. The orientation of the retinas is slightly different in each sample, but the layers are labelled. In all cases, the most emission of ^{42}Ca is seen in the inner and outer plexiform layers. This is particularly true for the ischemic (upper right) and high potassium (lower right) incubation conditions. The high emission of the OPL for both ^{40}Ca and ^{42}Ca was not seen in the glutamate incubated sample, even though the general morphology of this sample was neither better nor worse than any of the other incubation conditions.

SIMS Analysis, Quantitative Analysis: Several factors should be noted in the following analysis. First, SIMS analysis measures the total elemental content of a sample, not only ionized species that exist in situ. Rather the ions that are measured are formed during the sputtering process (4). Second, from preliminary, unpublished studies, we know that the ion emission reflects only a relative quantitation, not an absolute one. Therefore the data should be compared only between similar areas of retina, since there is a possibility that matrix effects exist that make comparisons between layers unreliable (9, 10). Thirdly, we cannot distinguish intra-and extracellular electrolyte content because 1) the instrument resolution is 1 μm or more, and 2) the tissue preservation is not designed to preserve intra- and extracellular space. Fourthly, we have not found it

useful, in practice, to normalize ion counts to carbon counts in a given area. First, the studies to be reported were done on the longest incubation times, 6 hours. We chose these samples first so that uptake of ^{42}Ca would be maximal. Analysis of the samples incubated for shorter times are in progress. Sixth, ion images of 45^+ did not give any specific distribution that would be expected from calcium localization as seen with ^{40}Ca and ^{42}Ca. We concluded that the signal at 45^+ did not correspond to ^{45}Ca, but rather a nonspecific organic species in the sample.

Comparison of Na, K, Mg and Ca <u>in vivo</u> and control incubation: The counts per pixel per second of 23^+, sodium, in retinal layers in shown in Figure 8. The sclera and choroid, being largely extracellular space have the highest levels of sodium emission. The RPE and inner retinal layers, with the exception of the ganglion cell layer, are less emissive which is consistent with the relatively small extracellular space of the retina. Values for the ganglion cell layer are less reliable than other layers for two reasons: this layer is very narrow and we are including ganglion cells and their axons, known as the nerve fiber layer; small blood vessels exist in this layer which are highly emissive for sodium and would contribute to the counts obtained; this layer tends to show freezing artifact and may have sodium which comes from the vitreous, a large aqueous extracellular compartment immediately adjacent to the inner retina. All layers of the retina in the control incubation sample show increased sodium emission. This is not unexpected, given the swelling of the retina that occurs during the 6 hour incubation time.

The potassium count rates for various retinal layers in the normal, <u>in vivo</u> sample

(Figure 9) reflect the ion image relative emission. The sclera, being extracellular space, is low in K^+ emission, but K^+ is high in the choroid, due to the emissivity of the melanin granules in this layer (10). The two nuclear layers are more emissive than the two plexiform layers. This distinction is lost in the control, in vitro, sample (Figure 9). Potassium is increased in the ONL, OPL and IPL, and decreased in the ROS and INL, although the count rates are not significantly different between the normal and control specimens. A problem which we have not yet solved is that the potassium count rates for these analyses are uniformly one half that of a previous series of determinations (unpublished). There seems to be a systematic reason for this, but we have not yet found the source of the discrepancy.

Magnesium count rates in various retinal layers are presented in Figure 10. Since these count rates are taken under low mass resolution conditions, it should be noted that there can be a discrepancy of ca. 10% due to counting the interfering ion, C_2^+. For the in vivo, normal retina, the levels of Mg are relatively even throughout the inner retina, and somewhat less in the photoreceptor cell layer. There appears to be some selective loss of magnesium from the INL, IPL and GC layer in the retina incubated in vitro for 6 hours.

Calcium count rates for normal and control conditions are shown in Figure 11. The highest count rates for calcium are found in the sclera, choroid and RPE for in vivo samples. Again, this is because the sclera and choroid are largely extracellular space and due to the large component of pigment granules in the choroid and RPE, which have a high intrinsic concentration of calcium (11) as well as showing more intense ion emission,

due to an intrinsic oxygen content (12). The in vivo control has counts of ^{42}Ca that are less than 1% of the ^{40}Ca counts, approximately what is expected from the natural isotope abundances. As we have seen from the images, the normal retina has more calcium in the plexiform layers than in the nuclear layers. The ganglion cell layer also shows high calcium emission, but this may be somewhat artifactual, for the same reasons discussed for the high sodium emission from this layer.

After incubation in vitro under control conditions, most retinal layers show a decreased level of ^{40}Ca. However, the loss of ^{40}Ca is compensated for by an increase in ^{42}Ca in these layers, resulting in reestablishment of the total calcium levels in the various retinal layers. The one exception is the outer plexiform layer which appears to concentrate ^{40}Ca during the incubation period, perhaps scavenging it from other retinal layers, since the only exogenous calcium is ^{42}Ca. This region also appears to concentrate exogenous calcium as the combined total ^{40}Ca + ^{42}Ca level in this layer is higher than any other retinal region. We will be adding more samples to validate these data. High mass resolution analysis of the ^{42}Ca peak showed that less than 1% of this peak could be due to polyatomic interferences.

SIMS Analysis of Experimental Conditions:

The data for electrolyte distributions in the retinas incubated under ischemia or high glutamate concentrations are given in Figures 12 through 16. With a few exceptions, there are no statistically significant differences between electrolyte concentrations in the different retinal layers. For example, sodium and potassium in the INL is higher in retinas incubated in high glutamate than in control conditions (Figure

12 and 13). This could reflect the swelling of the cell bodies seen in this layer and the increased levels of pyknotic nuclei observed. The level of K^+ in the photoreceptor outer segment layer is higher in ischemia but not in any other conditions examined (Figure 13). Magnesium is also higher in ischemic photoreceptor outer segments, as well as in the IPL (Figure 14).

There is loss of ^{40}Ca in ischemia and glutamate incubation that is not statistically different from that of control incubations (Figure 15). This is compensated for by influx of ^{42}Ca from the medium, that brings the total calcium level in the retinal layers within range of the normal, in vivo, retinas (Figure 16). We have limited data at the present time of the levels of calcium in the OPL, which shows an unusually high level, and so have not been able to statistically evaluate it.

The data for incubations in high potassium medium and in the presence of the calcium ionophore, A23187, are presented in Table II. These data show increases of Na, K, Mg, and Ca in different retinal layers, but the sampling size for these analyses is too small to feel confident about this data. Further analyses of these samples is in progress.

DISCUSSION

In this discussion, we are deliberately taking a limited view of the vast literature on the involvement of calcium in cell ischemic processes. This is because the technique, SIMS, which we are using offers unique capabilities for analysis that are not readily comparable to other methods used in this research. Some of these capabilities are the following: 1) The technique we are using is relatively new to analysis of biological

problems, particularly quantitative aspects; 2) SIMS measures total cellular electrolytes rather than ionized forms and therefore is difficult to correlate with published studies using either ion sensitive electrodes or imaging of ionized calcium with video systems (11,12); 3) This technique measures large areas rather than single cells, which is useful in following tissue level damage; 4) The inherent instrument resolution and tissue preservation methods do not permit a distinction between intra- and extracellular space; 5) The use of stable isotopes as tracers enables microlocalization studies in combination with "pulse-chase" labelling.

An important point is the degree of calcium exchange that we observed during the time course studied. Up to 6 hours in culture, as much as 70% of the tissue calcium was exchanged for the stable isotope added to the medium. And yet the total levels of calcium in the tissue was preserved, indicating that the cells appear to be able to maintain total calcium homeostasis, despite apparent damage as assessed by loss of cell nuclei and cell swelling, which was marked in the inner retinal layers. It thus appears that calcium is more mobile than might have been expected.

A question that remains is whether or not the exchangeable calcium is that normally found in the extracellular compartment, rather than internal cell calcium. If one accepts the commonly used figure of 5% for retinal extracellular space, one might expect only this amount of exchange, if the total intracellular and extracellular calcium concentrations are the same. Using SIMS, a recent determination of intracellular calcium concentration in fibroblasts would be ca. 1 mM (using some assumptions to convert the data to wet weight) (13). If we assume that the extracellular calcium

concentration is similar to serum (2.5 mM), then exchange of extracellular calcium only would be 2.5 x the extracellular volume estimation, or about 12 to 15%. Since the observed exchange is considerably more than that, it is likely that intracellular calcium was also exchanged during these experiments. Similar analyses using cell culture systems, and direct measurement of total tissue calcium concentrations would be desirable.

In this study, with the data we have at hand, we have not found evidence for massive influx of calcium above normal physiological concentrations that could be responsible for cell death. We thus conclude that it is more likely that release of intracellular stores of ionized calcium is responsible for derangment of cellular processes. We will collect more detailed data concerning this point by doing analyses on short time incubations, as well as trying to differentiate calcium in obviously pyknotic cell bodies from cell cytosolic locations.

The overall results of electrolyte analysis are not unexpected, in that, given the degree of cell swelling observed in the inner layers, the increase in sodium, but not potassium seen would reflect water movement into cells. Although one needs to be critically skeptical of a technique which is known to exhibit matrix effects (9), these results have an internal consistency, which is reassuring.

Other authors have reported swelling of the inner nuclear layers in retinal ischemia in vitro (14), but the Müller cells, the dominant glial cells of the retina were relatively spared. We have observed similar morphological findings, but our study of GFAP expression did not indicate stress of this cell. We also did preliminary studies measuring release of lactic dehydrogenase to the medium, an enzyme which is

predominantly in the Müller cell, and found insignificant release. These studies will be repeated using the current culture conditions. Since astrocyte cell swelling (and the Müller cell exhibits many astrocytic properties) is a characteristic of brain ischemia and edema (15,16), it is noteworthy that retinal glial cells seem relatively resistant to ischemia, by the measures tested. This bears further inquiry, and could perhaps be due to the capacity of the Müller cell to buffer extracellular K^+ (17), although astrocytes also possess this capacity (18).

The finding of high calcium emission, of both the normally abundant ^{40}Ca and the exogenous ^{42}Ca in the outer plexiform layer in all incubated retinas (except for glutamate treated) was dramatic. Normally, the plexiform layers of the retina contain more calcium than the nuclear layers (8), but this effect is exaggerated in the incubated retinas. The only other report that relates to this phenomenon was a study by Ripps, et al., (19) that showed accumulation of calcium rich deposits in the processes of the OPL layer by electron microprobe analysis, when high calcium concentrations were included in the fixative solutions. We have used normal calcium concentrations in these studies. They reported an increase in deposits in the postsynaptic elements during light adaptation of the retina and an decrease of deposits associated with the photoreceptor membranes. These relative locations were reversed in the dark. We have taken no precautions to define the light conditions of the experiments, although the retinas are incubated in the dark. This relative location of calcium may simply be a function of focal synaptic activity. Unlike other neurons, the photoreceptor cells release transmitter, which may be glutamate (20), in the dark, rather than upon stimulation by light. Thus it may be that

there is rapid turnover and accumulation of calcium in this region associated with the dark conditions. It may or may not be significant that this focal OPL calcium concentration was not seen in the glutamate treated retinas. At first we considered that this treatment resulted in severe damage to this area, and so the structures that might sequester calcium were not there. However, the damage in glutamate is not obviously worse morphologically than in other incubation conditions, particularly high potassium concentrations, although it is true that INL cell death is more extensive during glutamate incubation. It is tempting to speculate that the high glutamate incubation may be related to the normal neurotransmitter release, or saturation of the presumed glutamate receptors on the postsynaptic cells, but this is premature.

The studies reported need to be correlated with other measures of cell death and swelling and extended to the in vivo condition, which is part of our research plan for the coming year.

ACKNOWLEGEMENTS: We would like to thank Gayle Lux for assistance in operation of the Cameca IMS 4f and Mary E. Johnson for secretarial assistance. This study supported by the Office of Naval Research and an unrestricted grant from Research to Prevent Blindness, Inc., NY.

REFERENCES

1) Siesjo, B.K. (1988) Calcium, ischemia and death of brain cells. Ann. NY Acad. Sci. 522: 638-661.

2) Meyer, F.B. (1989) Calcium, neuronal hyperexcitability and ischemic injury. Brain Res. Reviews 14: 227-243.

3) Schanne, F.A.X., Kane, A.B., Young, E.E., and Farber, J.L. (1979) Calcium dependence of toxic cell death: A final common pathway. Science 206: 700-702.

4) Burns, M.S. (1988) Biological microanalysis by secondary ion mass spectrometry: status and prospects. Ultramicroscopy 24: 269-282.

5) Burns, M.S. and File, D.M. (1986) Quantitative microlocalization of diffusible ions in normal and galactose cataractous rat lens by secondary ion mass spectrometry. J. Microscopy 144: 157-182.

6) Davson, H. (1979) The little brain. Trans. Ophthalmol. Soc. UK 99:21-37.

7) Burns, M.S. and Robles, M. (1990) Müller cell GFAP expression exhibits gradient from focus of photoreceptor light damage. Current Eye Res. 9: 489-501.

8) Burns, M.S., File, D.M., Brown, K.T. and Flaming, D.G. (1981) Localization of calcium and barium in toad retina by secondary ion mass spectrometry. Brain Res. 220: 173-178.

9) Burns, M.S., File, D.M., Deline, V. and Galle, P. (1986) Matrix effects in secondary ion mass spectrometric analysis of biological tissue. SEM IV: 1277-1290.

10) Burns, M.S., Taffet, R. and Hitzman, C. (1989) Digital ion imaging of electrolyte movement in the retina-choroid complex: relative quantitation. In Secondary Ion Mass Spectrometry, SIMS VI (eds. A. Benninghoven, A. Huber, H. Werner) J. Wiley and Sons, Inc. pp. 891-892.

11) Lemaster, J.J., et al., (1990) Multiparameter digitized video microscopy (MDVM) of hypoxic cell injury. Video Microscopy (Eds. G. Herman and K. Jacobson) In press.

12) Trump, B.F. and Beresesky, I.K. (1989) Is $Ca^{2+}{}_i$ important in cell injury? ONR Annual Report, 1989.

13) Ausserer, W.A., Ling, Y-C., Chandra, S. and Morrison, G.H. (1989) Quantitative imaging of boron, calcium, magnesium, potassium and sodium distributions in cultured cells with ion microscopy. Anal. Chem. 61: 2690-2695.

14) Shay, J. and Ames, A. III (1976) Retina subjected to components of ischemia in vitro. Arch. Neurol. 33:715-721.

15) Lomneth, R. and Gruenstein, E.I. (1989) Energy dependent cell volume maintenance in UC-11MG human astrocytomas. Am. J. Physio. 257 (Cell Physiol. 26) C817-C824.

16) Kimelberg, H.K., Goderie, S.K., Higman, S., Pang, S. and Waniewski, R.A. (1990) Swelling induced release of glutamate, aspartate and taurine from astrocyte cultures. J. Neurosci. 10: 1583-1591.

17) Newman, E.A. (1985) Voltage dependent calcium and potassium channels in retinal glial cells. Nature 317:809-811.

18) Newman, E.A. (1986) High potassium conductance in astrocyte endfeel. Science 233:453-454.

19) Ripps, H., Shakib, M., Chappell, R.L. and MacDonald, E.D. (1979) Ultrastructural localization and X-ray analysis of calcium induced electron dense deposits in the skate retina. Neuroscience 4:1689-1703.

20) Copenhagen, D.R. and Jahr, E.E. (1989) Release of endogenous excitator amino acids from turtle photoreceptors. Nature 341:536-539.

LEGENDS

Figure 1a. Light micrograph of normal rat retinal eyeceup, quick frozen immediately after enucleation. The morphology of the entire retina appears normal. The choroid (C) and retinal pigment epithelium (RPE) are apposed. The RPE is immediately adjacent to the photoreceptor outer segments (ROS). The outer nuclear layer (ONL) and inner nuclear layer (INL) are compact. The outer and inner plexiform layers (OPL,IPL) are well formed. Bar = 20 μm.

1b. Rat retina incubated for 6 hours in control medium. The entire retina is swollen compared to freshly frozen retinas. The INL shows a large degree of swelling, as do the other retinal layers, but the overall morphology is retained. Careful comparison with Figure 1a indicates that most of the swelling is in the inner retina. Other specimens had even less damage and distortion than this example. Bar = 20 μm.

1c. Rat retina incubated for 6 hours in ischemic medium. The general retinal morphology is well retained, although there is marked swelling of cell soma in the INL layer. When compared with Figure 1a, it can be appreciated that most of the swelling is in the inner retinal layers. Bar = 20 μm.

1d. Rat retina incubated for 6 hours in glutamate containing medium. Although the general retinal morphology is apparent, there is pronounced swelling and pyknosis of nuclei of the INL and swelling of the inner plexiform layer (IPL) and nerve fiber layer (NFL). The outer retina in this area is relatively intact, but other specimens were more grossly distorted. Bar = 20 μm.

1e. Rat retina incubated for 6 hours in 40 mM K^+. The retina is grossly distorted and this was uniform throughout all specimens. Bar = 20 μm.

1f. Rat retina incubated for 6 hours in 4 μM A23187. The photoreceptor outer segments and nuclei (ONL) appear relatively normal, but the inner retinal layers are swollen, with apparently cystic spaces in the outer plexiform layer (OPL) and the NFL. Bar = 20 μm.

Figure 4. Ion Images of normal, in vivo, rat retina. The upper right image of sodium is labelled with the retinal layers. The other images of potassium, ^{40}Calcium and ^{42}Calcium are taken from exactly the same area, but with different times for integration of the image. Sodium and potassium images are accumulated for 10 sec, ^{40}Ca for 30 sec and ^{42}Ca for 60 sec. The diameter of the imaged field is 150 μm.

Figure 5. Ion images of control rat retina incubated for 6 hours. The images are discussed in the text.

Figure 6. Ion images of ischemic rat retina incubated for 6 hours. The images are

discussed in the text.

Figure 7. Ion images of ^{42}Ca in incubated rat retinas. The upper left image is of a control (the same specimen shown in Figure 5); upper right image of an ischemic retina (other images from this specimen are in Figure 6); lower left image of glutamate incubation; lower right image of high potassium incubated rat retina. Labelling is the same as in other figures.

Figure 8. Digital image analysis of sodium (23^+) counts per pixel per second in retinal layers. Scl = sclera; chor = choroid; rpe = retinal pigment epithelium; ros = photoreceptor outer segments; onl = outer nuclear layer; opl = outer plexiform layer; inl = inner nuclear layer; ipl = inner plexiform layer; gc = ganglion cell layer. Comparisons with the control condition that are statistically significant with $P \leq .05$ are marked with an asterisk in this and all following figures.

Figure 9. Digital image analysis of potassium (39^+) counts per pixel per second in retinal layers. Abbreviations in this and following histograms are the same as in Figure 8.

Figure 10. Digital image analysis of magnesium (24^+) counts per pixel per second in retinal layers.

Figure 11. Digital image analysis of calcium (40^+ or 42^+) counts per pixel per second in retinal layers.

Figure 12. Digital image analysis of sodium, comparing control and two experimental incubation conditions.

Figure 13. Potassium distribution in control and experimental conditions.

Figure 14. Magnesium distribution in control and experimental conditions.

Figure 15. 40-Calcium distribution in control and experimental conditions.

Figure 16. 42-Calcium distribution in control and experimental conditions.

1a

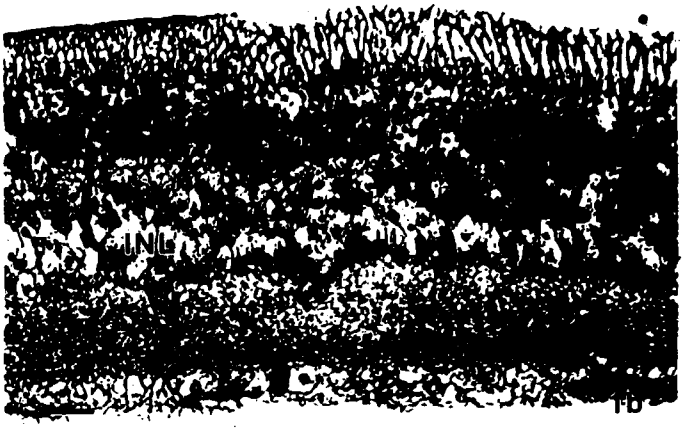

1b

1c

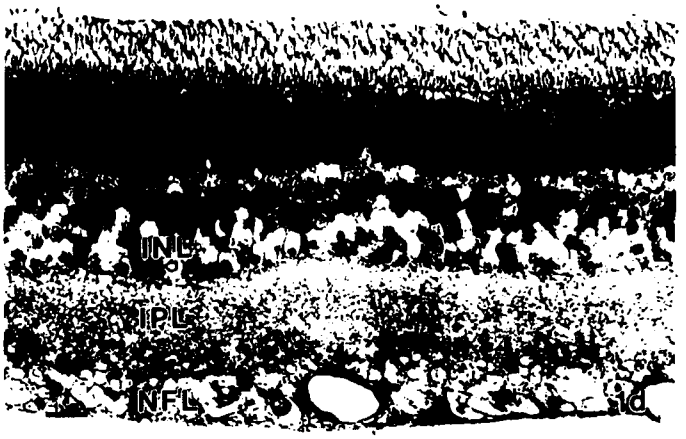

1d

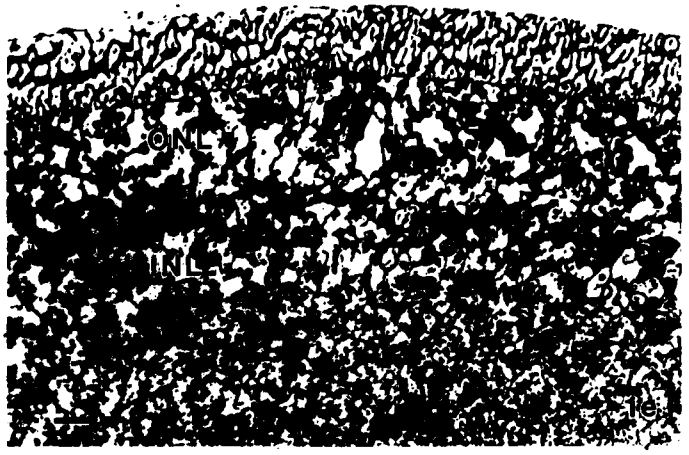

1e

1f

Table I

SURVIVING NUCLEI

	Incubation Condition				
	Control	Ischemia	5mM Glut	40mM KCl	A23187
1 min	144 ± 12	152 ± 31	159 ± 16	144 ± 7	150 ± 4
30 min	154 ± 18	157 ± 23	116 ± 4*	120 ± 8*	155 ± 8
120 min	132 ± 7	134 ± 11	99 ± 11*	107 ± 9*	118 ± 38
240 min	103 ± 12	111 ± 10	75 ± 6*	113 ± 8	109 ± 5
360 min	97 ± 7	106 ± 8	71 ± 8*	106 ± 3	113 ± 11

* Different from Control with $P \leq .05$.

Figure 2

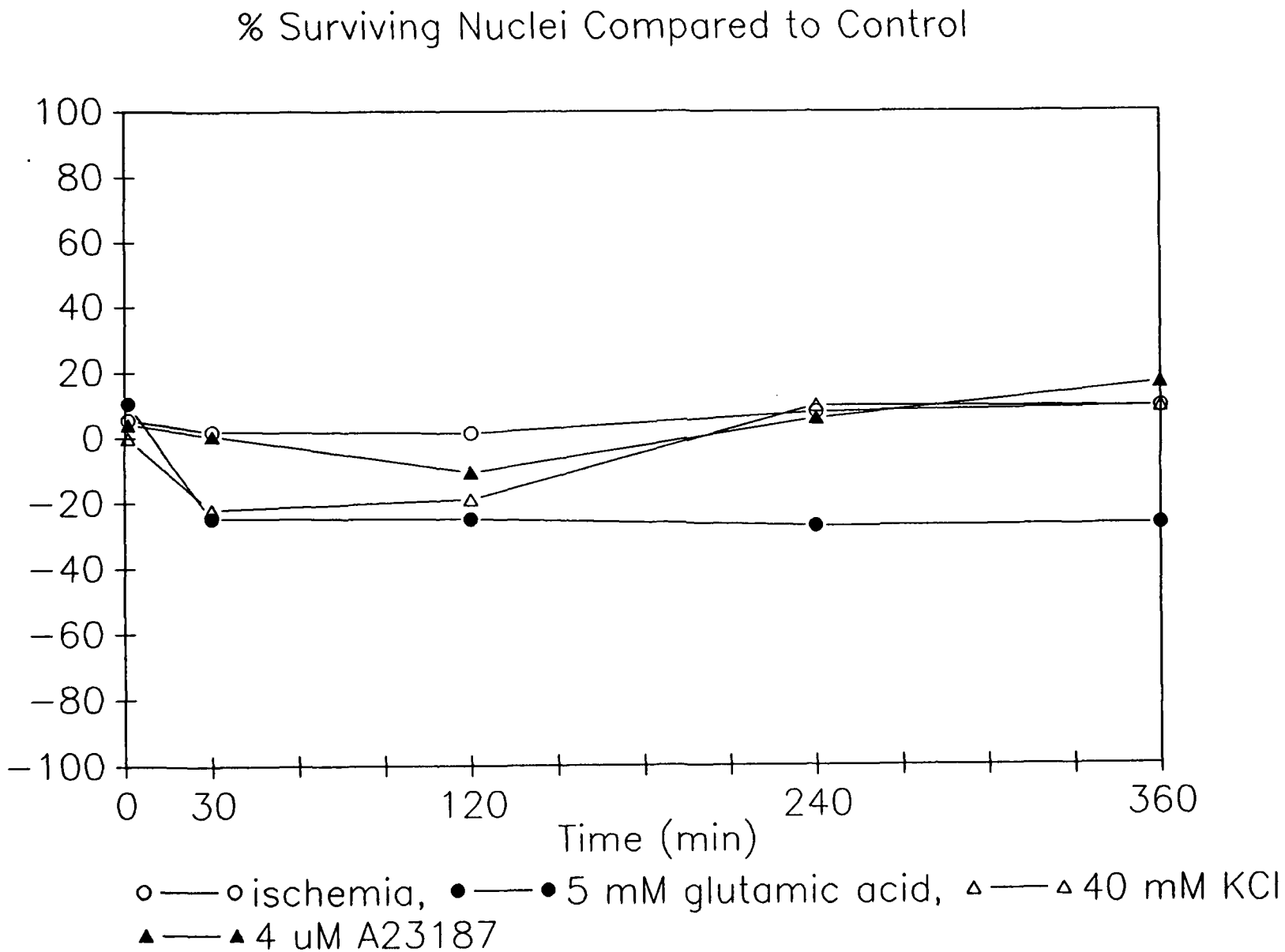
% Surviving Nuclei Compared to Control
100
80
60
40
20
0
−20
−40
−60
−80
−100
0
30
120
240
360
Time (min)
o—o ischemia, ●—● 5 mM glutamic acid, △—△ 40 mM KCl
▲—▲ 4 uM A23187

Figure 3a

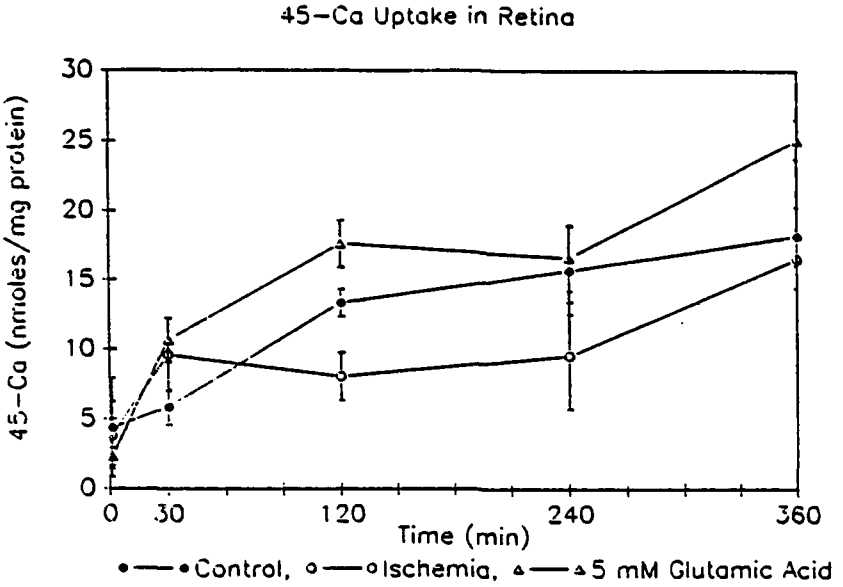

Figure 3b

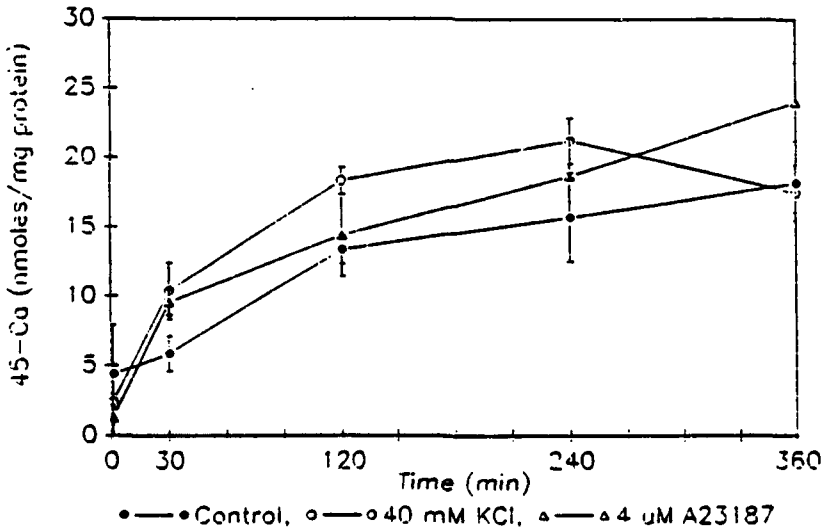

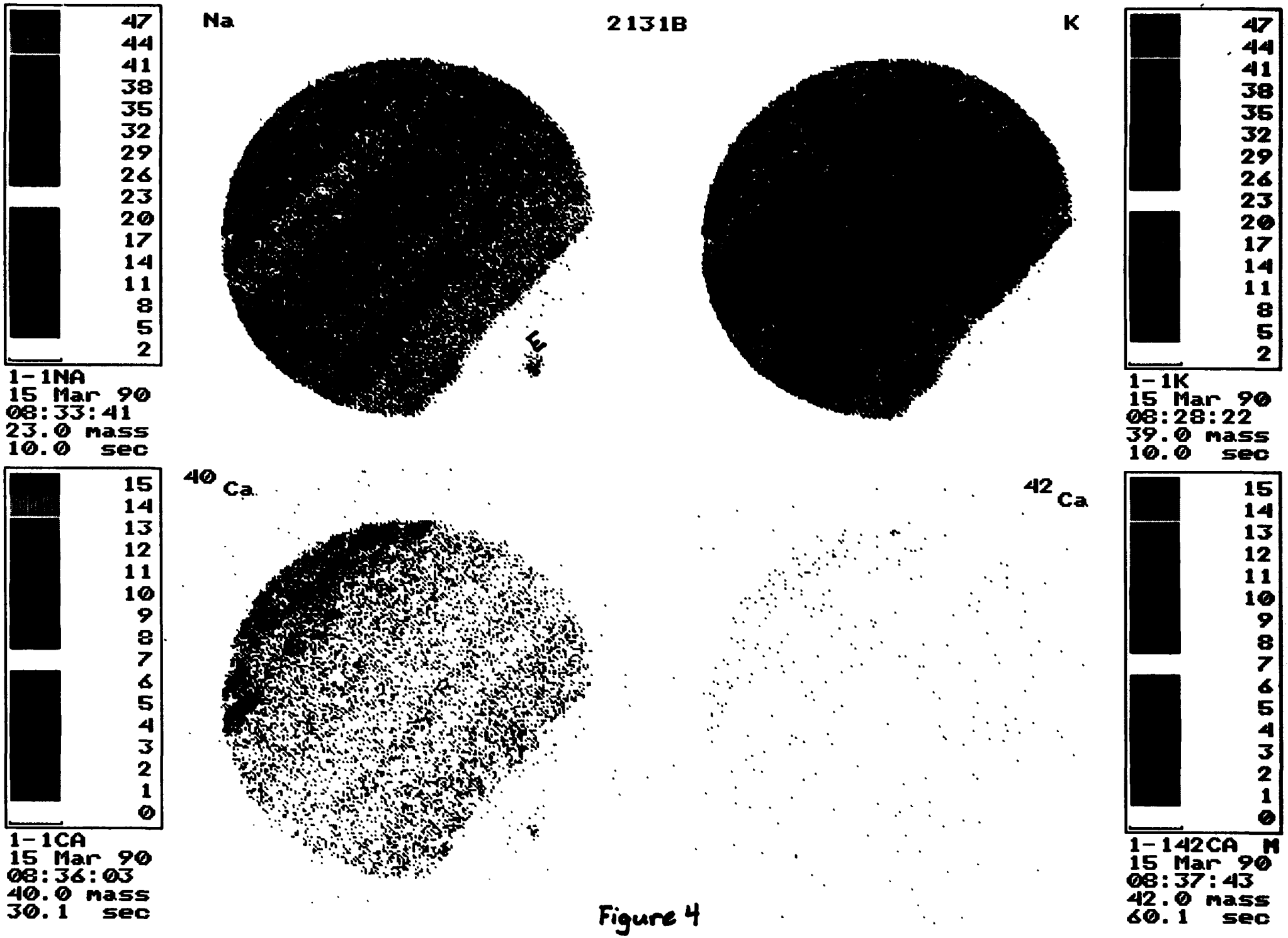
Na
2131B
K
47
44
41
38
35
32
29
26
23
20
17
14
11
8
5
2
1-1NA
15 Mar 90
08:33:41
23.0 mass
10.0 sec
1-1K
15 Mar 90
08:28:22
39.0 mass
10.0 sec
40 Ca
42 Ca
15
14
13
12
11
10
9
8
7
6
5
4
3
2
1
0
1-1CA
15 Mar 90
08:36:03
40.0 mass
30.1 sec
1-142CA M
15 Mar 90
08:37:43
42.0 mass
60.1 sec

Figure 4

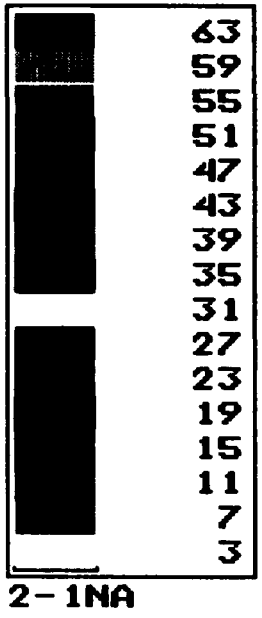

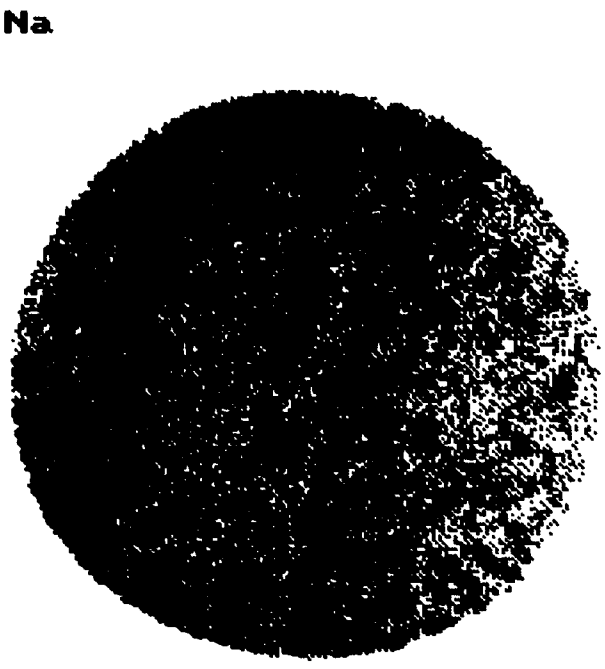

2429A

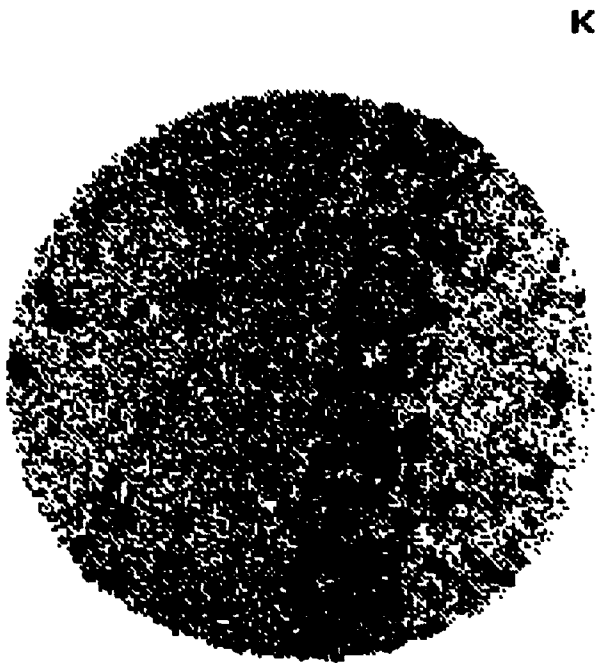

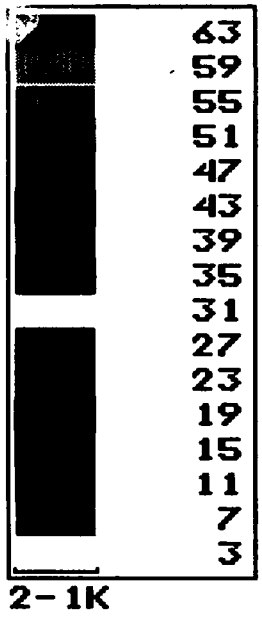

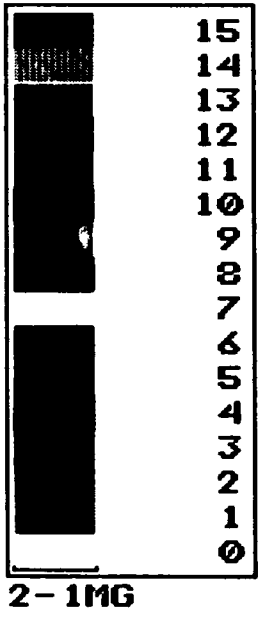

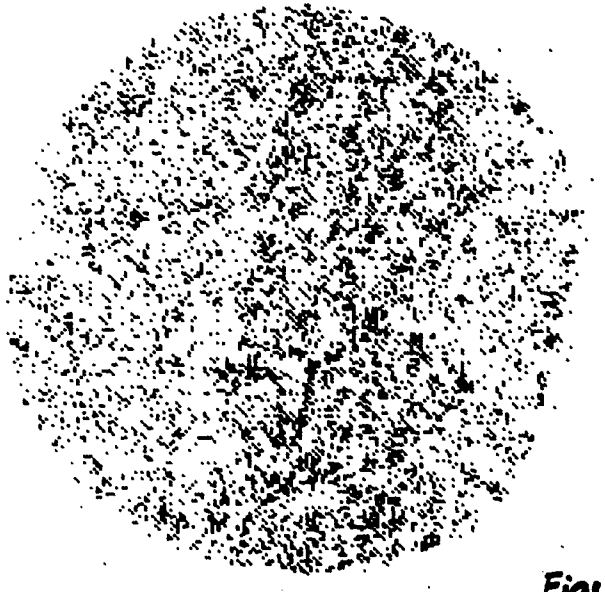

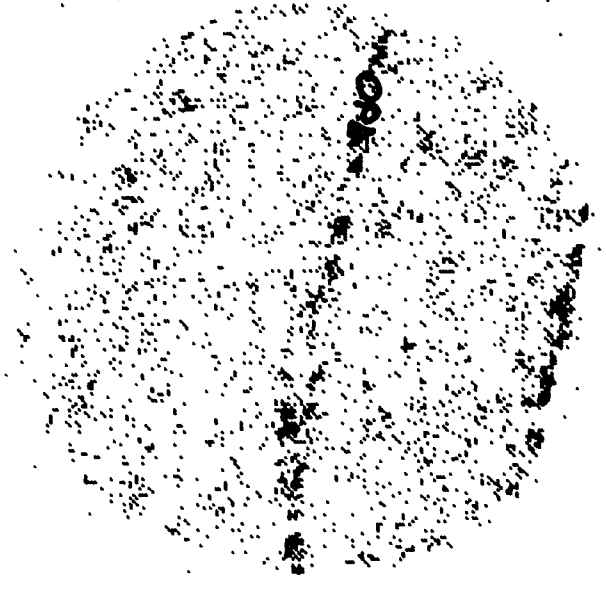

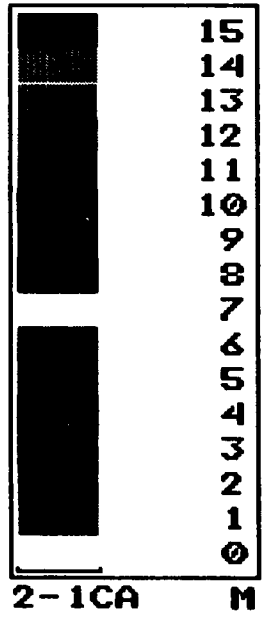

Figure 5

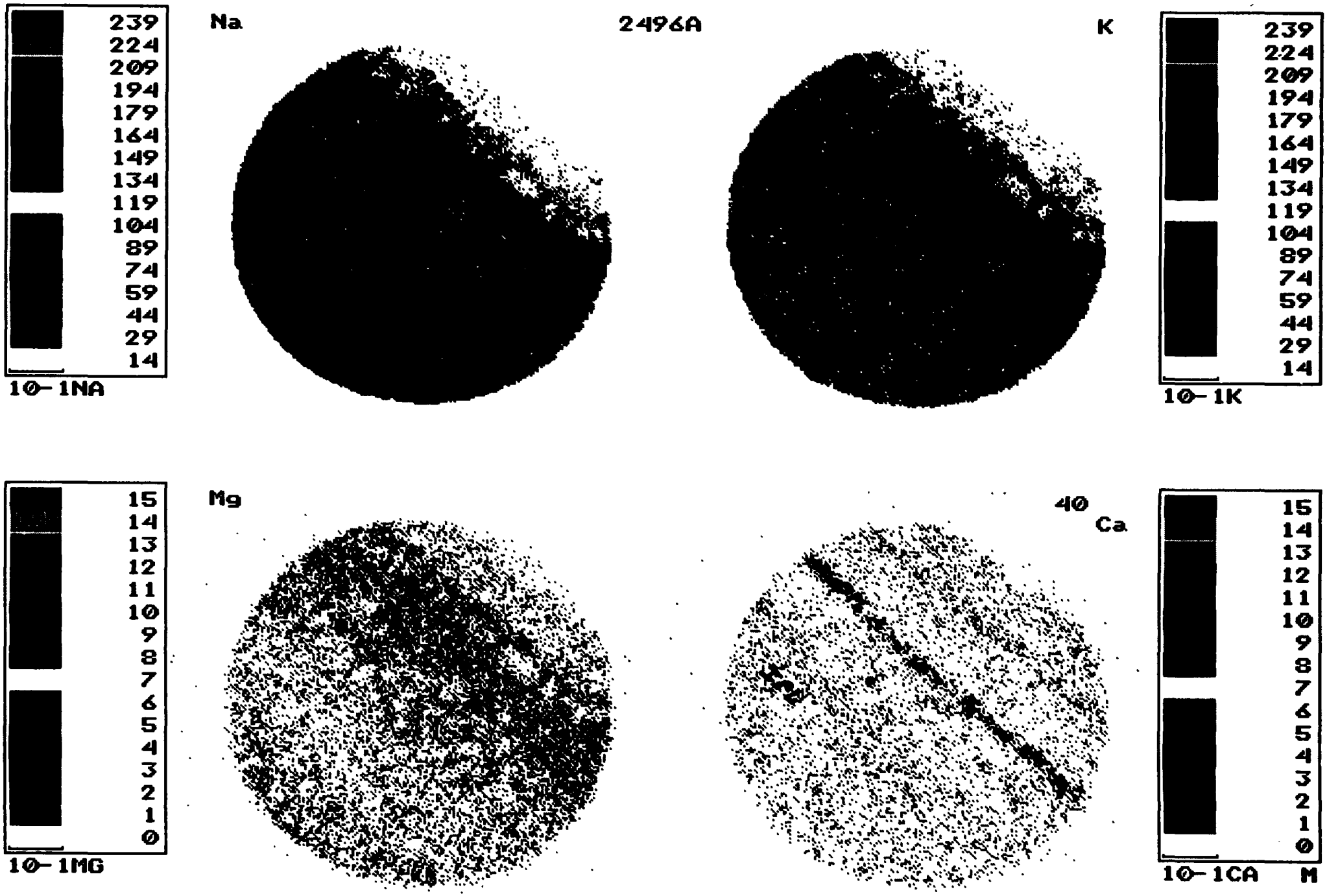
239
224
209
194
179
164
149
134
119
104
89
74
59
44
29
14
10-1NA
Na
2496A
K
239
224
209
194
179
164
149
134
119
104
89
74
59
44
29
14
10-1K
15
14
13
12
11
10
9
8
7
6
5
4
3
2
1
0
10-1MG
Mg
40
Ca
15
14
13
12
11
10
9
8
7
6
5
4
3
2
1
0
10-1CA
M

Figure 6

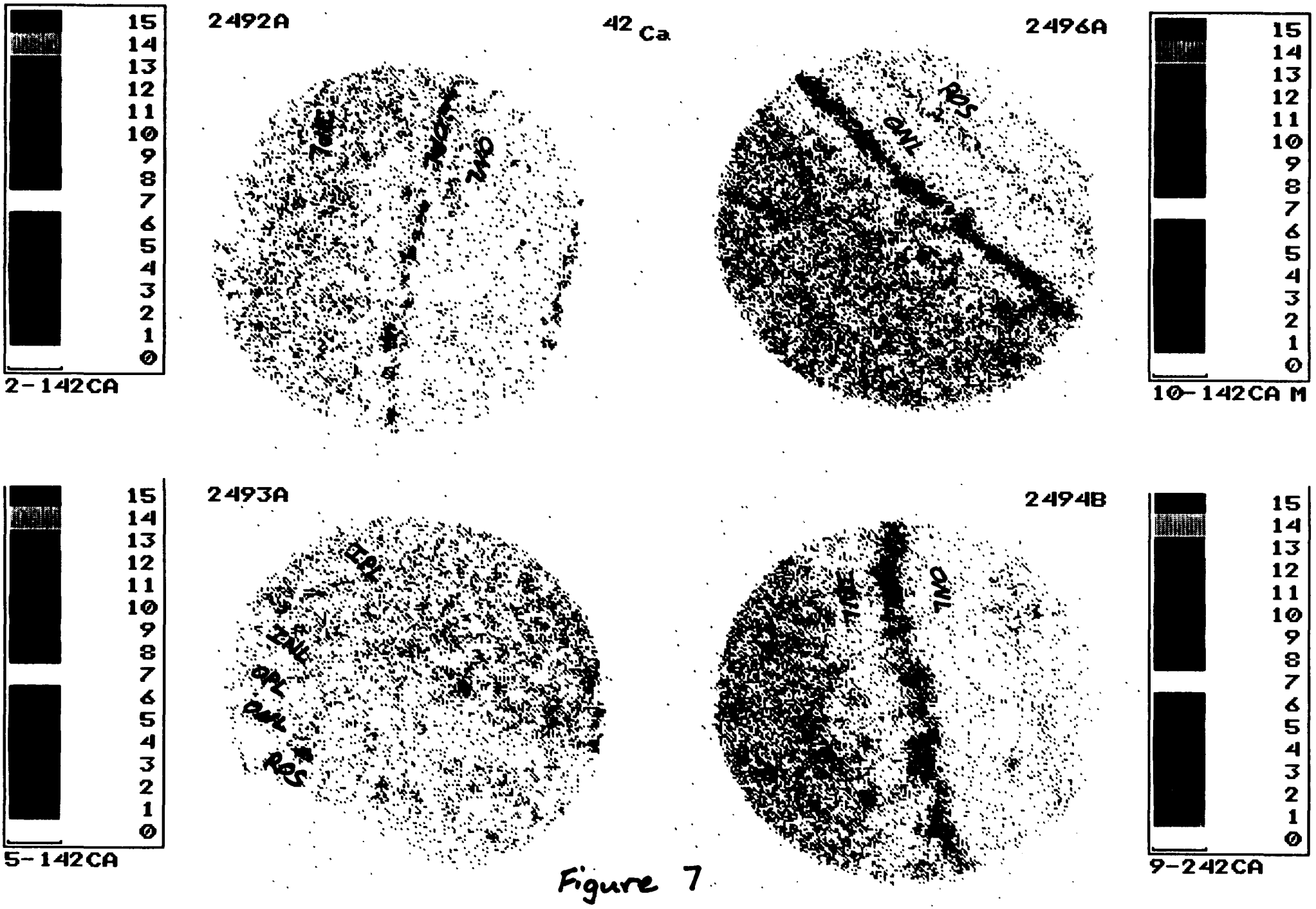
2492A
42 Ca
2496A
15
14
13
12
11
10
9
8
7
6
5
4
3
2
1
0
2-142CA
10-142CA M
2493A
2494B
5-142CA
9-242CA

Figure 7

Figure 8

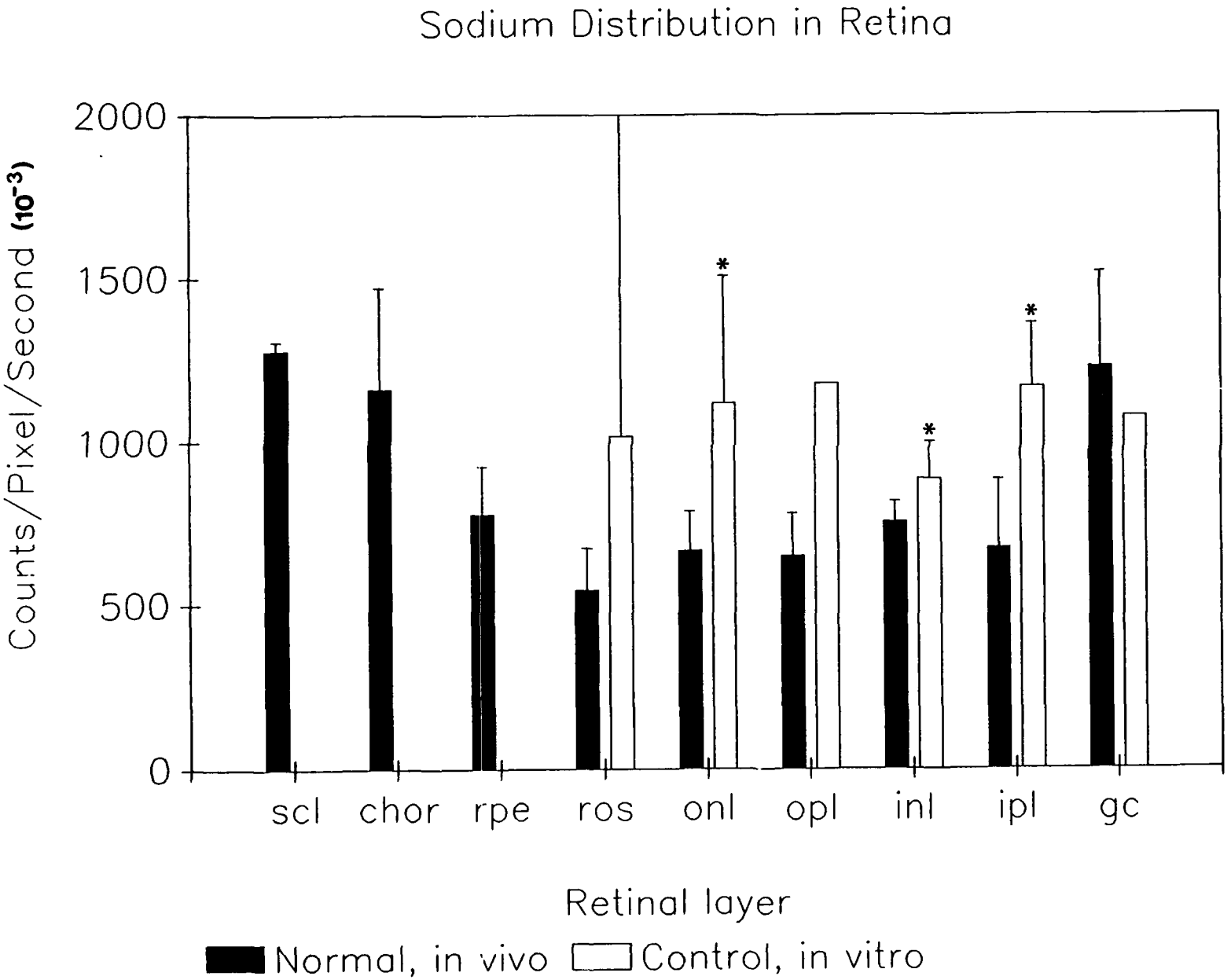
Sodium Distribution in Retina
Counts/Pixel/Second (10^-3)
2000
1500
1000
500
0
*
*
*
scl
chor
rpe
ros
onl
opl
inl
ipl
gc
Retinal layer
Normal, in vivo
Control, in vitro

Figure 9

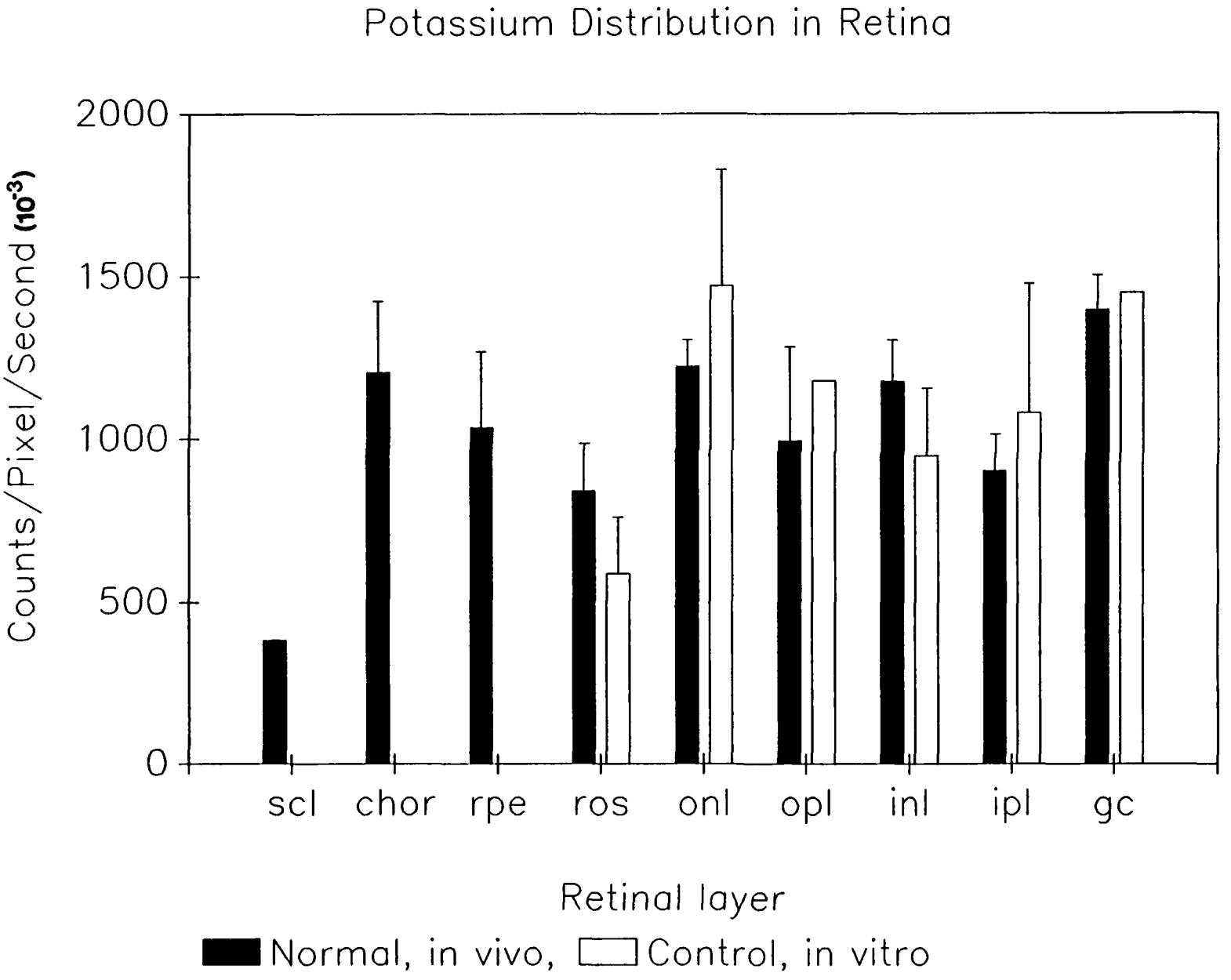
Potassium Distribution in Retina
2000
1500
1000
500
0
Counts/Pixel/Second (10^{-3})
scl
chor
rpe
ros
onl
opl
inl
ipl
gc
Retinal layer
Normal, in vivo,
Control, in vitro

Figure 10

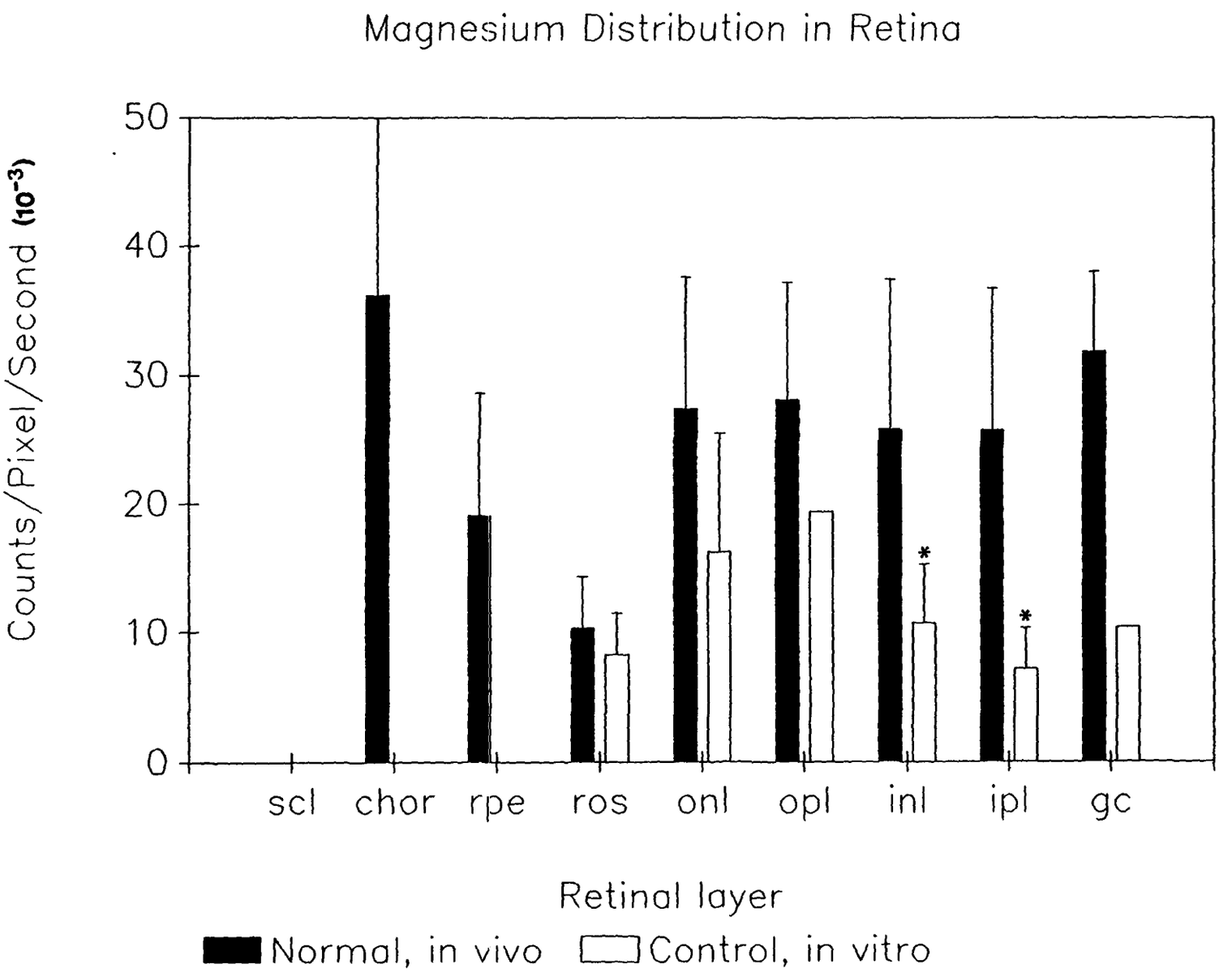
Magnesium Distribution in Retina
Counts/Pixel/Second (10^{-3})
50
40
30
20
10
0
scl
chor
rpe
ros
onl
opl
inl
ipl
gc
*
*
Retinal layer
Normal, in vivo
Control, in vitro

Figure 11

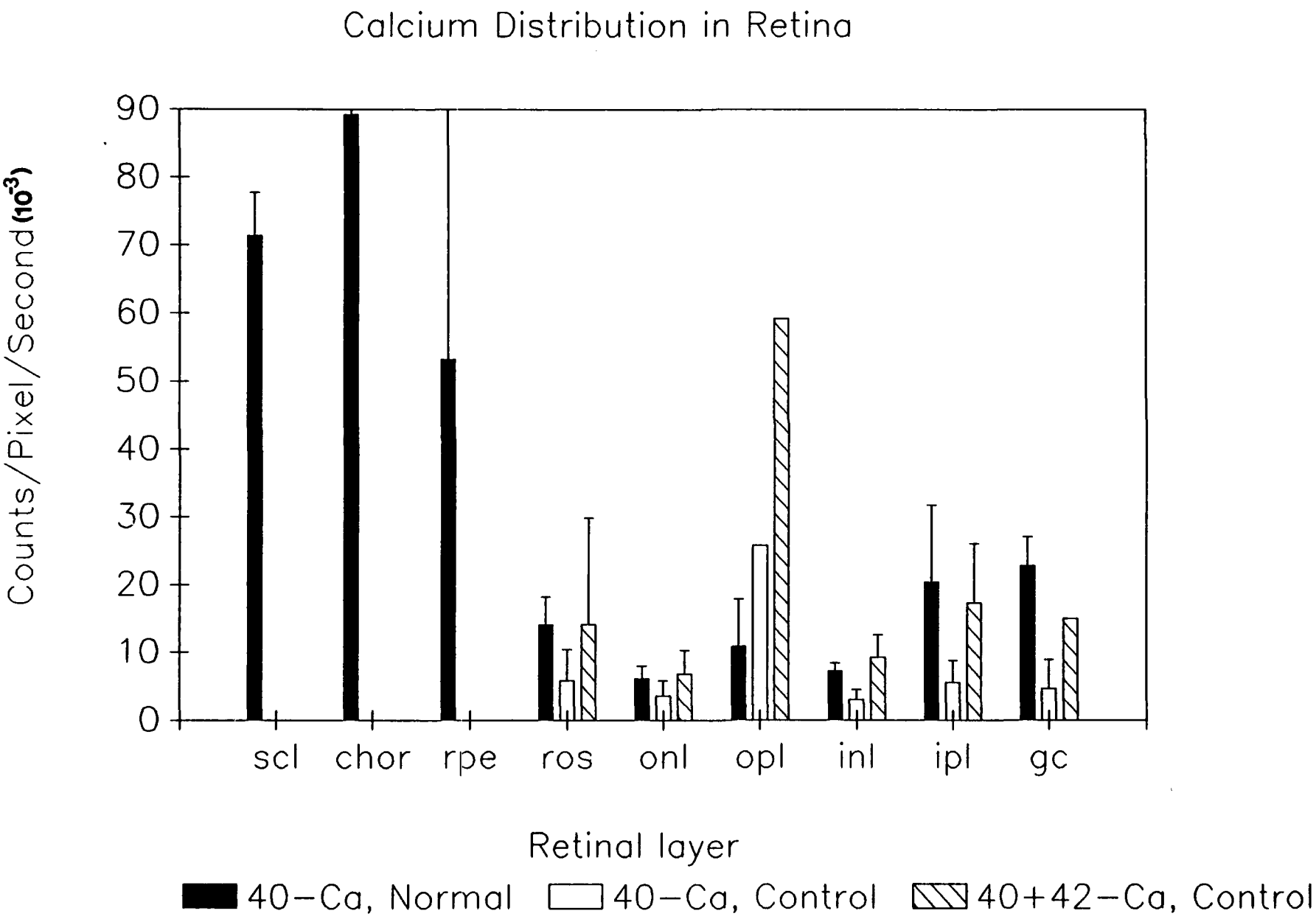
Calcium Distribution in Retina
Counts/Pixel/Second (10^{-3})
90
80
70
60
50
40
30
20
10
0
scl
chor
rpe
ros
onl
opl
inl
ipl
gc
Retinal layer
40−Ca, Normal
40−Ca, Control
40+42−Ca, Control

Figure 12

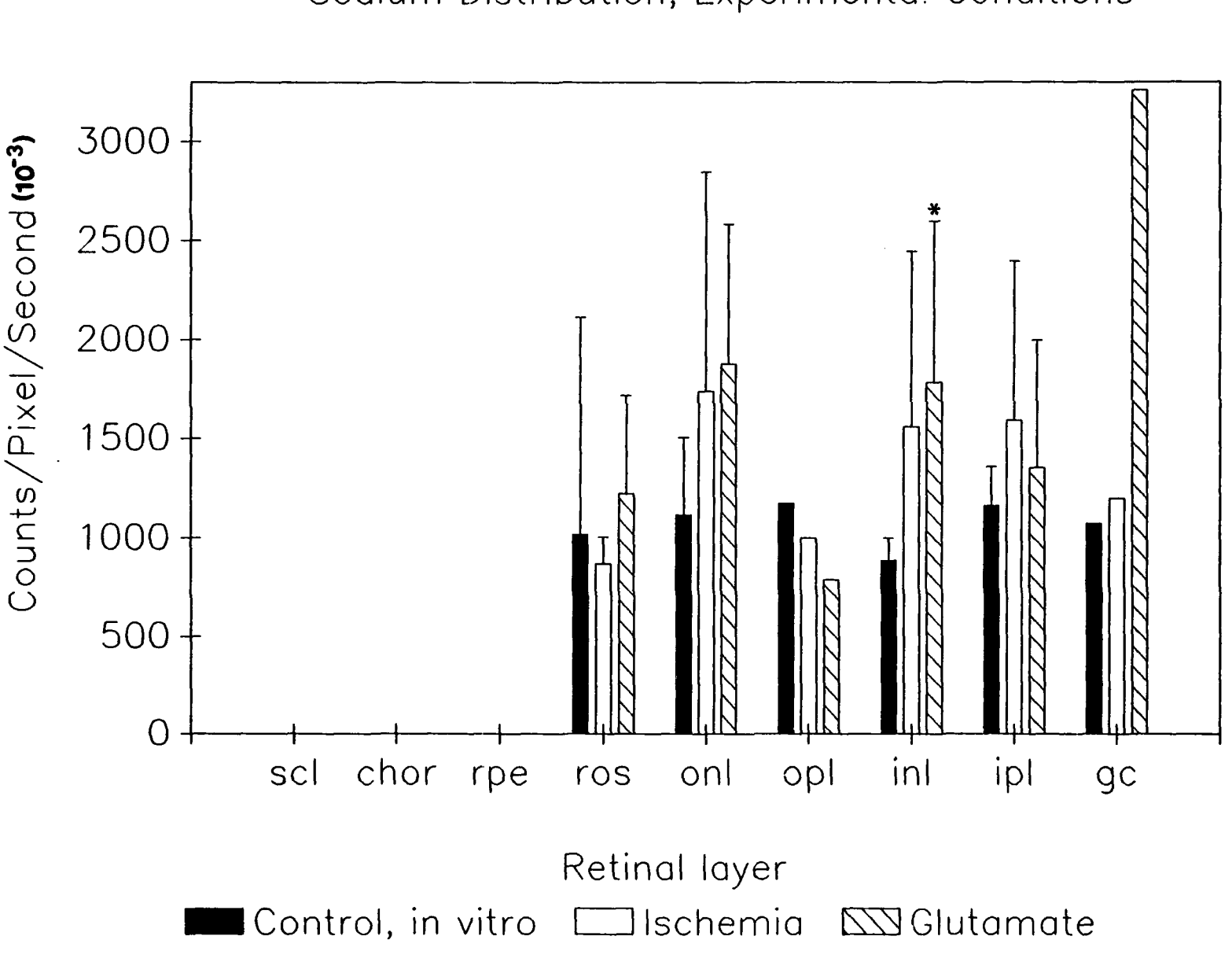
Sodium Distribution, Experimental Conditions
Counts/Pixel/Second (10-3)
3000
2500
2000
1500
1000
500
0
*
scl
chor
rpe
ros
onl
opl
inl
ipl
gc
Retinal layer
Control, in vitro
Ischemia
Glutamate

Figure 13

Potassium Distribution, Experimental Conditions

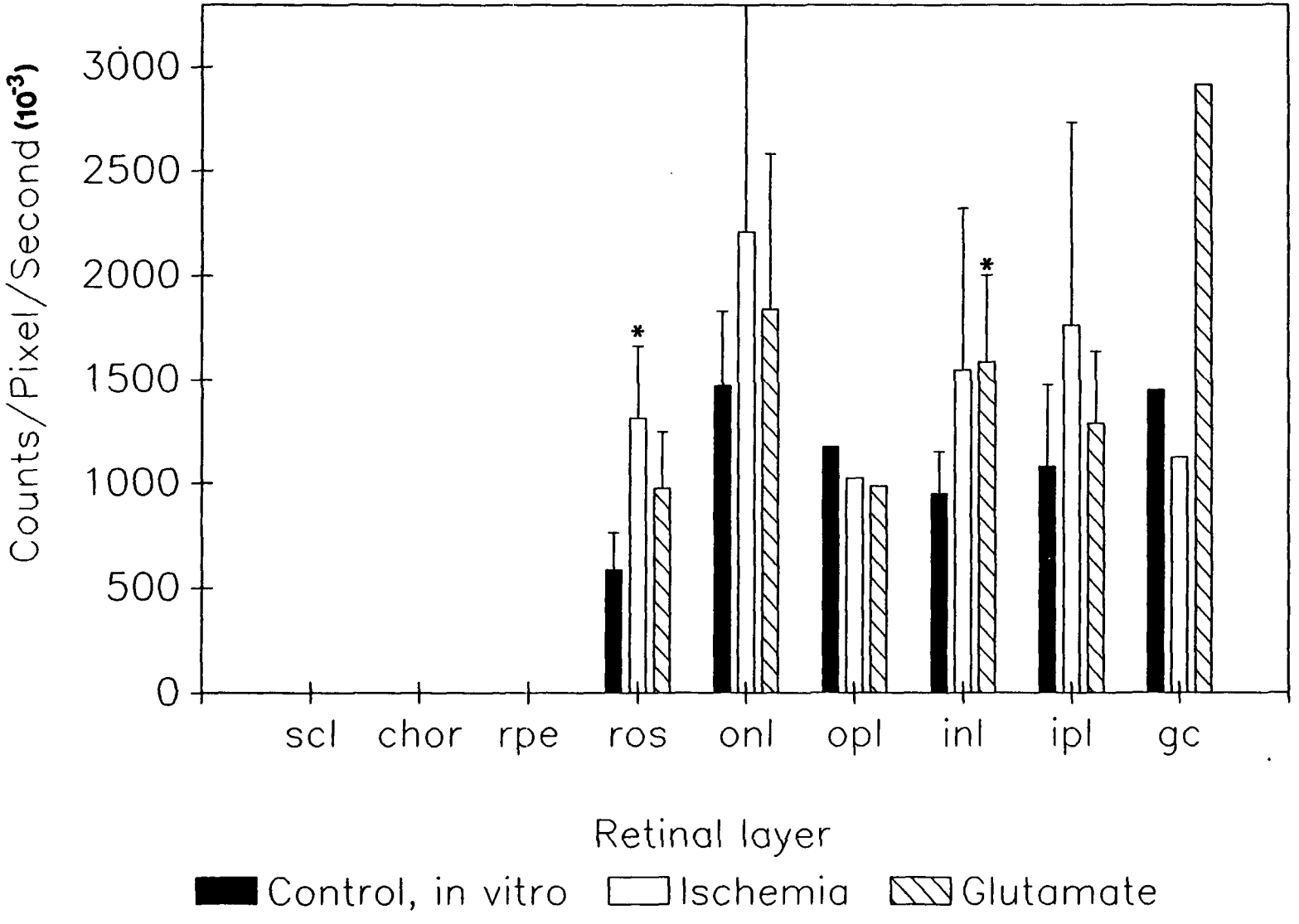

Figure 14

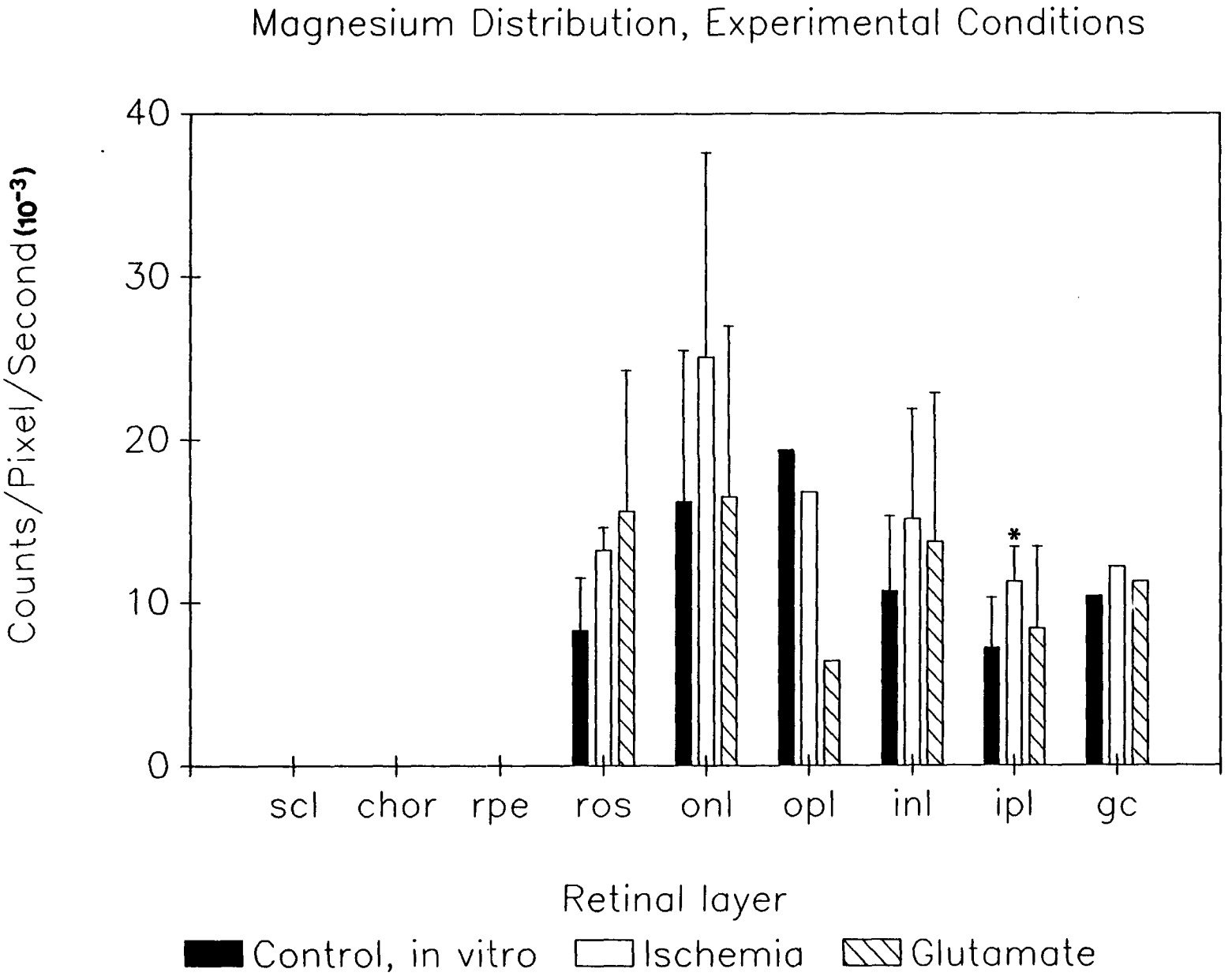
Magnesium Distribution, Experimental Conditions
Counts/Pixel/Second (10⁻³)
40
30
20
10
0
scl
chor
rpe
ros
onl
opl
inl
ipl
gc
*
Retinal layer
Control, in vitro
Ischemia
Glutamate

Figure 15

40–Calcium Distribution, Experimental Conditions

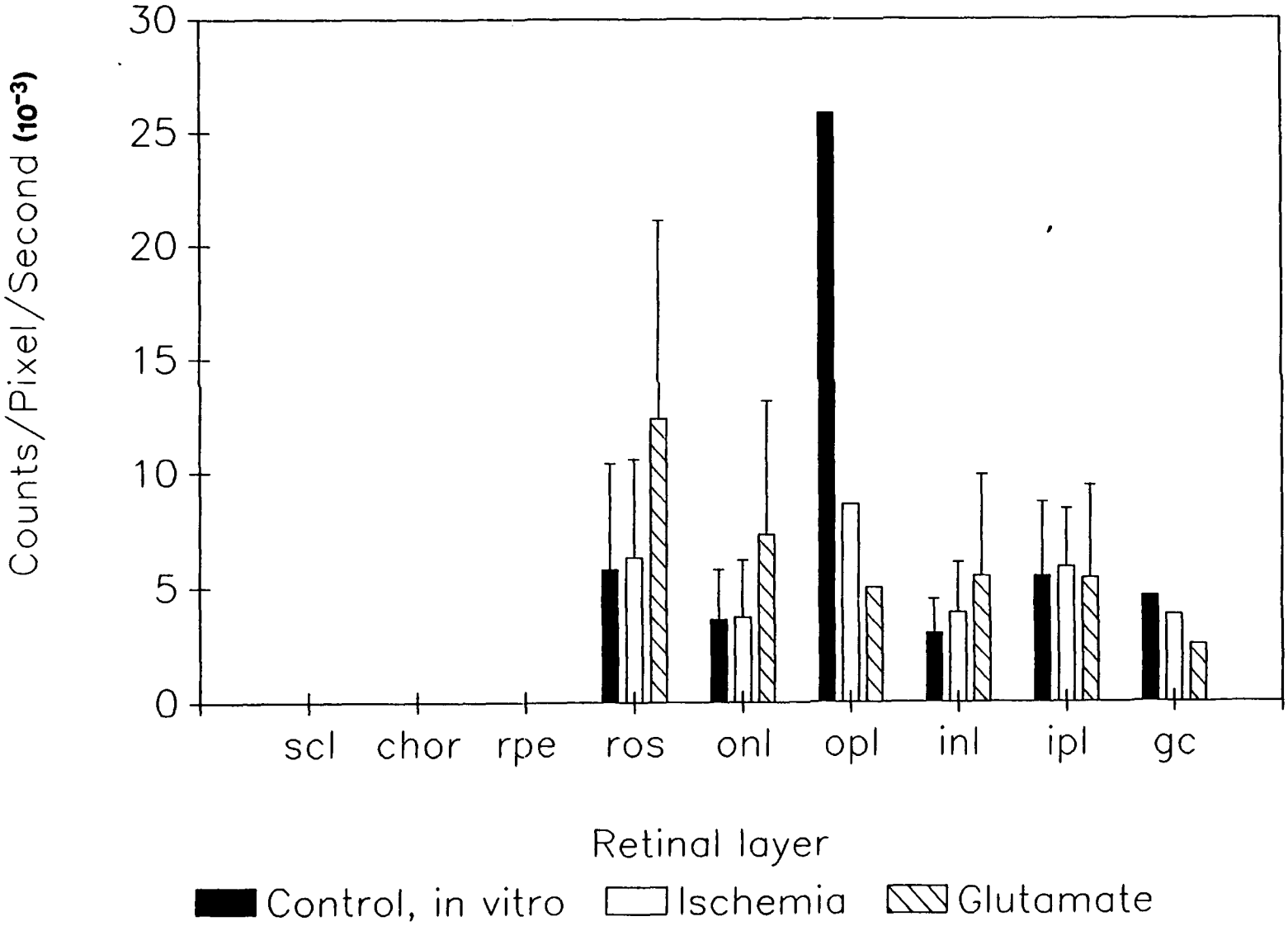

Figure 16

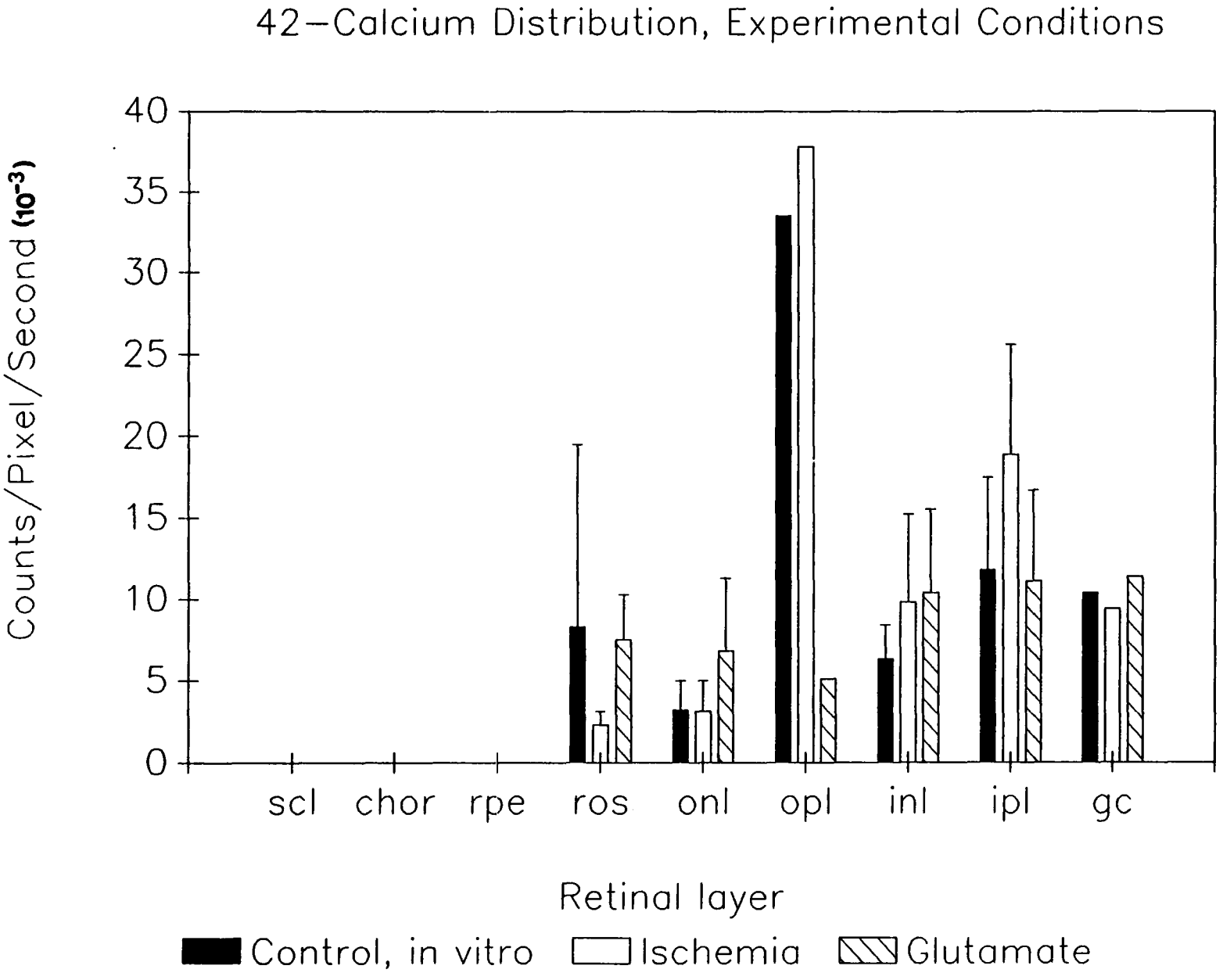
42–Calcium Distribution, Experimental Conditions
Counts/Pixel/Second (10^{-3})
40
35
30
25
20
15
10
5
0
scl
chor
rpe
ros
onl
opl
inl
ipl
gc
Retinal layer
Control, in vitro
Ischemia
Glutamate

Table II

Ion Counts in Retinal Layers

counts/pixel/second ($x10^{-3}$)

		Control				40 mM KCl				4 μM A23187			
Na	ROS	1017.9	±	1096.6	(3)	808.3	±	211.0	(4)	1079.0	±	380.8	(3)
	ONL	1119.1	±	387.4	(5)	1977.9	±	382.7	(4)*	2120.6	±	539.1	(3)*
	OPL	1178.5	±		(2)								
	INL	888.0	±	113.0	(5)	1837.0	±	744.5	(4)*	1733.5	±	365.0	(3)*
	IPL	1166.0	±	194.2	(5)	1383.5	±	740.0	(4)	2132.8	±	703.8	(3)
	GC	1076.3	±		(2)								
K	ROS	587.5	±	177.8	(3)	960.9	±	307.8	(4)	1568.3	±	594.1	(3)
	ONL	1473.1	±	354.6	(5)	2691.8	±	1018.0	(4)	3186.4	±	618.8	(3)*
	OPL	1178.5	±		(2)								
	INL	950.0	±	205.3	(5)	1797.6	±	935.5	(4)	2362.7	±	738.0	(3)*
	IPL	1080.5	±	397.6	(5)	1577.0	±	693.3	(4)	2474.0	±	462.8	(3)*
	GC	1450.8	±		(2)								
Mg	ROS	8.3	±	3.2	(3)	22.7	±	9.4	(4)*	18.9	±	2.4	(3)*
	ONL	16.2	±	9.3	(5)	48.1	±	12.6	(4)*	26.0	±	4.7	(3)
	OPL	19.4	±		(2)								
	INL	10.7	±	4.6	(5)	32.8	±	8.1	(4)*	19.6	±	9.0	(3)
	IPL	7.2	±	3.1	(5)	15.5	±	3.5	(4)*	15.8	±	4.2	(3)*
	GC	10.4	±		(2)								
^{40}Ca	ROS	5.8	±	4.6	(3)	13.5	±	3.4	(4)	7.6	±	1.1	(3)
	ONL	3.6	±	2.2	(5)	6.2	±	1.2	(4)	3.8	±	1.0	(3)
	OPL	25.8	±		(2)								
	INL	3.0	±	1.5	(5)	6.6	±	2.5	(4)*	5.0	±	1.2	(3)
	IPL	5.5	±	3.2	(5)	7.3	±	1.4	(4)	11.3	±	0.4	(3)*
	GC	4.6	±		(2)								
^{42}Ca	ROS	8.3	±	11.2	(3)	2.9	±	0.5	(4)	3.2	±	0.8	(3)
	ONL	3.2	±	1.8	(5)	4.4	±	1.5	(4)	1.7	±	0.5	(3)
	OPL	33.5	±		(2)								
	INL	6.3	±	2.1	(5)	19.3	±	2.2	(4)*	13.5	±	4.6	(3)
	IPL	11.8	±	5.7	(5)	27.0	±	5.5	(4)*	26.0	±	7.2	(3)*
	GC	10.4	±		(2)								

*Different from Control at $P \leq .05$.

SOCIETY FOR NEUROSCIENCE
1990 ABSTRACT FORM

Read all instructions before typing abstract.
See *Call for Abstracts* and reverse of this sheet.
Complete abstract and all boxes
at left and below before making copy.

____ **Check here if this is a REPLACEMENT of abstract submitted earlier. REMIT $25 for each replacement abstract. Replacement abstracts must be RECEIVED by MAY 11, 1990.**

First (Presenting) Author

Provide full name (no initials), address, and phone numbers *of first author on abstract. You may present only one abstract.*

Margaret Sue Burns
University of California, Davis
Department of Ophthalmology
1603 Alhambra Blvd.
Sacramento, CA 95816
Office: (916) 734-6590 Home: (916) 753-6956

SMALLEST RECOMMENDED TYPE SIZE: 10 POINT

SAMPLE:
1990 Annual Meeting
St. Louis, Missouri
October 28–November 2

DEADLINE FOR POSTMARKING:

MAY 1, 1990

Presentation Preference

Check one: [x] poster [ ] slide

Themes and Topics

See list of themes and topics. Indicate below a first and second choice appropriate for programming and publishing your paper.

1st theme title: Neurotran, Modul and Receptors theme letter: D
1st topic title Excitatory A.A.: excitotoxic. topic number: 44

2nd theme title: Disorders of the Nerv. Sys. theme letter: J
2nd topic title Ischemia
topic number: 136

Special Requests (e.g., projection requirements)

Include nonrefundable ABSTRACT HANDLING FEE of $25 payable to the Society for Neuroscience, DRAWN ON A U.S. BANK IN U.S. DOLLARS ONLY.

CALCIUM LOCALIZATION IN RETINA IN GLUTAMATE TOXICITY AND ISCHEMIA IN VITRO. M.S. Burns and C.M. Panattoni*, Ophthalmology Research Laboratories, UCDavis, Davis, CA 95616.

Increased intracellular calcium (Ca_i^{2+}) is thought to be a mechanism of toxic cell death in both neural and non-neural cells. Increases in Ca_i^{2+} can arise from redistribution of intracellular Ca and/or influx from extracellular calcium. To test if extracellular Ca influx occurs in retinal cell toxicity, and to localize exogenous Ca influx, we incubated retinas in the stable isotope, ^{42}Ca, and imaged total Ca content in retinal cell layers using Secondary Ion Mass Spectrometry (SIMS).

Rat retinas were incubated in modified Ames' medium for up to 6 hours under normal conditions or 5 mM glutamate or ischemia (100% N_2) and then prepared for SIMS analysis by low temperature freeze drying. Electrolyte localizations were compared to non-incubated control retinas.

Approximately 35% of the total retinal Ca was exchanged for ^{42}Ca in 6 hours of normal incubation conditions. The tracer was equally distributed in all retinal layers. With glutamate incubation, 50% of the endogenous total Ca content was lost from the inner plexiform layer (IPL), but little loss was seen in other retinal layers. Exogenous ^{42}Ca uptake occurred in all layers, but was greater in the inner nuclear (INL) and IPL. In ischemia, total retinal Ca loss was seen in all areas, but uptake occurred predominantly in the INL and IPL. Cell death in the INL was greatest in the glutamate treated retinas. Cell death under ischemic conditions was similar to normal incubation.

These results indicate that there is influx of exogenous Ca into retinas made toxic by either glutamate or ischemia, and there is preferential localization in the layer comprised by amacrine and bipolar cell synaptic processes and glial (Müller) cell processes.

Sponsored by the Office of Naval Research.

Do not type on or past blue lines (printers' cut lines) Dimensions of Abstract Form 4 ½" × 4 ¾"

KEY WORDS: (see instructions pg. 4)

1. Ion Mass Spectrometry
2. Electrolyte
3. Rat
4. _____

Signature of Society for Neuroscience member required below. ***No member may sign more than one abstract.***
The signing member must be an author on the paper.

The signing member certifies that any work with human or animal subjects related in this abstract complies with the guiding principles for experimental procedures endorsed by the Society.

Margaret S Burns — Society for Neuroscience member's signature
Margaret S Burns — Printed or typed name
916 734-6590 — Telephone number

Preprint Invest. Ophthal. Vis. Sci. 89-137RR

INTER-GLIAL CELL GAP JUNCTIONS INCREASE IN

URETHANE-INDUCED PHOTORECEPTOR DEGENERATION IN RATS

Margaret S. Burns, Ph.D. and Nancy K. Tyler, Ph.D.

Department of Ophthalmology, School of Medicine, University of California, Davis, CA 95616, U.S.A.

Short Title: Gap Junctions in Photoreceptor Degeneration

Author to whom correspondence should be directed:

Margaret S. Burns, Ph.D.
Department of Ophthalmology
School of Medicine
University of California, Davis
1603 Alhambra Boulevard
Sacramento, CA 95816

Acknowledgement of financial support:

This study was supported by grants from the National Eye Institute (EY 05979), the Office of Naval Research, and Research to Prevent Blindness, Inc., NY.

ABSTRACT

Gap junctions are found between astrocytes in the inner retina of normal rats, but are rare between Müller cells or between astrocytes and Müller cells in the inner retina. Following photoreceptor degeneration induced by urethane treatment of newborn animals, morphological alterations of glial cells occur in the inner retina. The Müller cells withdraw from the inner limiting membrane and the astrocytes hypertrophy and occupy the vitread surface of the inner limiting membrane. The frequency and size of the gap junctions between astrocytes increases with time in rats with urethane induced photoreceptor degeneration, more than expected from elaboration of additional astrocyte plasma membrane. The gap junction profile length per glial cell membrane contact length is 2.8 +/- 1.1 μm/1000 μm membrane in 8 week old normal animals and increases to 18.9 +/- 9.4 μm/1000 μm membrane at 56 weeks of age in urethane treated animals. The average size of the gap junction profile length doubles during this same period. This is the first study demonstrating pathological changes in gap junctions in central nervous system tissue. We speculate that this up-regulation of gap junctions occurs in response to an altered extracellular ionic composition in an attempt to increase the lateral spatial buffering of K^+ by these cells. The relative location of glial cells in retina can determine, in part, the vulnerability of the retina to edema.

INTRODUCTION

The retinal vasculature has an intimate relationship with retinal neurons and glia in normal and pathological responses.[1,2] Glial investment of the retinal vasculature is an important facet of its ultrastructure[3] but the physiological functions[5] of the perivascular glia is not known. Three types of glial cells - Müller cells, astrocytes and microglia - have been identified in retina and each has a relationship with the retinal vasculature.[4-6]

The radial Müller fibers are considered to be analogous to glioependymal cells in brain and are distributed throughout the retina, with the exception of the optic nerve head and fovea.[7] Fine processes of Müller cells invest both large vessels and capillaries in the inner and outer retinal vessel beds.[3] Morphological and functional polarity is exhibited by the Müller cell in that the Müller "end-feet" processes lining the vitreous have the highest concentration of mitochondria and potassium channels, facilitating removal of K^+ from the extracellular space into the vitreous.[3,8,9] Spatial buffering of K^+ by these cells could be extended over large areas if the Müller cells were coupled by communicating junctions.

Gap junctions are communicating junctions visible ultrastructurally as a heptalaminar array of apposed cell membranes with a discrete intercellular "gap" of 2 nm. They function to electrically couple the cells involved through low resistance pathways capable of transmitting ions and small molecules up to 1200 daltons in size.[10] Gap junctions between Müller cells at the external limiting membrane have been reported in some

vertebrates such as newt, frog, fish, mudpuppy and toad.[11-15] Gap junctions have not been found between Müller cells in cat, rat, rabbit, opossum, pigeon, turtle, eel and shark[13] using ultrastructural criteria. Electrophysiologically, Müller cells of turtle retina were found to be coupled in situ.[16] Using freeze-fracture techniques, Reale et al.,[17] reported gap junctions between Müller cells close to the inner limiting membrane in human retina.

Astrocytes have a distribution in retina which can be ubiquitous or highly restricted, depending upon the extent of retinal vascularization.[6,18,19] They invest inner, but not outer, retinal vessels in the holangiotic retina and are the only type of glial cell within the non-myelinated portion of the optic nerve.[7] Astrocytes from the optic nerve of salamanders have high K^+ conductance in their endfeet processes which abut on vessels.[20] Inter-astrocytic gap junctions are a frequent observation in brain astrocytes.[21,22] In retina, Quigley described gap junctions between optic nerve head astrocytes in man and monkey.[23] Büssow[7] demonstrated gap junctions between optic nerve head astrocytes in cat and monkey and discussed the existence of such junctions between retinal astrocytes, but not Müller cells.

The microglial cells of the retina are considered to be of mesodermal origin, possibly arising from vascular pericyte cells.[5] Credence is given to this hypothesis by findings of similar enzyme histochemical staining of microglial cells and the retinal vascular cells which are known to be of mesodermal origin.[24] The presence of a

macrophage specific antigen on microglia in mouse retina also supports a mesodermal origin of these cells.[25] Although gap junctions between microglia have not been demonstrated, Boycott and Hopkins[26] raised the possibility that the gap junctions reported by Reale, et al.,[17] were not between Müller cells, but rather, inner retinal glia, possibly microglia.

During the course of our studies of the cell-cell interrelationships in rat retina undergoing urethane-induced photoreceptor degeneration[27] we noticed prominent gap junctions between glial cells at the inner limiting membrane. This observation prompted us to perform a morphometric study of glial cells and gap junctions in normal and pathologic rat retina to ascertain the types of cells involved and the extent of cell coupling.

MATERIALS AND METHODS

Production of Urethane Retinopathy

Urethane retinopathy was produced in newborn Long-Evans rats as previously described.[27,28] We have adhered to the principles of the ARVO resolution on the Use of Animals in Research. Briefly, newborn rat pups were injected subcutaneously on Day 1, followed by seven weekly injections with urethane (ethyl carbamate, Aldrich Chemical Co.) in phosphate buffered saline (PBS) at a dose of 1 mg/gm body weight. Control animals were injected with the same volume of PBS. The rats were maintained under standard laboratory conditions with room light at 20 to 30 foot-candles on a 12 hour light (beginning at 7 am), 12 hour dark cycle until the time of sacrifice. Sacrifice was performed after 9:00 am to avoid the peak light-induced phagocytosis of rod outer segment discs. Five urethane and three control animals were sacrificed at age 8, 16 and 24 weeks. Tissue specimens from animals 56 weeks of age were available from earlier studies,[28] although no control animals of this age were available.

Preparation of Tissues

Following an overdose of sodium pentobarbital, the 12 o'clock limbal position was marked with a 6-0 silk suture, both eyes were rapidly enucleated, immersed for approximately 20 minutes in 3.0% glutaraldehyde in 0.1 M phosphate buffer at pH 7.4

and then the cornea and lens removed to facilitate fixative diffusion to the retina. Fixation continued until the next day, when the eye cups were rinsed with buffer, postfixed with osmium, dehydrated in a standard series of ethanol and propylene oxide and embedded in Polybed 812 (Polysciences, Inc.). The posterior eye cups were hemisected from 12 to 6 o'clock and oriented at embeddment so that light microscopic sections of the entire half eye cup could be made.

Microscopy and Morphometry

Light microscopic sections (1 to 2 μm) were cut with a glass knife on a Sorvall MT2B and stained with Toluidine Blue and Azure II in borax. The central half of the retina was cut into a superior and inferior portion and remounted for electron microscopy. Ultrathin sections were cut on a Reichert OmU3 ultramicrotome, placed on 200 mesh copper/palladium grids, stained with lead citrate and uranyl acetate and examined in a Philips 410 electron microscope.

For morphometric measurements, a grid window that had inner retina across the entire window, with no folds or other artifacts apparent, was randomly selected at very low magnification (1700 x). A montage of the inner retinal edge was made at 6900x. Preliminary experiments had shown that gap junctions were readily recognizable and could be accurately measured at this magnification. Depending upon the orientation of the retina relative to the grid window, 7 to 9 films covered the inner retinal edge. One

grid window from each of two grids was photographed for each animal. One grid was from the superior central retina and the other from the inferior central retina. There is no reason to think these two regions are different, since the retinopathy develops from central to peripheral regions[28] and we have controlled for selective light damage to the superior retina[29] in this experiment. The films were printed at approximately 2.6 x magnification (each set of films was measured independently and ranged from 2.55 to 2.63 x).

Since preliminary observations indicated that gap junctions exist only close to the inner retinal edge, we limited our area of examination to the 3 micrometers of retina closest to the inner limiting membrane. This area was defined on the photograph and all non-glial structures (such as ganglion cells, ganglion cell axons and blood vessels) within the area were excluded from measurement. Measurements of area, length of inner limiting membrane (ILM), length of gap junctions (GJ) and total glial membrane contact length were made using a Summagraphics Summasketch MM1201 attached to an IBM PC AT clone computer. The total glial membrane contact length included only those glial cell membranes that were adjacent to another glial cell membrane, since our initial observations had indicated that the gap junctions were formed only between glial cells. Thus, the glial cell membrane facing a nerve fiber bundle and the innermost plasma membrane facing the vitreous were not included in total glial cell membrane contact length. Statistical analysis of the data was performed by a one way analysis of variance (ANOVA). Tables I, II and III indicate that the sample size was the same in all groups.

RESULTS

Urethane Retinopathy

Urethane retinopathy (UR) is a primary degeneration of photoreceptor cells which follows the developmental pattern of these cells from central to peripheral retina.[27] By 8 weeks, no photoreceptor outer segments are apparent in the central retina and, by 24 weeks, few photoreceptor nuclei remain in the outer retina (Figure 1). The retinal pigment epithelium (RPE), choriocapillaris (CC) and inner plexiform layer (IPL) are not affected as a primary process in this photoreceptor degeneration.[27] Even at 24 weeks of age, the number of vessel profiles observed in the nerve fiber layer (NFL) is not different from normal.[30]

Inner Retina, Control Animals

In the control animals of all ages studied, the innermost aspect of the retina is formed primarily by the "end-feet" of the Müller cells, with their characteristic complement of mitochondria and smooth endoplasmic reticulum (SER). The organelles within the Müller cell are compartmentalized as seen, for example, in the bundles of intermediate filaments (IF), which are apparent at the level of the nerve fiber layer (Figure 2a).[9] Thick Müller endfeet processes appear to spread laterally and form most,

but not all, of the interface between the axons of the nerve fiber layer and the inner limiting membrane (Figure 2b).

Astrocytes are present within the innermost 3 micrometers of the retina, but are not particularly numerous. They are recognizable as relatively fine processes in the vicinity of the nerve fiber bundles and around retinal vessels in the inner retina (Figure 2c). In the control animals of all ages, these processes correspond to the protoplasmic astrocyte as described by Hogan and Feeney[3] and Büssow.[7] The processes tend to be electron lucent, and have a complement of IF placed sporadically throughout the cytoplasm and occasional ribosomes and rough endoplasmic reticulum.

Gap junctions are found in many, but not all, control specimens examined (Figure 2d). They are present in the innermost retinal area, close to the inner limiting membrane. During our initial observations, we searched for gap junctions among glial cell processes in the nerve fiber and the ganglion cell layer and did not find any. It was for this reason that we limited the morphometric study to the innermost 3 microns of retina.

Using morphological criteria described above, providing that the process involved in a gap junction is large enough to make identification certain, most of the gap junctions in normal retina are found between astrocyte processes (Table IV). In control animals, gap junctions are infrequent (Table IV and V). They are more likely to be found adjacent to blood vessels, but astrocyte processes are preferentially found in this area. In the

morphometric study, there is one gap junction that appeared to connect an astrocyte and Müller cell process. One gap junction photographed (but not as part of the morphometric study) would be classified as between Müller cells (Figure 2e) because of the SER present in the processes.

Inner Retina, Urethane Retinopathy

Although the inner retina of animals with urethane retinopathy appears normal at light microscopic magnification, there are ultrastructural alterations in the youngest animals examined, at 8 weeks, and the distortions become more marked with time. There is a change in the compartmentalization of organelles within the Müller cells.[9] The electron density is more variable than in controls, sometimes being more electron lucent than normal. SER is still present in the endfeet region. However, the regular pattern of the Müller cell endfeet at the ILM is sometimes disturbed, in that processes heavily laden with intermediate filaments extend horizontally across the area normally occupied by the Müller cell endfeet (Figure 3a).

Astrocyte cell processes and cell bodies in the innermost retina are filled with intermediate filaments and abundant rough endoplasmic reticulum (Figure 3b). The region closest to the ILM is occupied by profiles of fine processes filled with dense intermediate filaments that match the ultrastructural description of fibrous astrocytes, rather than the protoplasmic astrocytes commonly seen in control specimens.

Prominent gap junction profiles are found between glial processes, not infrequently in clusters (Figure 4a). They are often found between astrocyte processes adjacent to inner retinal vessels. Ultrastructurally, the inner retinal vessels and capillaries appear normal. The number of gap junction profiles per unit area of retina examined increases with duration of the retinopathy (Table V). Some profiles of the gap junctions are extremely long (Figure 4b).

Because of the pathological distortion, both Müller cell processes and astrocytic processes lack their normal characteristics. However, by noting the characteristics of the cell organelles in processes that clearly arise from the radial Müller cell stalk, we defined Müller cell processes in the UR animals as containing SER, rarely ribosomes or RER, sometimes lysosomes and intermediate filaments in a loosely arranged configuration (Figure 4a,b). In contrast, by following processes out from astrocyte cell bodies, we defined astrocytic processes as being densely, almost totally filled with intermediate filaments, containing RER and ribosomes, and, in general, not having either SER or lysosomes. The astrocytic processes also spread horizontally, aligned with the ILM, whereas the Müller cell processes tend to present rounded profiles near the ILM in the UR animals (Figure 4a,b).

Using these criteria, we assigned the gap junctional profiles to cell types as seen in Table IV. Approximately 60 % of the gap junctions in the experimental animals were assigned to the inter-astrocytic category. An additional 20% were between at least one

astrocytic cell, with the other cell unidentified. As the UR progressed and the morphology close to the ILM became more complex, the identity of cells connected by gap junctions became more difficult to define. Most of the remaining gap junctions could not be unambiguously assigned to cell type, but there were only 2 junctions between an astrocyte and Müller cell, and 1 junction that appeared to be between Müller cells.

Since there appears to be an increase in inter-glial gap junction frequency and length in the urethane treated retina, we wished to know if this increase is simply a result of increased glial membranes or if it represents a real increase in glial membrane occupied by gap junctions. The glial cell contact length per unit area is significantly greater in urethane treated retinas than in control retinas at 8, 24 and 56 weeks (Table VI). Since we do not have an age matched control for the 56 week UR animals, we compared them to the 24 week control animals, which are fully mature rats and there appears to be no significant change between control animals with age in any measured parameters. There is a trend for the glial cell membrane contact length per unit area to increase with increasing time of the retinopathy, but only the 8 to 56 week comparison was statistically significant. By 56 weeks of UR the length of glial cell membrane contact length was more than twice that of control animals.

In addition, the proportion of glial cell membrane occupied by gap junctions is greater in urethane than control animals (Table VII). The average length of gap

junction profile as a percent of the total glial cell membrane contact length is greater in UR versus controls and increases with time of retinopathy. Due to the large variability in these measurements, reflected in the large standard deviations, the only statistically significant difference is the comparison between the 56 week UR and the 24 week control. These numbers suggest that, in the oldest UR group, nearly 2% of the glial cell membrane contact length close to the inner limiting membrane is occupied by gap junctions. This is almost 10 times greater than in the control animals.

We also observed in UR that some profiles of gap junctions are exceedingly long compared to any observed in controls, as shown in Figure 4b. In Table VIII, the average length of gap junction profiles in the UR animals is 2 to 3 fold significantly larger than in the controls. The size distribution of all gap junctions is shown in Figure 5. Not only are there more gap junctions in UR animals, but their length can be greater than any seen in control animals.

DISCUSSION

Unambiguous identification of each cell connected by gap junctions is less difficult in normal animals and becomes more difficult in the urethane treated retinas. In both cases, gap junctions are often found between fairly fine processes, but the distinction between the normal protoplasmic astrocyte and the normal, electron dense, Müller cell is more obvious in the control animals. With increasing pathology, the array of glial cell processes increases, as evidenced by the increase in glial cell membrane contact length, and the morphological distinctions between the two glial cell types at the ILM become less clear. Despite the expression of glial fibrillary acidic protein, an intermediate filament component, in Müller cells in UR[9] the Müller cell does not exhibit a morphological increase in intermediate filaments to the same extent as does the astrocyte. However, using pattern recognition, an assignment of the gap junctions to astrocyte-astrocyte cell couples was possible in 60% of the examples in UR retinopathy. We think it likely that inter-astrocytic gap junctions are the predominant type in both normal and UR treated retinas.

Marc, et al., [31] have pointed out the difficulty of identifying small gap junctions in the inner plexiform layer of the goldfish retina, particularly in <u>en bloc</u> uranyl acetate stained material. Fortunately, our material was postfixed only with osmium tetroxide and the dark, fuzzy appearance of the gap junctions was apparent even at relatively low magnifications in the electron microscope. Since it is possible that we have missed

minute gap junctions, the actual incidence of gap junctions close to the ILM may be greater than we report. Although freeze fracture techniques can be used to identify gap junctions, the random fracturing process and difficulty of identifying cell membrane types in a complex tissue would make this technique less desirable than conventional electron microscopy.

Inter-astrocytic gap junctions are a common observation in brain astrocytes[21] and have been reported between astrocytes of the retina and optic nerve head in cat and monkey[7] and of the optic nerve head in man and monkey,[23] based on electron microscopy of thin sections. This report is the first to show and quantitate inter-astrocytic gap junctions in rat. Using freeze-fracture techniques, Reale et al.,[17] reported the existence of gap junctions between Müller cells in the inner retina in human. Our finding that the rat inter-astrocytic gap junctions are confined to the innermost retina, raises the possibility that the gap junctions observed by Reale et al., may have been between astrocytes rather than Müller cells; alternatively there may be species differences. Boycott and Hopkins[26] had also suggested that the gap junctions in human inner retina might be between microglia rather than between Müller cells.

Assignment of one or both cell processes participating in gap junction formation to Müller cells was possible in only 7 of the 128 (5%) gap junctions found in the morphometric study. This finding reinforces our view that gap junctions between Müller

cells or between Müller cells and astrocytes are rare at the inner limiting membrane in both normal and UR animals.

This is not to say that gap junctions may not exist between Müller cells at other locations in this polarized cell. Gap junctions have been reported between Müller cells at the external limiting membrane (ELM) in several species[11-15], but were not reported to be present anywhere on Müller cells in normal rat.[13] LaVail, et al.[32] reported that both tight and gap junctions were found between Müller cells and retinal pigment epithelial cells in rats with a hereditary photoreceptor degeneration. Since our current study did not include examination of the outer retina, we do not know if gap junctions form between these two cell types in UR photoreceptor degeneration.

Astrocytes in the brain act as a spatial buffering mechanism, in that K^+ liberated into the extracellular space by neuronal activity is taken up in astrocyte processes surrounding the neurons and ejected from the cells at the "end-feet," which rest on the basement membrane of capillaries. Evidence supporting this hypothesis is the demonstration that astrocytic end-feet have a higher K^+ conductance than other portions of the cell.[20] The existence of gap junctions between astrocytes would enlarge the area over which these cells could remove K^+ from the extracellular space. This is analogous to the function of gap junctions between horizontal cells in fish retina, which enlarges the receptive fields of these neurons.[31] Thus, in normal rats, the existence of gap junctions between retinal

astrocytes probably allows them to spatially buffer extracellular K^+ in the inner retina, delivering it to the perivascular space.

In the retina, the Müller cell is also polarized with reference to K^+ conductance, with the end-feet facing the vitreous having the largest potassium conductance, thus acting as a siphon to remove extracellular K^+ from the distal to the proximal retina.[8] Calculations of the spatial buffering capacity of the Müller cells of axolotl retina indicated that gap junctional coupling can increase the capacity of the Müller cell to buffer extracellular potassium by 60 %.[33]

However, this type of analysis is unlikely to pertain to all animal species, since many mammalian vertebrates do not have gap junctions between Müller cells.[13] For example, in the rat, the Müller cell could remove K^+ from the outer retina to the vitreous within the radius of the Müller cell processes, but not from larger areas since the Müller cells are rarely coupled by gap junctions.

If our speculations concerning the lack of Müller cell gap junctions in humans are accurate, then human retina would be similar to rat in being able to spatially buffer K^+ from a vertical volume encompassed by one Müller cell, but not more. If the normal human retina, like rat, has gap junctions between astrocytes, only these glia could spatially buffer K^+ over larger areas in a lateral direction. Given the restricted location of astrocytes to the inner retina in rat and human,[6] this area should be more protected

from the deleterious effects of localized high extracellular potassium than the outer retina. The optic nerve head, which has astrocytes coupled by gap junctions,[21] should be capable of extensive spatial K^+ buffering, and less susceptible to local changes in extracellular K^+. The opposite would be true of the macula, a region in human and primate retina[6] devoid of astrocytes.[6,7] This region should be particularly susceptible to cell edema, caused by high local extracellular K^+ concentration.

The major observation of this study is that inter-glial gap junctions increase in number and size following photoreceptor degeneration. To our knowledge, this is the first report of a change in gap junctions as part of a pathological process. Increased numbers of gap junctions have been shown in uterine smooth muscle at parturition.[34] Gap junctions of brain astrocytes were not different after 1 hour of ischemia[35] and were stable to hyperosmotic solutions.[21] Although another plasma membrane structure of astrocytes, the orthogonal arrays of intramembrane particles, are extremely labile to anoxia and cold,[36-38] alterations in gap junctions have not been seen in these studies (Brightman, personal communication).

The morphological increase of inter-glial gap junctions during urethane induced photoreceptor degeneration does not necessarily mean that there is increased functional coupling of these cells. Electrical coupling can be altered by changes in intracellular pH and calcium concentration without modification of the morphological appearance.[10,39]

The increased gap junction profiles are not due simply to increased glial cell membranes, since the proportion of glial cell membrane occupied by gap junctions is close to 2% of the glial cell membrane length at 56 weeks in UR, a 10 fold increase over the controls. This could result either from de novo synthesis of gap junction proteins or recruitment of pre-existing precursors.[40] Without additional studies, we cannot discriminate between these two alternatives. The increase in total glial cell membranes might argue for de novo synthesis of both membranes and gap junctions. The long time course of the observations would be sufficient to permit new synthesis, but does not rule out assembly of pre-existing precursors. In an in vitro system, assembly of gap junctions from pre-existing precursors was ascribed to disturbances of the cytoskeleton. As described in the accompanying paper,[9] there are alterations of cytoskeletal elements in both astrocytes and Müller cells that could participate in the appearance of formed gap junctions. The glial cell gap junctions may also play a role in glial cell migration and proliferation in retinal degenerations. Since the gap junctions are seen predominately between astrocytes in both control and experimental animals, the stimulus to increase gap junctional profiles may be cell-type specific.

What might the stimulus for up-regulation of gap junctions in retinal glial cells be? Loss of photoreceptor cells is the primary lesion in UR.[27] Secondary changes in the cytoskeleton, as mentioned above, might be sufficient to cause enhanced appearance of gap junctions. However, given the role of astrocytes in brain to spatially buffer

extracellular potassium, we speculate that the increased gap junction profiles are related to this function.

Several factors may contribute to this possibility. The photoreceptors normally release neurotransmitter at their synapses in the dark, and this release is decreased with light. Thus, in the UR, with the absence of photoreceptors, the residual inner retina is in a state equivalent to being in constant light and those neuronal cells responsive to this state could be activated. This could lead to increased extracellular K^+. In later stages of UR, the blood retinal barrier at the level of the retinal pigment epithelium breaks down, which has the potential to contribute to an abnormal extracellular space in the residual retina.[41] We have previously commented on cystic spaces occurring in the inner retina in UR.[28] Whatever the mechanism, we think the increased astrocyte cell membrane and gap junction profles are an attempt to spatially buffer an increasingly abnormal extracellular compartment.

ACKNOWLEDGEMENT

The authors wish to acknowledge the excellent electron microscope facility directed by Robert Munn, secretarial services of Mary E. Johnson and technical assistance of Mariana Robles.

Key words: astrocytes, Müller cells, gap junctions, retinal degeneration, spatial bufferering, glia

REFERENCES

1. Burns MS, Bellhorn RW, Korte GE, and Heriot WJ: Plasticity of the retinal vasculature. Prog Retinal Res 5:253, 1986.

2. Korte GE, Burns MS, Bellhorn RW: Epithelial - capillary interactions in the eye: the retinal pigment epithelium and the choriocapillaris. International Review of Cytology 114:221, 1989.

3. Hogan MJ and Feeney L: The ultrastructure of the retinal vessels. J Ultrastructure Res 9:47, 1963.

4. Ripps H and Witkovsky P: Neuron-Glia interaction in the brain and retina. Prog Retinal Res 4:181, 1985.

5. Gallego A: Comparative studies on horizontal cells and a note on microglial cells. Prog Retinal Res 5:165, 1986.

6. Schnitzer J: Astrocytes in mammalian retina. Prog Retinal Res 7:209, 1988.

7. Büssow H: The astrocytes in the retina and optic nerve head of mammals: A special glia for the ganglion cell axons. Cell and Tissue Research 206:367, 1980.

8. Newman E A: Membrane physiology of retinal glial (Müller) cells. J Neuroscience 5:2225, 1985.

9. Tyler NK and Burns MS: Alterations in glial cell morphology and GFAP expression in urethane induced retinopathy. Invest Ophthal Vis Sci, submitted.

10. Loewenstein WR: Junctional intercellular communication: the cell-to-cell membrane channel. Physiol Rev 61:828, 1981.

11. Lasansky A: Functional implications of structural findings in retinal glial cells. Prog Brain Res 15:48, 1965.

12. Miller RF and Dowling JE: Intracellular responses of the Müller (Glial) cells of mudpuppy retina: Their relation to b-wave of the electroretinogram. J Neurophysiol 33:323, 1970.

13. Uga S and Smelser GK: Comparative study of the fine structure of retinal Müller cells in various vertebrates. Invest Ophthal Visual Sci 12:434, 1973.

14. Fain GL, Gold GH, and Dowling JE: Receptor coupling in the toad retina. Cold Spring Harbor Symposium 40:547, 1975.

15. Tonus JG and Dickson DH: Neuro-glial relationships at the external limiting membrane of the newt retina. Exp Eye Res 28:93, 1979.

16. Conner JD, Detwiler PB, and Sarthy PV. Ionic and electrophysiological properties of retinal Müller (glial) cells of the turtle. J Physiol 362:79, 1985.

17. Reale E, Luciano L, and Sptiznas M: Communicating junctions of the human sensory retina. Albrecht v. Graefes Arch Klin Exp Ophthal 208:77, 1978.

18. Ikui H, Uga S, and Kohno T: Electron microscopic study on astrocytes in the human retina using ruthenium red. Ophthalmol Res 8:100, 1976.

19. Stone J and Dreher Z: Relationship between astrocytes, ganglion cells and vasculature of the retina. J Comp Neurol 255:35, 1987.

20. Newman EA: High potassium conductance in astrocyte endfeet. Science 233:453, 1986.

21. Brightman MW and Reese TS: Junctions between intimately apposed cell membranes in the vertebrate brain. J Cell Biol 40:648, 1969.

22. Dermietzel R: Junctions in the central nervous system of the cat. III. Gap junctions and membrane-associated orthogonal particle complexes (MOPC) in astrocytic membranes. Cell Tissue Res 149:121, 1974.

23. Quigley H.A: Gap junctions between optic nerve head astrocytes. Invest Ophthalmol Visual Sci 16:582, 1977.

24. Terubayashi H, Murabe Y, Fujisawa H, Itoi M, and Ibata Y: Enzymhistochemical identification of microglial cells in the rat retina: Light and electron microscopic studies. Exp Eye Res 39:595, 1984.

25. Hume DA, Perry VH, and Gordon S: Immunohistochemical localization of a macrophage-specific antigen in developing mouse retina: Phagocytosis of dying neurons and differentiation of microglial cells to form a regular array in the plexiform layers. J Cell Biol 97:253, 1983.

26. Boycott BB and Hopkins JM: Microglia in the retina of monkey and other mammals: its distinction from other types of glia and horizontal cells. Neuroscience 6:679, 1981.

27. Burns MS and Bellhorn RW: Early degeneration of photoreceptor cells in urethane induced retinopathy of rats. In Degenerative Retinal Disorders:

Clinical and Laboratory Investigations, Hollyfield JG, Anderson RE, and LaVail MM, editors. Alan R. Liss, Inc., NY, 1987, pp. 531-549.

28. Bellhorn RW, Bellhorn MS, Friedman AH, and Henkind P: Urethane induced retinopathy in pigmented rats. Invest Ophthal 12:65, 1973.

29. Noell WK: There are different kinds of retinal light damage in the rat. In The Effects of Constant Light on Visual Processes, Williams TP and Baker BM, editors. Plenum Press, NY, 1979, pp 3-28.

30. Burns MS and Tyler NK: Retinal vessels incorporated into retinal pigment epithelium after total loss of photoreceptor nuclei. Invest Ophthal Vis Sci 29(Suppl):381, 1988.

31. Marc RE, Liu W-LS and Muller JF: Gap junctions in the inner plexiform layer of the goldfish retina. Vision Res 28:9, 1988.

32. LaVail MM, Sidman M, Rausin R and Sidman RL: Discrimination of light intensity by rats with inherited retinal degeneration: A behavioral and cytological study. Vision Res 14:693, 1974.

33. Mobbs P, Brew H, and Atwell D: A quantitative analysis of glial cell coupling in the retina of the axolotl (Ambystoma mexicanum). Brain Res 460:235, 1988.

34. Sims SM, Daniel EE, and Garfield RE: Improved electrical coupling in uterine smooth muscle is associated with increased numbers of gap junctions at parturition. J Gen Physiol 80:353, 1982.

35. Cuevas P, Gutierrez-Diaz JA, Reimers D, Dujovny M, Diaz FG, and Ausman JI: Aspects of interastrocytic gap junctions in blood-brain barrier in the experimental penumbra area, revealed by transmission electron microscopy and freeze-fracture. Experientia 40:471, 1984.

36. Anders JJ and Brightman MW: Assemblies of particles in the cell membranes of developing, mature and reactive astrocytes. J Neurocytol 8:777, 1979.

37. Anders JJ and Brightman MW: Particle assemblies in astrocytic plasma membranes are rearranged by various agents in vitro and cold injury in vivo. J Neurocytol 11:1009, 1982.

38. Anders JJ and Brightman MW: Freeze-fracture studies of plasma membranes of astrocytes in freezing lesions. Adv Neurol 44:765, 1986.

39. Spray DC, Saez JC, Burt JM, Watanabe T, Reid LM, Hertzberg EL and Bennett MVL: Gap junctional conductance: Multiple sites of regulation. In Modern Cell Biology, Hertzberg EL and Johnson RG, editors. Alan R. Liss, 1988, pp. 227-244.

40. Tadvalkar G and DaSilva PP: In vitro, rapid assembly of gap junctions is induced by cytoskeleton disruptors. J Cell Biol 96:1279, 1983.

41. Korte GE, Bellhorn RW, and Burns MS: Urethane-induced rat retinopathy: Plasticity of the blood-retinal barrier in disease. Invest Ophthal Vis Sci 25:1027, 1984.

LEGENDS

Figure 1a. Light micrograph of central retina of a 24 week control rat retina. The choroid (C), rod outer segment (ROS), outer nuclear layer (ONL), inner nuclear layer (INL) and inner plexiform layer (IPL) appear normal. Vessels (arrowheads) are present in the nerve fiber layer. Bar = 50 μm.

1b. Central retina of a 24 week urethane rat retina. The photoreceptor cells are absent, while the INL and IPL appear normal. The RPE (white arrow) and choriocapillaris (white arrowhead) appear intact. Vessels (black arrowheads) are present in the NFL and one extends toward the RPE. Bar = 50 μm.

Figure 2a. Electron micrograph of 24 week control rat retina showing the heavy stalk of a Müller cell (M) between bundles of ganglion cell axons (A). The electron dense radial process has a mitochondria rich region containing smooth endoplasmic reticulum closest to the vitreous body. Bundles of intermediate filaments (IF) occur at the level of the ganglion cell axons. Bar = 2 μm.

2b. Electron micrograph of an 8 week control rat retina showing the inner limiting membrane composed of lateral processes of Müller cells filled with smooth endoplasmic reticulum (SER). Profiles of two electron lucent astrocytic

processes contain small bundles of intermediate filaments (arrowheads), some ribosomes and rough endoplasmic reticulum, and are joined by a small gap junctional profile (arrow). Ganglion cell axons at the top of the picture contain neurotubules (NT) and no rough endoplasmic reticulum. Bar = 0.5 μm.

2c. Electron micrograph of a 24 week control rat retina with an astrocyte cell body (A) with prominent nucleolus immediately adjacent to a small inner retinal capillary. Electron lucent astrocyte processes (arrows) are adjacent to the capillary basement membrane, which is also contacted by denser Müller cell processes (arrowhead). Bar = 1 μm.

2d. Electron micrograph of a typical gap junctional profile in a control 24 week rat retina, found between two small electron lucent processes. The typical heptalaminar morphology was present. Bar = 0.1 μm.

2e. Electron micrograph of a junctional profile adjacent to a retinal vessel basement membrane (BM) in a control 16 week rat retina. Occasional small gap junction profiles (arrow) are accompanied by profiles indicative of maculae adherens (arrowhead) as described by Büssow (1980). Due to the presence of SER within these processes, this gap junction would be classified as a Müller-Müller cell junction. Bar = 0.5 μm.

Figure 3a. Electron micrograph of inner retina in 24 week old urethane treated rat retina. The Müller (M) cell looks relatively normal, except that it does not extend to the inner retinal edge, nor does it spread laterally. That space is occupied instead by a fibrous astrocyte process (asterisk). Ganglion cell bodies (G) and axon bundles (A) look normal. Bar = 1 μm.

3b. Astrocyte soma near the ILM in a 56 week UR retina. The cell is filled with abundant intermediate filaments (IF) and contains much rough endoplasmic reticulum close to the soma. Bar = 1 μm.

Figure 4a. The astrocyte processes are more numerous at the inner limiting membrane in older animals as in this 56 week UR example. The gap junction profiles frequently occur in clusters (arrowheads). Individual processes are labelled as astrocytes (A) or Müller cells (M), as described in the text. Bar = 1 μm.

4b. Compared to controls, some gap junctions have an extremely lengthy profile (arrows) as seen in this 56 week UR specimen. Based on the text description, Müller cell (M) and astrocyte (A) processes are labelled. Bar = 1 μm.

Figure 5. Histogram of gap junction profile length.

Table I

Length of Inner Limiting Membrane Measured, μm

	Control	Urethane	
8 Week (n = 3)	182 +/- 10	184 +/- 10	*
16 Week (n = 3)	188 +/- 8	192 +/- 8	*
24 Week (n = 3)	192 +/- 31	203 +/- 2	*
56 Week (n = 5)@	-	127 +/- 42	#

*No difference between control and urethane.

#No difference between 56 week urethane and 24 week control.

@ n is the same for all tables.

Table II

Area of Inner Retina Measured, μm^2

	Control	Urethane	
8 Week	425 +/- 72	440 +/- 23	*
16 Week	452 +/- 52	459 +/- 15	*
24 Week	463 +/- 74	491 +/- 88	*
56 Week	-	322 +/-123	#

*No difference between control and urethane.

#No difference between 24 week control and 56 week urethane.

Table III

Measured Area per Inner Limiting Membrane Length, μm

	Control	Urethane	
8 Week	2.33 +/- .27	2.39 +/- .12	*
16 Week	2.41 +/- .18	2.39 +/- .05	*
24 Week	2.41 +/- .02	2.42 +/- .46	*
56 Week	-	2.51 +/- .27	#

*No difference between control and urethane.

#No difference between 24 Week control and 56 Week urethane.

Table IV

Cell Type Involved in Gap Junctions

	A - A*	A - ?	? - ?	Other
8 Week Control	3	1		A - M
16 Week Control	6	1		
24 Week Control	1	1		
8 Week Urethane	7	2	2	M - ?
16 Week Urethane	9	1	1	
24 Week Urethane	12	8	5	A - M
				M - M
56 Week Urethane	40	14	7	A - M
				? - M
				? - M
TOTAL	78	28	15	7

*A = Astrocyte; M = Müller cell

Table V

Average Number of Gap Junction Profiles Per 100 μm^2 Retinal Area

	Control	Urethane
8 Week	.47	.76
16 Week	.66	1.02
24 Week	.14	2.10
56 Week	-	3.98

Table VI

Glial Cell Membrane Contact Length, μm per 100 μm^2 Area

	Control	Urethane
8 Week	58 +/- 12	82 +/- 6*
16 Week	69 +/- 3	101 +/- 22
24 Week	64 +/- 9	119 +/- 23@
56 Week	-	137 +/- 24^#

*Significantly different from control at P <.05.

@ Significantly different from control at P < .02.

^Significantly different from 24 week control at P < .01.

#Significantly different from 8 week urethane at P < .05.

Table VII

Gap Junction Profile Length Per Glial Cell Membrane Contact Length

(μm per 1000 μm)

	Control	Urethane
8 Week	2.8 +/- 1.1	5.2 +/- 2.3
16 Week	3.3 +/- 2.9	5.5 +/- 1.9
24 Week	1.1 +/- 2.0	13.6 +/- 7.9
56 Week	-	18.9 +/- 9.4*

* Significantly different from 24 Week control at $P < .05$.

Table VIII

Gap Junction Profile Length, μm

	Control	Urethane
8 Week	.36 +/- .07	.61 +/- .30
16 Week	.26 +/- .23	.54 +/- .09
24 Week	.17 +/- .30	.73 +/- .13*
56 Week	-	.73 +/- .20^

*Significantly different from control at $P < .05$.

^Significantly different from 24 week control at $P < .05$.

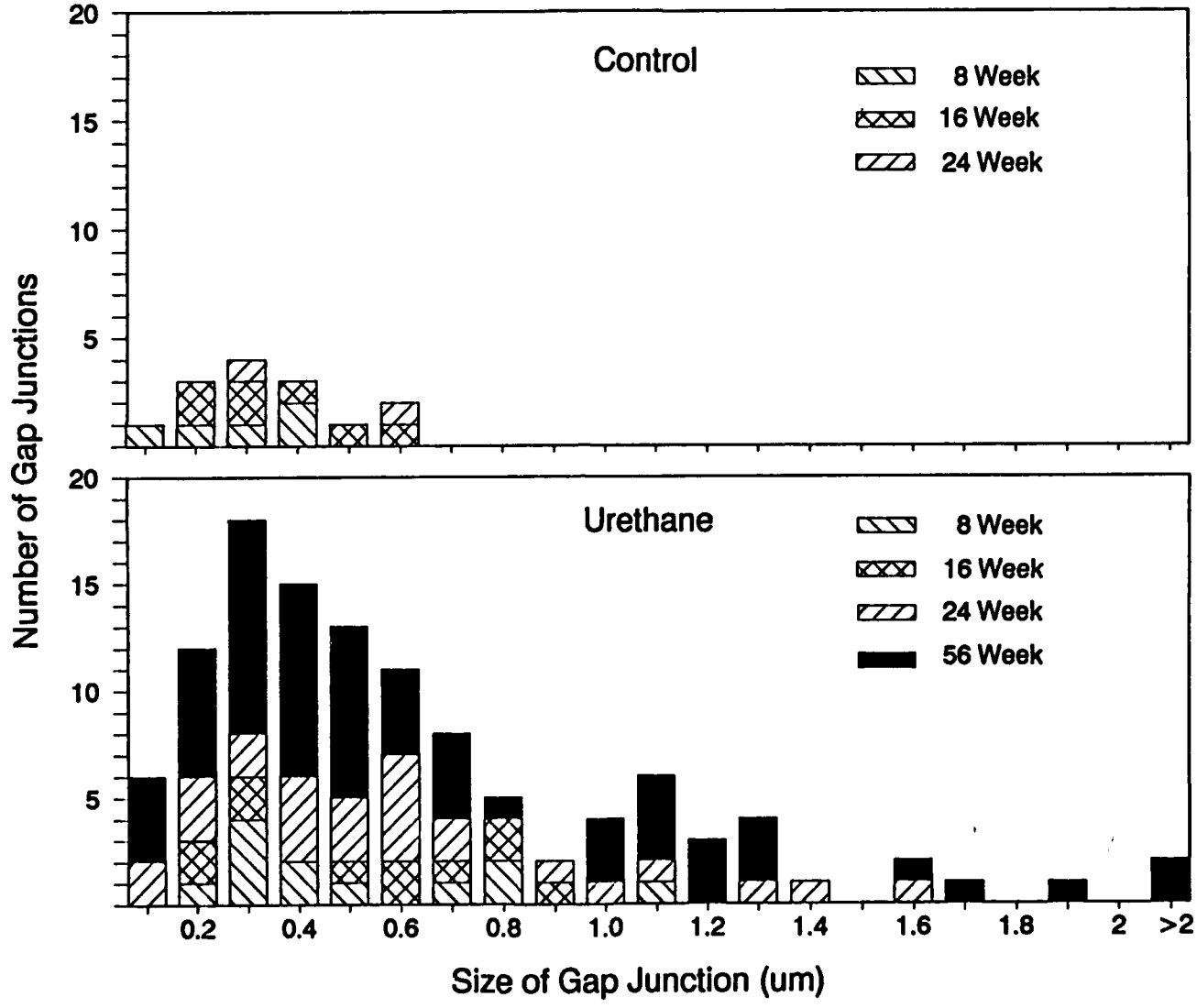
Control
8 Week
16 Week
24 Week
Urethane
8 Week
16 Week
24 Week
56 Week
Number of Gap Junctions
20
15
10
5
0.2
0.4
0.6
0.8
1.0
1.2
1.4
1.6
1.8
2
>2
Size of Gap Junction (um)

Figure 5


C
ROS
ONL
INL
IPL
1a
INL
IPL
1b

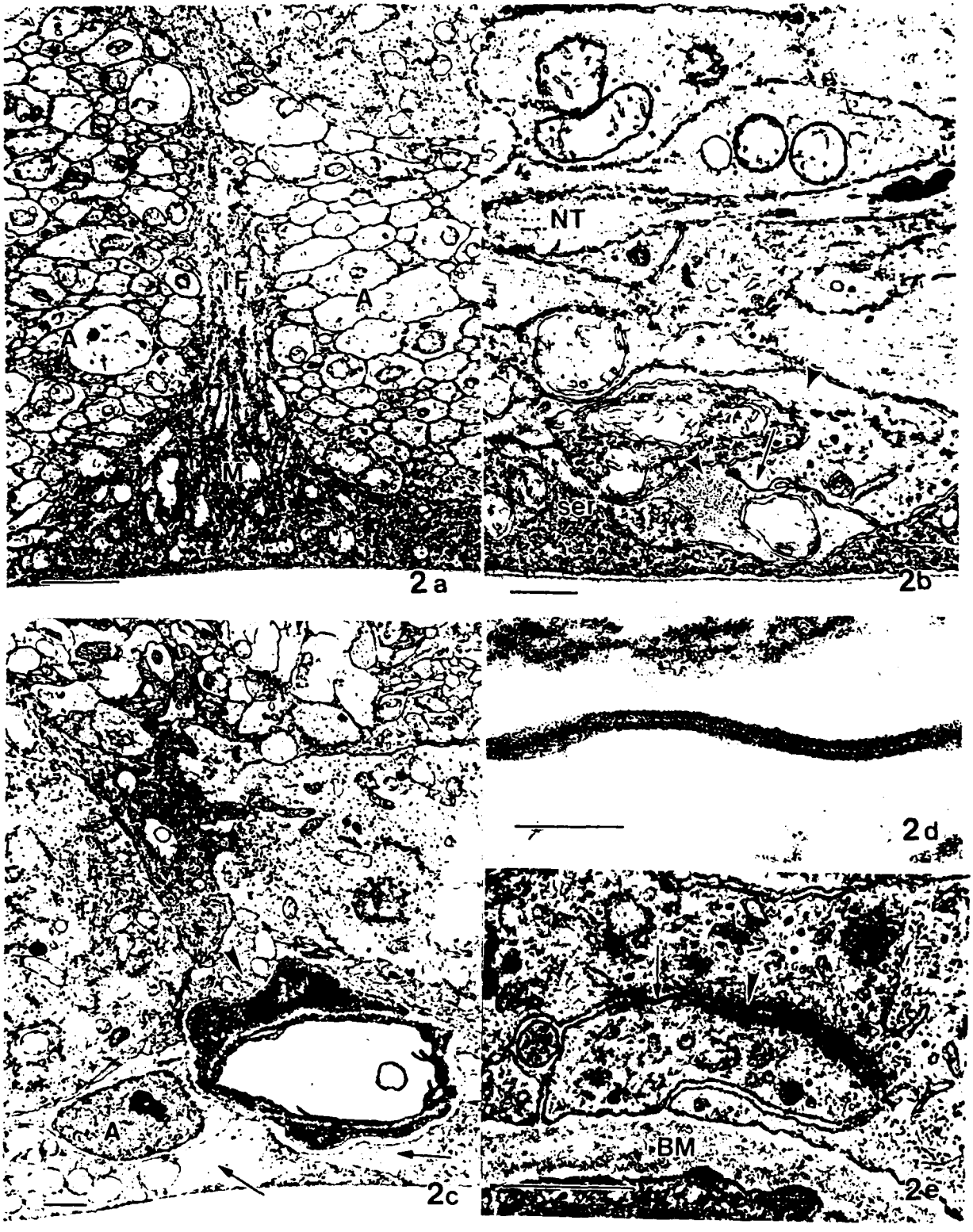
A
IF
A
M
2a
NT
ser
2b
A
2c
2d
BM
2e

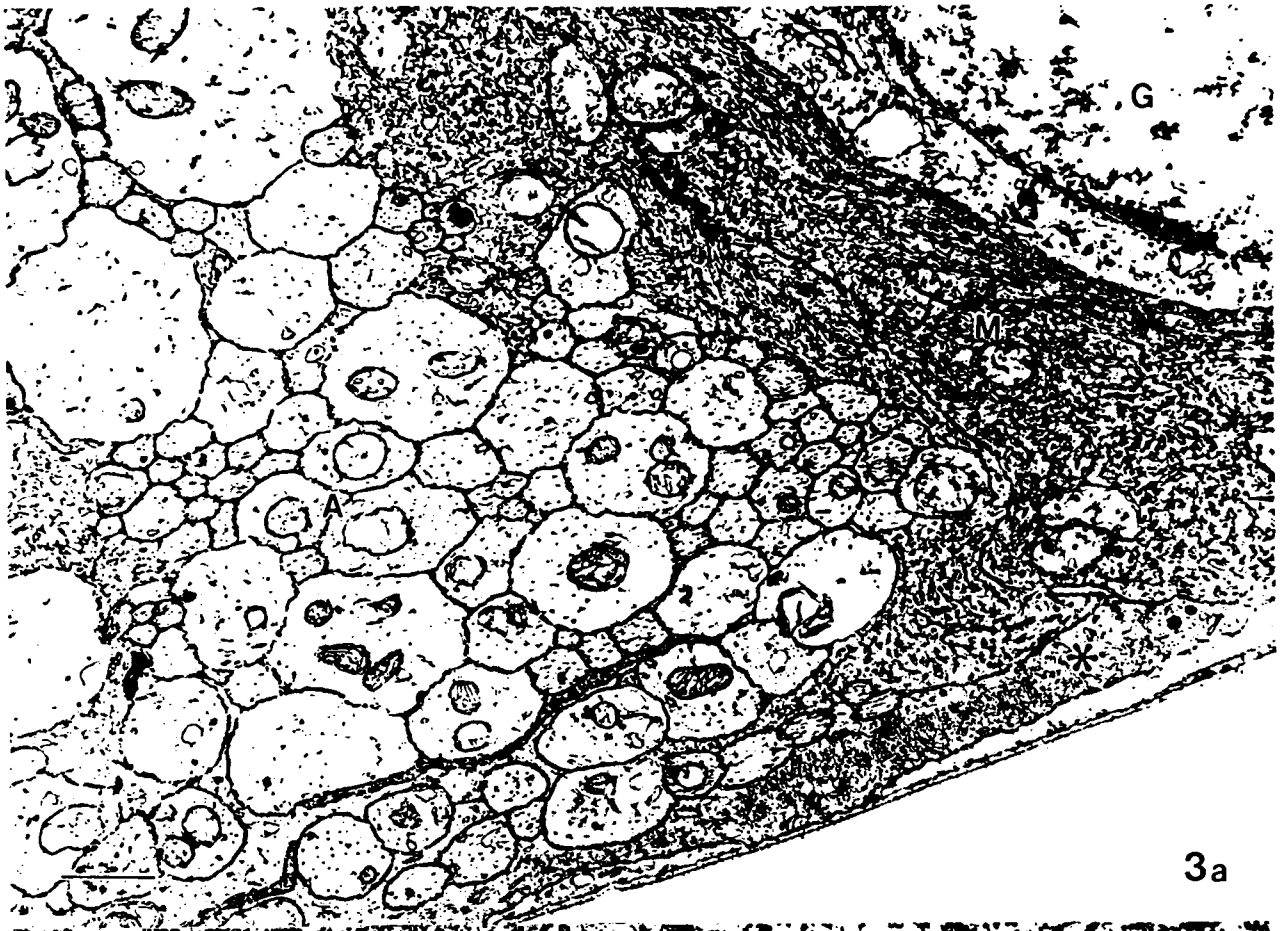

3a

3b

4a

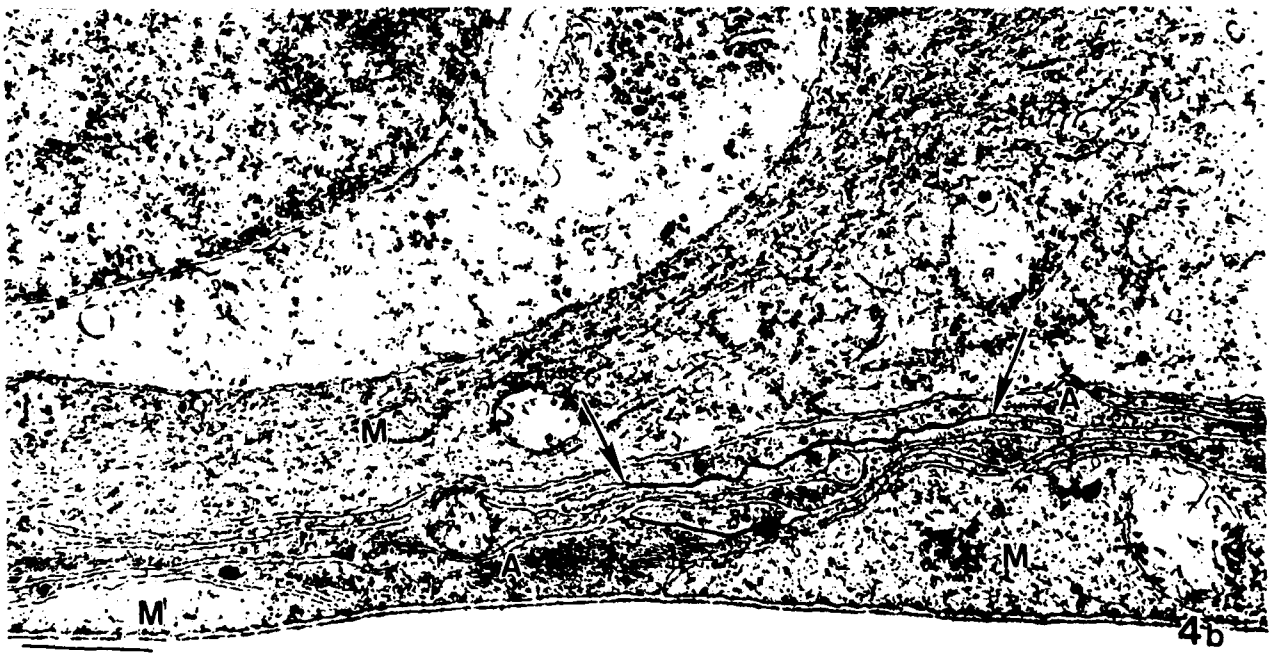

4b

Submitted: Current Eye Res

RETINAL PIGMENT EPITHELIUM (RPE) STIMULATION OF RPE NEOVASCULARIZATION IN VIVO

Margaret S. Burns and Nancy K. Tyler

Department of Ophthalmology, School of Medicine
University of California, Davis

KEY WORDS: Retinal vessels, Photoreceptor cells, Retinal pigment epithelium, Urethane, Rats, Morphometry, Retinal degeneration

Running Title: RPE Stimulation of Neovascularization In Vivo

ABSTRACT

Photoreceptor cell degeneration in rodents from a variety of causes results in neovascularization of the retinal pigment epithelium as a late stage phenomenon. Even though the vessels within the pigment epithelium arise from the retinal circulation, they can manifest the choroidal endothelial cell phenotype of fenestrated endothelial cells. In order to study the detailed cellular events which result in incorporation of retinal vessels within the retinal pigment epitheiium, a morphological and morphometric analysis of the RPE and vasculature was performed in rats. Urethane, given subcutaneously to newborn rats, results in a photoreceptor degeneration but does not affect the RPE, choroid or inner retinal layers. Retinas were studied from 8 to 24 weeks of age, the time period when vascularization of the RPE occurs.

Loss of retinal vessels is first seen at 12 weeks, primarily in substantial dropout of vessel profiles in the outer plexiform layer (OPL) vessel bed. There is a gradient of loss from the OPL bed to the nerve fiber layer (NFL) bed and from the central to peripheral region. Total vessel density of the retina is initially greater than controls, but decreases from 8 to 20 weeks, and appears to stabilize at 20 and 24 weeks. Analysis of the separate vessel beds shows that this is due to continued loss of vessels within the sensory retina, but increased presence of vascular profiles within the RPE. Total absence of the photoreceptor cell is necessary for incorporation of vessels within the RPE. The RPE stimulates the development of new vessel profiles within this layer, but not in the adjacent sensory retina. A model of the cellular events leading to RPE neovascularization is proposed.

INTRODUCTION

In photoreceptor cell (PRC) degeneration in rodents neovascularization of the retinal pigment epithelium (RPE) occurs subsequent to the PRC loss. (1) We have previously shown in both phototoxic and urethane induced PRC degeneration that the source of the vessels within the RPE is from the retinal vasculature. (2,3) Even though these vessels arise from the retinal circulation, they can exhibit the choroidal endothelial cell phenotype, which is a fenestrated endothelial cell, unlike the continuous endothelial cell of the normal retinal vessel. (3)

Both neovascularization and vessel degeneration

have been demonstrated in various rodent models. For example, early studies using trypsin digest preparations, showed that in both hereditary and toxic induced PRC degeneration, the retinal vasculature exhibited capillary dropout. (4,5) Early loss of retinal vessels during development has been shown in several hereditary mouse retinal dystrophies. (6-9) In later stages of the PRC degeneration, neovascularization, as assessed by tritiated thymidine labelling of endothelial cells, has been demonstrated in urethane induced retinopathy (UR) and RCS rats. (10,11) An absolute increase in vessel density has been reported in the retinas of RCS rats. (12)

We are interested in the cellular mechanisms by which retinal endothelial cells can be induced to change their phenotype. Our purpose in this study is to understand the detailed cellular events which permit vascularization of the RPE. As a study model, we have used PRC degeneration in the rat induced by urethane, which causes PRC degeneration during the neonatal period. (13) This toxic model is highly reproducible, even though the mechanism of action of urethane on the developing PRC is not known. Unlike the hereditary retinal degnerations, there is no apparent defect in, or direct effect of urethane on, the RPE, choriocapillaris or inner retinal neurons. The response of the retinal vasculature and RPE can be followed without underlying genetic defects that could modulate the pathologic response. A detailed morphologic and morphometric study of the discrete retinal vessel beds and their relationship to the RPE and PRC degeneration is reported.

MATERIALS AND METHODS

Production of Urethane Retinopathy

Urethane retinopathy was produced in newborn Long-Evans rats as previously described. (4,14) All animals were treated in accord with the Guiding

Principles in the Care and Use of Animals (DHEW Publication, NIH 80-23). Briefly, newborn rat pups were injected subcutaneously on Day 1, followed by seven weekly injections with urethane (ethyl carbamate, Aldrich Chemical Co.) in phosphate buffered saline (PBS) at a dose of 1 mg/gm body weight. Control animals were injected with the same volume of PBS. The rats were maintained under standard laboratory conditions with room light at 20 to 30 foot-candles on a 12 hour light (beginning at 7 am), 12 hour dark cycle until the time of sacrifice. Sacrifice was performed after 9:00 am to avoid the peak light-induced phagocytosis of rod outer segment discs. Five urethane and three control animals were sacrificed at age 8, 12, 16, 20 and 24 weeks. This is the same cohort of animals that were used for other studies. (14,15)

Preparation of Tissues

Following an overdose of sodium pentobarbital, the 12 o'clock limbal position was marked with a 6-0 silk suture, both eyes were rapidly enucleated, immersed for approximately 20 minutes in 3.0% glutaraldehyde in 0.1 M phosphate buffer at pH 7.4 and then the cornea and lens removed to facilitate fixative diffusion to the retina. Fixation continued until the next day, when the eye cups were rinsed with buffer, postfixed with osmium, dehydrated in a standard series of ethanol and propylene oxide and embedded in Polybed 812 (Polysciences, Inc). The posterior eye cups were hemisected from 12 to 6 o'clock and oriented at embeddment so that light microscopic sections of the entire half eye cup could be made.

Microscopy and Morphometry

Light microscopic sections (0.5 to 1 um) were cut with a glass knife on a Sorvall MT2B and stained with Toluidine Blue and Azure II in borax.

For morphometric measurements, the posterior

eyecup was divided into three segments: superior peripheral, central, and inferior peripheral. The central section was approximately one-half of the entire retina, and the two peripheral regions were each one-fourth of the total retinal length. The sections were photographed on an Olympus BH2 microscope at 2x magnification and enlarged 40 fold. The length of each segment and retinal thickness were measured from the enlargements using a Summagraphics Summasketch digitizing pad, connected to an AT clone computer. The total number of vessel profiles in each segment and in each layer of vessels was counted at the microscope with 400x magnification. The residual nuclei of the outer nuclear layer were counted similarly. Values for the superior and inferior peripheral retinas were combined. One half eyecup of both eyes of each animal was counted and the values combined to give an average for that animal, and then the group averages calculated. Number of vessel profiles per unit retinal length was calculated. Vessel density, the number of vessel profiles per unit area of retina, was derived from the length and thickness measurements. Data were analyzed using an independent t-test of the CRUNCH interactive statistical package (CRISP), as well as by analysis of variance (ANOVA).

RESULTS

Control Rat Retina

The control rat retinas at all ages were normal (Figure 1a, 2a). There are three layers of retinal vessels in the holangiotic rat retina. The innermost vessel bed is adjacent to the inner limiting membrane (ILM) in the nerve fiber layer (NFL) and consists of the large arteries and veins as well as a capillary network. More sclerad, a capillary plexus arborizes at the inner edge of the inner nuclear layer (INL). The deepest vessels are found within the outer plexiform

layer (OPL), at the outer edge of the inner nuclear layer, and do not impinge on the synaptic endings of the photoreceptor cells. We refer to these three vessel beds as the NFL bed, the INL bed, and the OPL bed, respectively.

The average central retinal thickness in control animals diminished somewhat with age (Table I). Since the retina thins from the equator to the ora serrata, we did not attempt to make average thickness measurements in the peripheral retina.

In the normal rat retina the OPL vessel bed contains the most vessel profiles per unit length in both central and peripheral areas (Tables II, III), and showed no differences at any ages studied. Vessel profiles in the INL layer are the least frequent of the three vessel beds. There is no statistically significant difference between the central and peripheral vessel profiles in the OPL and NFL layers, but the central INL layer has greater numbers of vessel profiles ($P \leq .02$ for 8, 16, 20 and 24 week comparisons) than the peripheral IPL. No statistically significant differences in vascularity with age were noted in the central or peripheral retina, with the lone exception of the values for 16 week control rats in the IPL vessel bed. This average is larger than other measurements in this layer, for which we have no explanation except for biological variability.

There was no age related difference in the density of total retinal vessels (number of vessel profiles per unit area) in the central region of normal animals (Table IV).

Experimental Rat Retina

Pathology In the experimental animals with urethane induced photoreceptor degeneration, we have made observations primarily in the central area, as that is where the photoreceptor degeneration first appears and then spreads peripherally. (3) At 8 weeks of age,

there are approximately 2 rows of photoreceptor nuclei remaining in the central region, although formed photoreceptor outer and inner segments are gone, with only some fragments in the residual interphotoreceptor space (Figure 1b). The RPE layer retains its configuration as a single layer of epithelial cells with normal polarity. The inner nuclear and inner plexiform, ganglion cell and nerve fiber layers appear normal at 8 weeks. At this age, as in all subsequent ages, the choriocapillaris appears normal.

During the subsequent weeks, there is additional loss of photoreceptor cell nuclei. By 16 weeks there are areas without any PRC nuclei, but on average, there is one row of PRC nuclei remaining (Figure 1c). This loss continues through 20 weeks and by 24 weeks there are only sporadic PRC nuclei present (Figure 1d). Where vessels are observed traversing from the inner retina into the RPE, there are no PRC nuclei remaining (Figure 2b, 2c). We have not observed macrophage *like cells in the outer retina at any time* period studied.

In general, the RPE cells continue to form their usual compact row abutting on Bruch's membrane, up to 24 weeks of age (Figure 1d). In areas where there is substantial loss of PRC nuclei, some subtle changes of RPE cells such as swelling or attenuation are seen. As the PRC cells are lost, the apical microvilli of the RPE cells become more apparent and form a lightly staining sheet in the former interphotoreceptor space, up to the external limiting membrane, which remains in many areas (Figure 1c, 1d).

The quiescent appearance of the RPE cells is sometimes lost in areas in which vessel profiles are found within the RPE. Here, the RPE cells tend to surround the vessels, and sometimes extend along the vessel into the retina (Figure 2b). However, in other areas, vessel profiles approach the RPE, or are even

found within the RPE without gross distortion of RPE morphology at the light microscopic level (Figure 2c, 2d).

The pattern of the inner retinal layers is relatively normal even at 24 weeks of age (Figures 1d, 2b, 2c). There can be some disruption of the INL morphology in some areas. We occasionally see pyknotic nuclei in the INL that seem to correspond to Müller cell nuclei (Figure 2d), but we have no observations which suggest Müller cell nuclear migration up to 24 weeks of age.

Morphometry The thickness of the residual central retina in experimental animals was about 65% of normal by 8 weeks of age and decreased to circa 50% of age matched control retinas by 24 weeks of age (Table I).

Changes in the number of vessel profiles per mm length of retina are due primarily to decreased vascularity of the OPL (Table II). In the central retinal region at 8 weeks of age, the OPL vessel content is not statistically different from normal, although by 12 weeks the numbers of vessel profiles in the OPL are half that at 8 weeks. At 16 and 24 weeks, the INL vessel layer is decreased compared to the control group (although the 16 week control value is not representative of the other ages, see above). Of the NFL vessels, none of the values are significantly different from controls, although there are diminished numbers of vessel profiles of the 24 week experimental group compared to the 8 week experimental group.

Decreased vascularity of the peripheral retina is also due primarily to loss of vessels in the OPL, although the rate of loss appears to be somewhat slower (Table III), as would be expected since the photoreceptor degeneration is less complete in the

periphery than in the central retina during these time periods.

The total vessel density of the experimental retinas is significantly greater than controls at 8 and 12 weeks, but not at later times (Table IV). This is due to the loss of retinal thickness, but no decrease in retinal vessel profiles at 8 weeks. Although there is vessel loss in the OPL at 12 weeks of age, the further reduction in retinal thickness at this age keeps the vessel density in the experimental retinas statistically significantly greater than in controls at the same age.

The apparent stabilization of total vessel density in later stages of the retinopathy as seen in Table IV is due to decreased vascularity of the neural retina and increased vascularity of the RPE. When the relative contribution of the retinal and RPE vessels is distinguished (Table IV), it can be appreciated that the vessel density of the neural retina continues to decrease with duration of the PRC degeneration and is significantly less than control animals by 24 weeks. As we have seen, this is due to loss of vessels primarily in the OPL.

In contrast, the vessel density within the RPE increases enormously from 16 weeks to 24 weeks, reaching average values that are much higher than vessel density in any control retina (Table IV). For the purposes of calculation, we have assumed a constant thickness of the RPE of 10 μm. Although the numbers are not statistically significant (due to the sporadic appearance of the vessels within the RPE - they tend to occur in tufts and are variable between animals), the figures give some appreciation for the degree of vascularity of the RPE.

The pathology suggested that there was a relationship between loss of photoreceptor cell nuclei and neovascularization of the RPE. However, the appearance of blood vessels within the RPE does not occur evenly throughout the RPE, but rather, there

are focal areas of inclusion with many profiles in that area, as coils of vessels arborize within the RPE. (16) There is also biological variability between animals so that some animals have a large number of vessels and others many fewer. The morphometric correlation between loss of photoreceptor nuclei and appearance of vessels in the RPE is seen in Figure 3. This correlation is tight, but not linear, which suggests that the process is more complicated than simply loss of nuclei.

It is our impression that in sections where a vessel can be seen traversing from the retina into the pigment epithelial layer, that pigmentation of the RPE in that region is light or non-existent. We attempted to assess this in a quantitative manner by counting vessel profiles seen within the RPE and noting whether or not they were present in a pigmented or non-pigmented RPE area (Table V). Both in the 20 and the 24 week specimens there were large numbers of vessel profiles seen with lack of pigmentation of the surrounding epithelial cells.

DISCUSSION

Sequence of cellular events leading to RPE neovascularization

We believe the following temporal sequence of cellular events leads to neovascularization of the RPE in urethane induced photoreceptor degeneration (UR): 1) Following partial loss of the PRC layer, retinal vessels in the outer neural retina degenerate. 2) Only after total degeneration of the PRC cell in a focal region do remaining retinal vessels in the OPL approach and contact the RPE. 3) The contact of the retinal vasculature stimulates the RPE to enfold and surround the existing retinal vessels. 4) The RPE stimulates retinal vessel endothelial cells to divide and form new vessels, but only within the RPE layer. 5) These new vessels are of the choroidal phenotype.

6) The choriocapillaris remains intact throughout this process due to the continued presence of the RPE.

Evidence and deductive analysis that supports this sequence of cellular events, as well as speculation on the mechanisms involved are as follows:

1) Partial loss of the PRC layer is sufficient to cause retinal vessels in the outer neural retina to degenerate.

By 12 weeks of age the number of vessels of the OPL is reduced to half, as is the retinal thickness. There are still many PRC cell nuclei remaining, often in a continuous single layer, so total loss of the PRC is not necessary to induce retinal vessel degeneration. Correlation of retinal vascular degeneration and loss of photoreceptor cells has been described in a variety of genetic and toxic retinopathies. (2-9,12) A cogent argument that the vascular loss is associated only with the PRC cell degeneration and not changes in the RPE or inner retinal layers is made by Dantzker and Gerstein (5) and supported by the experiments reported here. A question which remains unanswered is whether it is the physical presence of the PRC or their intense metabolic activity which is required to prevent retinal vessel degeneration (see below).

The mechanism for vessel degeneration has been suggested to be increased oxygen tension in the outer retinal layers, due to decreased retinal tissue mass. (4) Our experiments support this general hypothesis. There is no morphological change seen in the choriocapillaris up to 24 weeks, so we assume that there is no difference in blood flow, and therefore oxygen delivery to the retina. In the absence of photoreceptor cells to utilize oxygen, the intraretinal oxygen tension would be higher than normal and exhibit a gradient from outer to inner retina. Our studies have shown a gradient of vessel degeneration from the OPL to the NFL, which could correspond to the presumed oxygen gradient. There is also a

gradient of retinal vessel loss in the OPL from central to peripheral retina, which would conform to a lateral central to peripheral oxygen gradient, generated by increasing survival of PRC cells towards the periphery. The only other study of alterations in vascularization of individual retinal layers was reported by Blanks and Johnson (6), and they also found a gradient of vessel loss from the outer to inner retina in hereditary mouse retinal degenerations. They suggest that toxic lipid peroxidative products may be responsible for vessel degeneration, which is plausible. In vitro studies have shown inhibition of retinal endothelial cell growth in hyperoxic conditions. (17)

The above considerations of the potential importance of high oxygen tension in the retina being responsible for vascular cell death would lead to the prediction that the mere presence of photoreceptor cells would not be sufficient to prevent vascular degeneration. Rather, the PRC would need to be metabolically active, *and thus keep retinal oxygen* tension in a normal range to prevent vessel dropout. 2) Only after total degeneration of PRC cells in a focal region do retinal vessels in the OPL come in contact with RPE.

We and others have made and commented on this observation previously. (3,7,12) However, in order to understand the subsequent events of neovascularization of the RPE, this point needs to be highlighted. It is not sufficient for the outer and inner segment of some individual PRC cells to be gone for the OPL blood vessels to come in contact with the RPE. Rather, the entire PRC cell, including its nucleus, must be absent. In reading slides for this study, the presence of a moderately complete, even though discontinuous, row of PRC nuclei was an unfailing indicator that no vessels would be found within the RPE. Since the vessels of the OPL are

continuously decreasing in number, in order for retinal vessels to come into contact with the RPE, not only must the PRC nuclei be gone within a focal region, but there must also be a residual, presumably metabolically viable, vessel in that region.

This suggests that the RPE cell in UR does not produce an active diffusible chemotactic or chemokinetic molecule that is able to initiate migration of retinal blood vessels across residual PRC nuclei from the OPL towards the RPE. Rather, loss of the PRC nuclei is a permissive condition which allows neovascularization of the RPE to occur.

An alternative explanation for this observation would be that the PRC cell, or its products, are inhibitory to vessel cell migration and proliferation. In the RCS rat, it has been remarked that vascularization of the RPE does not occur until the "debris" layer, which consists of photoreceptor outer and inner segments, has been cleared. (1,7) It is possible that the components of the interphotoreceptor matrix are inhibitory to vascular outgrowth.

3) The contact of the retinal vasculature stimulates the RPE to enfold and surround the existing retinal vessels.

The RPE appears morphologically quiescent in UR, even up to 24 weeks of age, in most regions, except where blood vessels are in contact with this epithelial layer. If anything, in areas of loss of PRC cells, the RPE is attenuated, and perhaps degenerating, rather than being hypertrophic. Korte, et al., (18) has emphasized that the presence of retinal vessels within the RPE results in loss of polarity of the RPE cell and organization around the invading blood vessel. Caldwell and Roque (19) have reported expression of vimentin, an intermediate filament protein, in RPE cells of RCS rats during vascular remodelling, indicating that cytoskeletal

elements can undergo substantial change during this process. These observations are supportive of the hypothesis that proximity of the retinal vasculature has a stimulatory effect on the RPE cell. Several studies in vitro have demonstrated both stimulatory and inhibitory activity of RPE cells or conditioned medium on vascular endothelial cells. (20,21) We are not aware of studies which address the reverse - that is, the stimulation of RPE by vascular cells.

Our observation of the relative lack of pigment in many RPE cells surrounding the RPE vessels could be explained if the RPE cells are induced to divide at these sites, which would result in a dilution and relative loss of pigment. Mitotic figures in RPE cells in rodent dystrophies has not been reported (although thymidine labelling has been observed (1), but this must be a relatively rare event. (1,10,11) The time periods studied, which are weeks to months, are relatively prolonged, so the probability of observing a mitotic event is low. Alternatively, the RPE cells may degenerate, and the remaining RPE cells hypertrophy and slide to fill the space along Bruch's membrane (22), which would also result in pigment dilution.

4) The RPE stimulates retinal vessel endothelial cells to divide and form new vessels, but only within the RPE layer.

Our evidence that the vessel profiles within the retina, specifically the OPL layer, continue to decrease in number shows that the RPE does not stimulate neovascularization of the retinal vessels in general. However, the exuberant increase in vessel profiles within the RPE leads to the conclusion that there is a specific, local interaction of the RPE cell and the apposed retinal endothelial cells that results in endothelial proliferation only within this layer. Caldwell, et al., (12) have shown an increase in vessel density within the retina in the RCS rat at later stages, but could not differentiate retinal from RPE

vessels, since the RPE appears to be hypertrophic and proliferative at an early stage in this model.

Thus, there is the apparent contradiction of simultaneous death of vessels within the neural retina and stimulation of neovascularization within the RPE. This difference in behaviour occurs within a distance of only a few tens of microns, at most, and suggests that non-diffusible, local acting stimuli are responsible for the neovascularization. A likely candidate is basic fibroblast growth factor, which is produced by both the RPE and capillary endothelial cells, and may be regulated by binding to extracellular heparan sulfate. (23-26)

Alterations in extracellular matrix (ECM) could also stimulate neovascularization (27), and it is possible that the vessels within the RPE have a different ECM environment than normal retinal vessels. Caldwell (28) has reported changes in charge of the RPE ECM prior to neovascularization in RCS rats. Whether this is a function of the genetic abnormality in these animals is not known. We do not have information on whether a similar early difference in ECM charge is seen in the urethane model, which does not have a genetic component.
5) The new vessels that are formed are of the choroidal phenotype.

In previous electron microscopic studies we (3) and others (29-31) have noted that the vessels within the RPE are pleiomorphic in appearance. Some vessels have a typical retinal phenotype, others have endothelial cells with fenestrae, and there is also residual vessel basement membrane material, suggesting that some retinal vessels that become encapsulated by the RPE degenerate within this layer. It has been suggested (31,32) that the appearance of the fenestrae increases with age, but this has not been proved. It would, however, be logical, since, during development, nascent choriocapillaries first have

continuous endothelial cells, and only later develop the fenestrated phenotype. (33) It would also be logical to think that the vessel type that is stimulated to form within the RPE is capable of resistance to high oxygen concentrations, which is apparently true of the choriocapillaris.

A characteristic of all retinal vessels is that they are entirely surrounded by glial cell processes, either of Müller cells or astrocytes. (343) However, the vessels within the RPE do not have a glial investment. (15) The lack of surrounding glial cells may be a permissive condition which allows the fenestrated phenotype to develop.

6) The choriocapillaris remains intact throughout this process due to the continued presence of the RPE.

Since there is profound loss of retinal vessels, why does the choriocapillaris not degenerate? First, the choriocapillaris must have a totally different reactivity to high oxygen concentrations and high blood flow than the retinal vasculature. Secondly, there is abundant information in the literature, that the existence of the RPE is sufficient to maintain choriocapillaris viability. (for review, 35) So, as long as the RPE forms a continuous sheet along Bruch's membrane, we would expect the choriocapillaris to remain functional. But why is the choroidal capillary bed not stimulated to proliferate? In vitro studies have shown that RPE can stimulate choroidal endothelium . (36)

Comparison with other rodent photoreceptor degenerations

We think it likely that the mechanisms for RPE neovascularization that occur in rodent photoreceptor degenerations are similar (1) but there may be differences between the time course or details that would illuminate the relative importance of different factors.

Comparing the RCS rat with UR rat photoreceptor degeneration:

1) Up to 8 weeks of age, the UR shows no change in vessel profiles per mm retinal length. Caldwell, et al. (12) showed a slight decrease in this measurement in RCS rats (8 to 16 weeks) compared to controls at 8 weeks. Matthes and Bok (7), using a different measuring technique, which did not include RPE vessels, found no change in RCS rat retina vascularity up to 16 weeks of age. By 24 weeks of age, the RCS rat had 70% of the control retinal blood vessels.

The RCS rat shows increased vessel density (number of vessels/mm^2 retina) at 30 to 52 weeks when compared to control. (12) The UR rat has an increased vessel density at 8 and 12 weeks, but at later times is not different from the control. Since the measurements of vessel density in the RCS rat included both retinal and RPE vessels, it is not possible to distinguish retinal vessel loss from RPE vessel proliferation, as we have done in UR. Since the RPE cell appears more reactive in the RCS rat, it is difficult to discriminate the vessel location, but the increased vessel density appears in the RCS rat appears to be due to proliferation of vessels surrounded by RPE. (12)

A curious finding is that, in the control animals of these two studies, there are major differences in vessel density within the retina. At 8 weeks the control RCS-rdy^+ retina had 275 +/- 18 vessels/mm^2 retina, while the Long-Evans control retina had 122 +/- 21 vessels/mm^2 retina. Matthes and Bok (7) also showed a difference in vessel density between two control strains of mice, and attributed that to a difference in retinal thickness. Calculations show that this does not account for the difference between the UR and RCS rats. Apparently there may be a strain difference in vessel density.

2) In the RCS rat, duplication and proliferation of RPE cells has been observed at 8 weeks (12), but in UR, we have not observed RPE duplication or possible proliferation until vessels come into contact with the RPE, first seen at 16 weeks. It may be that the RPE in RCS rats is more reactive than in UR.

3) In UR, there does not appear to be Müller cell migration up to 24 weeks, as has been observed in RCS rats. (37) In both retinopathies, GFAP is expressed in Müller cells, as early as 8 weeks in UR. (15,37)

4) Vascularized vitreoretinal membranes (VRM) have been observed in some RCS rats as early as 8 weeks of age, and more commonly in older ages (11,12) but always in association with RPE neovascularization. The vitreoretinal vessels are accompanied by proliferating RPE, but the vessels are apparently not fenestrated. Why are these vessels, in association with RPE, not fenestrated? In UR, in this study, up to 24 weeks of age, we have not seen VRMs that extend into the vitreous, although they may occur in later stages.

Clinical relevance

The participation of RPE in stimulating neovascularization in proliferative retinopathies is widely accepted (38), and the role of RPE in stimulating choroidal neovascularization in age-related macular degeneration has been examined. (36) However, vascularization of the RPE is not known to occur in human diseases of photoreceptor degeneration, such as retinitis pigmentosa although other forms of neovascularization do occur. (39) The occurence of RPE neovascularization in the rodent models suggests a significant difference in the disease processes, or species difference in the capacity of the RPE cell to interact with the retinal vasculature.

ACKNOWLEDGEMENTS

This study supported by NIH Grant #EY05979, Office of Naval Research, and an unrestricted grant from Research to Prevent Blindness, Inc., NY. We are appreciative of Mary E. Johnson's excellent secretarial assistance.

CORRESPONDING AUTHOR

Margaret S. Burns, Ph.D., Department of Ophthalmology, 1603 Alhambra Blvd., Sacramento, CA 95816.

REFERENCES

1. LaVail, M.M. (1979) The retinal pigment epithelium in mice and rats with inherited retinal degeneration. In "The Retinal Pigment Epithelium", (Eds. Marmor, M.F., Zinn, K.M.). Pp. 357-380. Harvard University Press, Cambridge.
2. Bellhorn, R.W., Burns, M.S. and Benjamin, J.V. (1980) Retinal vessel abnormalities of phototoxic retinopathy in rats. Invest. Ophthalmol. Vis. Sci. 19, 584-592.
3. Bellhorn, R.W., Bellhorn, M, Friedman, A.H. and Henkind, P. (1973) Urethane induced retinopathy in pigmented rats. Invest. Ophthalmol. 12, 65-79.
4. Gerstein, D.D. and Dantzker, D.R. (1969) Retinal vascular changes in hereditary visual cell degeneration. Arch. Ophthalmol. 81, 99-105.
5. Dantzker, D.R. and Gerstein, D.D. (1969) Retinal vascular changes following toxic effects on visual cells and pigment epithelium. Arch. Ophthalmol. 81, 106-114.
6. Blanks, J.D. and Johnson, L.V. (1985) Vascular atrophy associated with photoreceptor degeneration in mutant mice. In "Retinal Degeneration: Experimental and Clinical Studies", (Eds. LaVail, M.M., Hollyfield, J.G. and Anderson, R.E.). Pp. 189-207. Alan R. Liss, Inc., New York.
7. Matthes, M.T. and Bok, D. (1985) Blood vascular abnormalities in animals with inherited retinal degeneration. In "Retinal Degeneration: Experimental and Clinical Studies", (Eds. LaVail, M.M., Hollyfield, J.G. and Anderson, R.E.). Pp. 209-237. Alan R. Liss, Inc., New York.
8. Blanks, J.D. and Johnson, L.V. (1986) Vascular atrophy in the retinal degenerative rd mouse. J. Comp. Neurol., 254, 543-553.

9. Matthes, M.T. and Bok, D. (1984) Blood vascular abnormalities in the degenerative mouse retina (C57BL/6j-rdle). Invest. Ophthalmol. Vis. Sci. 25, 364-369.
10. Shiraki, K. and Burns, M.S. (1986) Neovascularization in urethane rat retinopathy demonstrated by thymidine labelling. Curr. Eye Res., 5, 683-695.
11. Weber, M.L., Mancini, M.A. and Frank, R.N. (1989) Retinovitreal neovascularization in the Royal College of Surgeon's rat. Curr. Eye Res., 8, 61-74.
12. Caldwell, R.B., Roque, R.S., and Solomon, S.W. (1989) Increased vascular density and vitreo-retinal membranes accompany vascularization of the pigment epithelium in the dystrophic rat retina. Curr. Eye Res. 8. 923-937.
13. Burns, M.S. and Bellhorn, R.W. (1987) Early degeneration of photoreceptor cells in urethane induced retinopathy of rats. *In* "Degenerative Retinal Disorders: Clinical and Laboratory Investigations", (Eds. Hollyfield, J.G., Anderson, R.E. and LaVail, M.M.) Alan R. Liss, Inc., NY. Pp. 531-549.
14. Burns, M.S. and Tyler, N.K. (1990) Inter-glial cell junctions increase in urethane induced photoreceptor degeneration in rats. Invest. Ophthalmol. Vis. Sci. In press.
15. Tyler, N.K. and Burns, M.S. (1990) Alterations in glial cell morphology and GFAP expression in urethane induced retinopathy. Submitted.
16. Shiraki, K., Burns, M.S. and Bellhorn, R.W. (1982) Abnormal vessel patterns in phototoxic rat retinopathy studied by vascular replicas. Curr. Eye Res., 2, 545-551.
17. D'Amore, P.A. and Sweet, E. (1987) Effects of hyperoxia on microvascular cells in vitro. In Vitro Cell. Develop. Biol. 23, 123-128.
18. Korte, G.E., Bellhorn, R.W. and Burns, M.S. (1986) Remodelling of the retinal pigment epithelium in response to intraepithelial capillaries: evidence that capillaries influence the polarity of the epithelium. Cell and Tissue Res. 245, 135-142.
19. Caldwell, R.B. and Roque, R.S. (1990) Changes in RPE and Müller cell intermediate filament protein expression during vascular remodelling in the dystrophic rat retina. Invest. Ophthalmol. Vis. Sci. 31 (Suppl.), 492.
20. Wong, H.C., Boulton, M., McLeod, D., Bayly, M., Clark, P. and Marshall, J. (1988) Retinal pigment epithelial cells in culture produce retinal vascular mitogens. Arch. Ophthalmol. 106, 1439-1443.
21. Glaser, B.M., Campochiaro, P., Davis J.L. Jr., Sato, M. (1985) Retinal pigment epithelial cells release an inhibitor of neovascularization. Arch. Ophthalmol. 103, 1870-1875.

22. Korte, G.E., Burns, M[illegible]nd Bellhorn, R.W. (1989) Epithelium-capillary interactons in the eye: the retinal pigment epithelium and the choriocapillaris. Intern. Rev. Cytology 114, 221-248.
23. Schweigerer, L., Malerstein, B., Neufeld, G., and Gospodarowicz, D. (1987) Basic fibroblast growth factor is synthesized in cultured retinal pigment epithelial cells. Biochem. Biophys. Res. Communs. 143, 934-940.
24. Schwigerer, L., Neufeld, G., Friedman, J., Abraham, J.A., Fiddes, J.C. and Gospodarowicz, D. (1987) Capillary endothelial cells express basic fibroblast growth factor, a mitogen that promotes their own growth. Nature 325, 257-259.
25. Bensaid, M., Malecaze, F., Prats, H., Bayard, F., and Tauber, J.P. (1989) Autocrine regulation of bovine capillary endothelial cell (BREC) proliferation by BREC-derived basic fibroblast growth factor. Exp. Eye Res. 48, 801-813.
26. Bensaid, M., Malecaze, F., Bayard, F., and Tauber, J.P. (1989) Opposing effects of basic fibroblast growth factor and transforming growth factor-b on the proliferation of cultured bovine retinal capillary endothelial (BREC) cells. Exp. Eye Res. 48, 791-799.
27. Gospodarowicz, D. and Ill, C. (1980) Extracellular matrix and control of proliferation of vascular endothelial cells. J. Clin. Invest. 65, 1351-1364.
28. Caldwell, R.B. (1989) Extracellular matrix alterations precede vascularization of the retinal pigment epithelium in dystrophic rats. Curr. Eye Res. 9, 907-921.
29. Dowling, J.E. and Sidman, R.L. (1962) Inherited retinal dystrophy in the rat. J.Cell Biol. 14, 73-109.
30. Bok, D., and Hall, M.O. (1971) The role of the pigment epithelium in the etiology of inherited retinal dystrophy in the rat. J. Cell Biol. 49, 664-682.
31. Mancini, M.A., Frank, R.N., Keirn, R.J., Kennedy, A., and Khoury, J.K. (1986) Does the retinal pigment epithelium polarize the choriocapillaris? Invest. Ophthalmol. Vis. Sci. 27, 336-345.
32. Korte, G.E., Bellhorn, R.W. and Burns, M.S. (1984) Urethane induced rat retinopathy. Plasticity of the blood-retinal barrier in disease. Invest. Ophthalmol. Vis. Sci. 25, 1027-1034.
33. Ozanics, V., Rayborn, M.E. and Sagun, D. (1978) Observations on the ultrastructure of the developing primate choroid coat. Exp. Eye Res. 26, 25-45.
34. Hogan, M.J. and Feeney, L. (1963) The ultrastructure of the retinal vessels. J. Ultrastructure Res. 9, 47-62.

35. Burns, M.S., Bellhorn, R.W., Korte, G.E. and Heriot, W.J. (1986) Plasticity of the retinal vasculature. Prog. Retinal Res. 5, 253-307.
36. Morse, L.S., Terrell, J., and Sikikaro, Y. (1989) Bovine retinal pigment epithelium promotes proliferation of choroidal endothelium in vitro. Arch. Ophthalmol. 107, 1659-1663.
37. Roque, R.S. and Caldwell, R.B. (1989) Glial cell migration accompanies RPE cell alterations and vascular proliferation in the RCS retina. Invest. Ophthalmol. Vis. Sci. 30(Suppl.), 464.
38. Glaser, B.M. (1986) Cell biology and biochemistry of endothelial cells and the phenomenon of intraocular vascularization. In "The Retina, Part II," (Eds. Adler, R. and Farber, D.) Academic Press, NY. Pp. 215-243.
39. Uliss, A.E., Zdenek, J.G., and Bird, A.C. (1986) Retinitis pigmentosa and retinal neovascularization. Ophthalmology 93, 1599-1603.

Figure 1a: Control rat retina, 8 weeks of age, central region. All retinal structures appear normal. The OPL vessel bed has evenly spaced capillary profiles (arrows) vitread to the synaptic endings of the photoreceptor cells. The INL vessels are at the inner edge of the INL (arrowhead). The NFL vessels are close to the inner limiting membrane. A capillary profile traversing from the NFL to the INL bed is seen in the inner plexiform layer (IPL). Cone nuclei with lobulated chromatin are present (double arrowhead) in the outer nuclear layer (ONL). Bar = 20 μm.

Figure 1b: Experimental rat retina, 8 weeks of age, central region. Although the choriocapillaris (C), RPE, INL, IPL and NFL appear normal, the photoreceptor cell nuclei (ONL) has been reduced to approximately 2 rows of nuclei with a predominance of cone nuclei remaining. Two vessel profiles are seen in the usual location in the OPL (arrows) and in the NFL (arrowheads). The interphotoreceptor space contains some rod nuclei and residual photoreceptor inner and outer segment material. Bar = 20μm.

Figure 1c: Experimental rat retina, 16 weeks of age, central region. The photoreceptor cell nuclei (ONL), which are primarily cone nuclei, are reduced to one almost continuous layer and the apical microvilli of the RPE cells fill the residual interphotoreceptor space, with indication of the external limiting membrane (arrowheads) remaining. The C, RPE, INL, IPL and NFL appear normal. Bar = 20 μm.

Figure 1d: Experimental rat retina, 24 weeks of age, central region. A few photoreceptor nuclei remain at the inner edge of the external limiting membrane (arrowheads), above which the apical microvilli of the RPE form a translucent layer. The C, RPE, INL, IPL and NFL appear normal. Vessel profiles are not seen in the residual OPL, although they are frequent in control retinas in this layer (compare Figure 1a). Bar = 20 μm.

Figure 2a: Control rat retina, 24 weeks of age, central region. All retinal structures appear normal, including the choriocapillaris (C) and retinal pigment epithelium (RPE). Two vessel profiles of the outer plexiform layer are present (arrows). Three cone nuclei with lobulated chromatin are present (arrowheads) in the outer nuclear layer (ONL). Bar = 20 μm,

Figure 2b: Experimental rat retina, 24 weeks of age, central region. A vessel profile that appears continuous with an inner retinal vessel is partially enveloped by RPE in an area with no photoreceptor cell nuclei remaining. The choriocapillaris (C) and

residual retinal structures are relatively normal in appearance. The RPE cell layer is slightly thickened in an area which probably contains a small vessel (arrow). Bar = 20 μm.

Figure 2c: Experimental rat retina, 16 weeks of age, central region. A retinal vessel profile (arrow) enters the RPE in an area without photoreceptor cell nuclei. Pigmentation of the RPE at this spot is relatively lacking. One RPE cell (arrowhead) in this region is attenuated and condensed. The residual retina is not particularly distorted. A small hyalocyte is at the inner limiting membrane. Bar = 20 μm.

Figure 2d: Experimental rat retina, 24 weeks of age, central region. Three vessel profiles (arrows) are visible within the RPE which is somewhat swollen, but not grossly distorted, though light in pigmentation. An attenuated and condensed RPE cell (double arrowhead) is adjacent to the vessel cluster. A few Müller cell nuclei of the INL have a somewhat pyknotic appearance (arrowheads). The C, INL, IPL and NFL appear normal. Bar = 20 μm.

Figure 3: Relationship of number of residual nuclei in the outer nuclear layer and number of vessels in the RPE for each individual eye. As the nuclei degenerate, the vessels in the RPE increase. Regression coefficient, R = 0.829.

Table I

Retinal Thickness, Central

Average Thickness (μm) ± SD

Age	Control	Experimental
8 weeks	225 ± 17[#]	144 ± 11[*]
12 weeks	213 ± 6[#]	115 ± 9[*,a]
16 weeks	215 ± 8[#]	113 ± 12[*,a]
20 weeks	203 ± 19	118 ± 7[*,a]
24 weeks	197 ± 3[#]	107 ± 8[*,a]

[#]Eight, 12 and 16 week average thickness was statistically different from 24 week average with $P \leq .05$.

[*]Significantly different from age matched control group at $P \leq .001$.

[a]Significantly different ($P \leq .01$) from 8 week urethane group.

Table II

Number of Vessel Profiles/mm Retinal Length

Central Region

	8 weeks	12 weeks	16 weeks	20 weeks	24 weeks
OPL					
Control	15.5 ± 2.3	12.4 ± 2.9	16.2 ± 1.0	15.1 ± 1.9	15.2 ± 3.1
Experimental	12.4 ± 2.4	6.2 ± 1.6[•,‡]	5.6 ± 2.3[•,‡]	4.5 ± 2.6[•,‡]	1.9 ± 1.0[•,‡]
INL					
Control	3.9 ± 0.7	3.3 ± 0.6	6.5 ± 0.3[a]	4.3 ± 0.8	4.5 ± 0.9
Experimental	4.6 ± 1.4	3.4 ± 1.5	3.6 ± 0.9[•]	3.3 ± 1.8	1.7 ± 1.1[•,‡]
NFL					
Control	7.9 ± 0.2	6.8 ± 1.6	7.3 ± 1.2	8.4 ± 2.0	6.6 ± 1.1
Experimental	8.4 ± 1.2	7.7 ± 1.4	8.3 ± 0.7	6.4 ± 1.9	6.2 ± 0.9[‡]

[a]Significant at $P \leq .02$, as described in text.

[•]Significant at $P \leq .05$ compared to control of same age and area.

[‡]Significant at $P \leq .05$ compared to 8 week experimental of same area.

Table III

Number of Vessel Profiles/mm Retinal Length

Peripheral Region

	8 weeks	12 weeks	16 weeks	20 weeks	24 weeks
OPL					
Control	11.7 ± 1.5	11.3 ± 1.0	12.9 ± 0.9	11.4 ± 0.4	11.9 ±1.1
Experimental	12.2 ± 0.7	7.5 ± 0.9[•,‡]	6.5 ± 1.0[•,‡]	6.8 ± 2.4[•,‡]	4.4 ± 1.8[•,‡]
INL					
Control	1.6 ± 0.5	2.7 ± 1.1	1.9 ± 0.4	1.5 ± 0.5	1.8 ± 0.8
Experimental	2.3 ± 0.9	1.2 ± 0.6[‡]	1.4 ± 0.4	1.7 ± 1.2	0.9 ± 0.6[‡]
NFL					
Control	8.3 ± 2.6	6.8 ± 1.0	7.0 ± 0.7	7.1 ± 0.5	8.0 ± 1.0
Experimental	7.5 ± 0.8	6.0 ± 0.5[‡]	6.4 ± 0.6[‡]	7.4 ± 1.6	5.4 ± 1.1[‡]

[a]Significant at $P \leq .02$, as described in text.

[•]Significant at $P \leq .05$ compared to control of same age and area.

[‡]Significant at $P \leq .05$ compared to 8 week experimental of same area.

Table IV

Vessel Density, Central Retina

	Number of Vessels per mm2 Retina			per mm2 RPE
		Experimental		
Age	Control	Total	Retinal	RPE
8 weeks	122 ± 21	178 ± 28*	178 ± 28	0
12 weeks	105 ± 22	150 ± 32*	150 ± 32	0
16 weeks	139 ± 12	156 ± 31‡	155 ± 32‡	14 ± 29
20 weeks	138 ± 37	124 ± 34‡	117 ± 39‡	80 ± 95
24 weeks	133 ± 29	124 ± 17‡	91 ± 18‡	340 ± 264

*Different from Control at $P \leq .05$.

‡Different from 8 week Experimental, Total, at $P \leq .05$.

Table V

Vessels Profiles Within The RPE, Central Region

Age	Surrounded by Pigmented RPE	Surrounded by Non-pigmented RPE
8 weeks	0	0
12 weeks	0	0
16 weeks	3	1
20 weeks	18	21
24 weeks	49	94


RPE
ONL
OPL
INL
IPL
NFL

1a


C
RPE
ONL
INL
IPL
NFL

1b

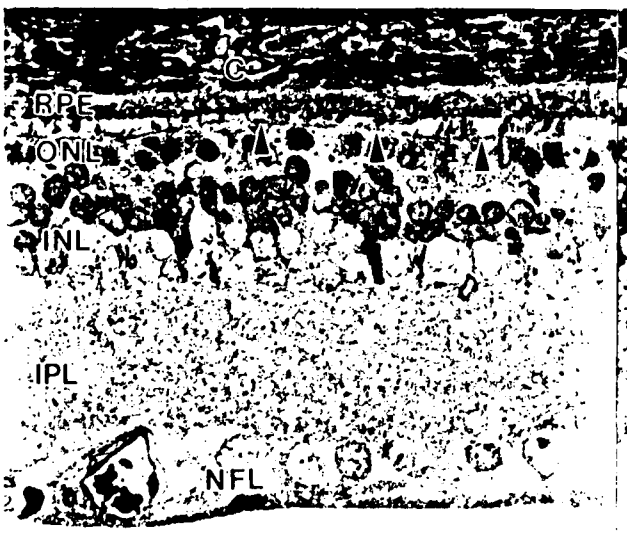
C
RPE
ONL
INL
IPL
NFL

1c

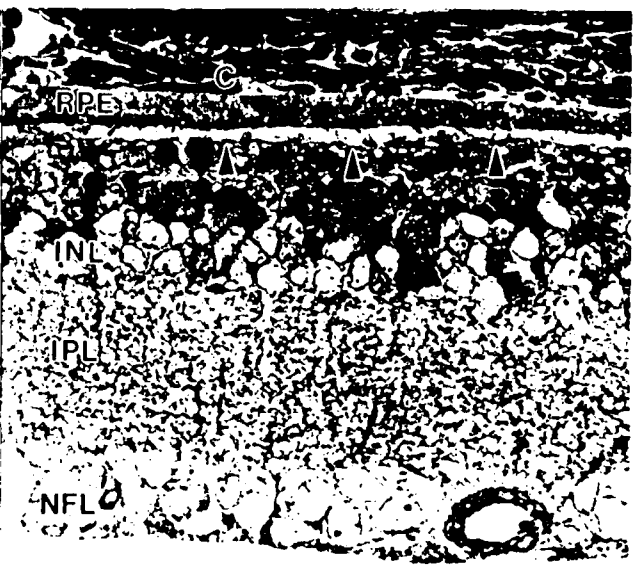
C
RPE
INL
IPL
NFL

1d

2a

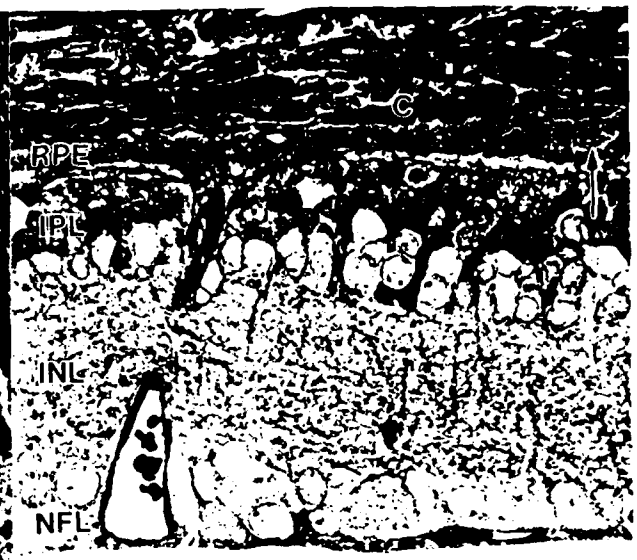

2b

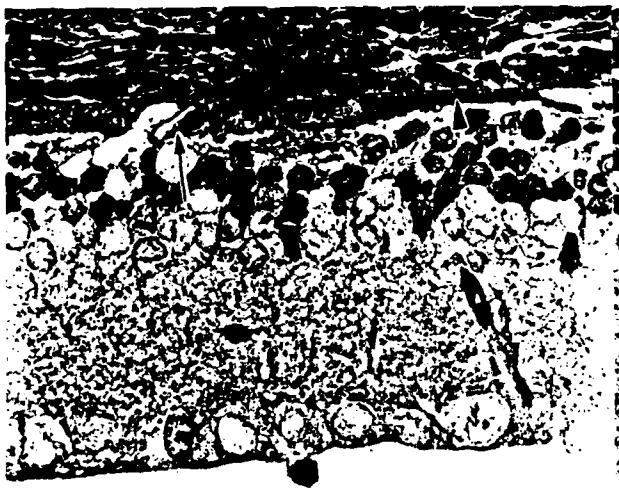

2c

2d

Figure 3

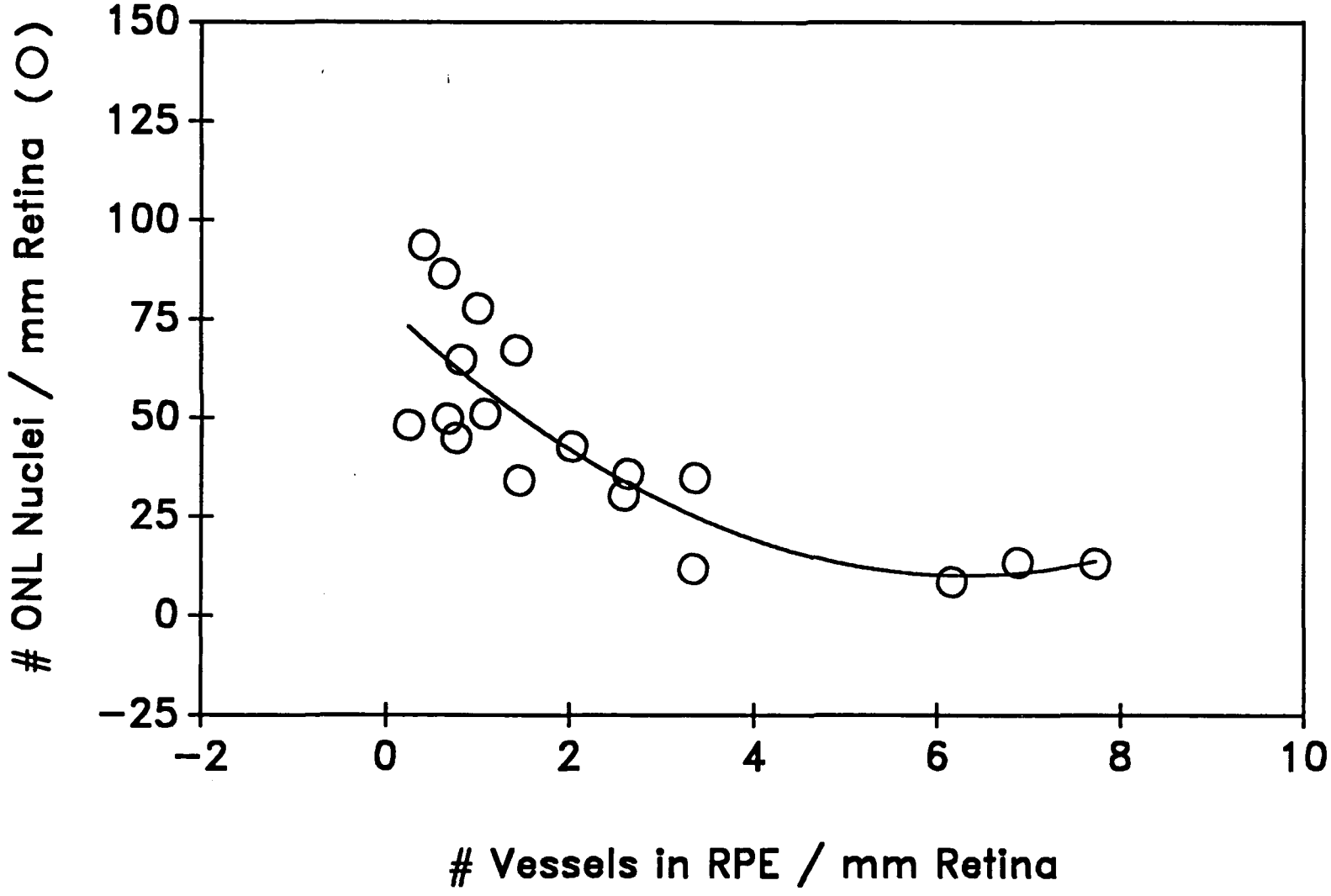
150
125
100
75
50
25
0
−25
−2
0
2
4
6
8
10
ONL Nuclei / mm Retina (O)
Vessels in RPE / mm Retina

DISTRIBUTION LIST

Cell Biology of Trauma Program

Annual, Final and Technical Reports (one copy each)

INVESTIGATORS

Dr. Michael Artman
Dept. of Pediatrics
Univ. of South Alabama
Medical Center
2451 Fillingim Street
Mobil, AL 36617

Dr. Margaret S. Burns
Dept. of Ophthalmology
Univ. of California, Davis
1603 Alhambra Boulevard
Sacramento, CA 95816

Dr. Robert J. Cohen
Dept. of Biochemistry and
Molecular Biology
College of Medicine
Box J-245, JHMHC
University of Florida
Gainesville, FL 32610

Dr. Dipak K. Das
Department of Surgery
Univ. of Connecticut
Health Center
Farmington, CT 06032

Dr. Thomas M. Devlin
Chairman, Dept. of Biological Chemistry
Hahnemann University
230 Broad Street
Philadelphia, PA 19102

Dr. Marvin A. Karasek
Dept. of Dermatology
Stanford University School of Medicine
Stanford, CA 94305

Dr. John J. Lemasters
Dept. of Cell Biology and Anatomy
School of Medicine
University of North Carolina
Campus Box 7090
Chapel Hill, NC 27599

Dr. Alfred H. Merrill, Jr.
Dept. of Biochemistry
Emory University School
of Medicine
Atlanta, GA 30322

LCDR Douglas H. Robinson
Diving Medicine Dept.
Naval Medical Research Inst.
NMC NCR
Bethesda, MD 20814-5055

Dr. Benjamin F. Trump
Dept. of Pathology
Univ. of Maryland
School of Medicine
Baltimore, MD 21201

Annual, Final and Technical Reports (one copy each except as noted)

ADMINISTRATORS

Dr. Jeannine A. Majde, Code 1141SB
Office of Naval Research
800 N. Quincy Street
Arlington, VA 22217-5000

Program Manager, Code 1213
Human Factors/Biosciences
Division
Office of Naval Research
800 N. Quincy Street
Arlington, VA 22217-5000

Administrator (2 copies) (Enclose DTIC Form 50)
Defense Technical Information Center
Building 5, Cameron Station
Alexandria, VA 22314

Program Manager, Code 223
Support Technology
Directorate
Office of Naval Technology
800 N. Quincy Street
Arlington, VA 22217-5000

Administrative Contracting Officer
ONR Resident Representative
(address varies - obtain from business office)

Annual and Final Reports Only (one copy each)

DoD ACTIVITIES

Commanding Officer
Naval Medical Center
Washington, DC 20372

Directorate of Life Sciences
Air Force Office of
Scientific Research
Bolling Air Force Base
Washington, DC 20332

Commanding Officer
Naval Medical Research & Development Command
National Naval Medical Center
Bethesda, MD 20814

Library
Armed Forces Radiation
Research Institute
Bethesda, MD 20814-5145

Library
Naval Medical Research Institute
National Naval Medical Center
Bethesda, MD 20814

Commander
Chemical and Biological Sciences Division
Army Research Office, P.O. Box 12211
Research Triangle Park, NC 27709

Commander
U.S. Army Research and Development Command
Attn: SGRD-PLA
Fort Detrick
Frederick, MD 21701